Glacial Earthquakes and Glacier Seismicity in Greenland

Stephen A. Veitch

Submitted in partial fulfillment
of the requirements for the degree of
Doctor of Philosophy
in the Graduate School of Arts and Sciences

COLUMBIA UNIVERSITY

2016

Abstract

Glacial Earthquakes and Glacier Seismicity in Greenland

Stephen A. Veitch

The loss of ice from the Greenland ice sheet is an important contributor to current and future sea level rise occurring due to ongoing changes in the global climate. A significant portion of this ice mass loss comes through the calving of large icebergs at Greenland's many marine-terminating outlet glaciers. However, the dynamics of calving at these glaciers is currently not well understood, complicating projections of future behaviour of these glaciers and mass loss from the Greenland ice sheet. The use of seismological tools has shown promise as a means of both monitoring and better understanding the dynamics of the calving process at these glaciers. On the global scale, data from the long-standing global seismic network has recorded the occurrence of glacial earthquakes, large long period earthquakes that occur during large calving events at near-grounded outlet glaciers. The occurrence and source parameters of these earthquakes provide insight into the link between glacier calving and climatic and oceanic forcings, as well as information on the large-scale glacier-dynamic conditions under which these major calving events occur. On the more local scale, a deployment of seismometers around an individual glacier has provided insights on the seismic environment of a calving glacier, as well as the more immediate, short-term external drivers of calving events. We consider both local and global seismic data in order to further understanding of the dynamics of

the calving process at Greenland outlet glaciers, and find that glacial earthquake production is indicative of a near-grounded terminus at the source glacier. We find that the locations derived from these events are accurate and are sensitive to changes in the calving-front position of the source glacier, and that the active-force azimuths are representative of the orientation of the glacier at the time of calving. We also find that these glaciers are the source of abundant small icequakes, which are strongly tied to the occurrence of major calving events. The small icequakes that occur at Helheim glacier are modulated by semi-diurnal variations in tide height, and potentially control the timing of major calving events by progressively damaging the glacier tongue.

Contents

List of Figures

List of Tables

Page

Chapter 1

Introduction

The Greenland Ice Sheet is the second largest body of ice in the world, and the largest in the Northern Hemisphere. It represents an important reservoir of landfast water with the potential to contribute to future sea-level changes in response to the changing climate. It has been observed to be undergoing rapid changes over the past several decades that may generally be characterized as rapidly increasing mass loss [*Enderlin et al.*, 2014] and negative mass balance [*Shepherd et al.*, 2012] throughout Greenland.

The most rapid changes currently observed in Greenland are occurring at its margins [e.g *Krabill et al.*, 2004], where numerous studies have shown Greenland's outlet glaciers to be undergoing widespread retreat [e.g. *Joughin et al.*, 2004; *Howat et al.*, 2005; *Luckman et al.*, 2006; *Moon and Joughin*, 2008], acceleration [e.g. *Joughin et al.*, 2004; *Howat et al.*, 2005; *Rignot and Kanagaratnam*, 2006; *Joughin et al.*, 2010], and thinning [e.g. *Thomas et al.*, 2000; *Abdalati et al.*, 2001; *Krabill et al.*, 2004; *Howat et al.*, 2005; *Stearns and Hamilton*, 2007] coincident with oceanic [e.g. *Holland et al.*, 2008; *Straneo et al.*, 2010] and atmospheric [e.g. *Box and Cohen*, 2006; *Hanna et al.*, 2008] warming surrounding Greenland. Mass loss at outlet glaciers represents a large portion of overall mass loss from Greenland, where iceberg calving represents at least $1/3$–$1/2$ of mass lost from the Greenland Ice Sheet [*van den Broeke et al.*, 2009; *Enderlin et al.*, 2014]. Thus, understanding the behaviour of these outlet glaciers is key to developing models of the future behaviour

of the Greenland Ice Sheet both in the immediate and long term.

Iceberg calving is one of the most important and complex dynamic behaviours that occurs at marine-terminating glaciers. However, the calving process is not well understood, and may show a variety of modes during different glacier-dynamic conditions. While remote sensing studies in Greenland have provided important insights into the dynamics of calving glaciers, such remote studies are limited to temporally coarse observations which may not clearly observe processes that occur over short timescales. Remote studies are not able to address the glacier-dynamic processes underlying each event or the effect of calving events on other aspects of the glacier's behaviour, and behaviours that are ephemeral may not be observed at all.

As part of the efforts to better understand the calving process at Greenland outlet glaciers, there has been an increasing use of seismological techniques, and the application of seismological techniques to the understanding of the dynamics of marine-terminating glaciers is the primary concern of this work.

The application of a newly developed earthquake detection method [*Ekström*, 2006] to previously recorded global seismic data led to the detection of a large number of previously undetected long-period earthquakes located in Greenland [*Ekström et al.*, 2003]. These events, now referred to as glacial earthquakes, were initially recognized as noteworthy because of their unusual source spectra, their location in tectonically inactive Greenland, and their poor fit to the 'double-couple' moment tensor source-model that is nearly universally used for studies of tectonic earthquakes [*Ekström et al.*, 2003]. Further study revealed both seasonality and a rapid increase in their occurrence [*Ekström et al.*, 2006] which clearly identified glacial earthquakes as a distinct phenomena warranting further study.

Glacial earthquakes were initially inferred to be the result of sudden acceleration of large portions of the source glacier's trunk [*Ekström et al.*, 2003]. Their unique patterns of occurrence were suggested to be of climatic origin [*Ekström et al.*, 2006]. However, the links between the occurrence of glacial earthquakes and glacier dynamics were not clear. Since their initial discovery, glacial earthquakes have been modeled [e.g. *Tsai et al.*, 2008] and observed [e.g *Amundson et al.*,

2008; *Joughin et al.*, 2008a; *Nettles et al.*, 2008a] to occur as the result of iceberg capsize during large-scale calving events at marine-terminating outlet glaciers. This has provided insight into the nature of the climatic link to glacial earthquakes, but the glacier-dynamic conditions under which they occurred remained unclear. The iceberg-capsize source model also requires further validation.

The earthquakes themselves must also be revisited in light of the new source model. The intermediate-period surface waves generated by glacial-earthquakes may be used to perform waveform modeling to determine source parameters for each event, which are best represented by a single-force (CSF) model *Kawakatsu* [1989] initially developed for seismic modeling of landslides. Existing studies of these source parameters rely on the basal-sliding model [*Ekström et al.*, 2003, 2006; *Tsai and Ekström*, 2007], and have not been evaluated as events resulting from iceberg capsize. This improved source model must be applied to an analysis of previously published glacial-earthquake parameters in order to better assess the physical meaning and accuracy of the source parameters with respect to glacier dynamics.

While glacial earthquakes provide a great deal of information about the glacier dynamics underlying the occurrence of calving events, they are limited to observations of the calving event itself, and do not provide insight into the glacier dynamics immediately preceding and following their occurrence. Additionally, glacial earthquakes are only observable at periods greater than $\sim$25 seconds [e.g *Ekström et al.*, 2003; *Nettles and Ekström*, 2010], and do not provide information on behaviours which occur over shorter time scales. In order to explore these questions, the local deployment of seismometers is required. These local deployments can provide further insights into the calving process by recording the seismic environment of the glacier during periods between large calving events, as well as recording high-frequency seismicity that would not otherwise be observable by established, longer term seismic networks.

In this dissertation, consisting of a series of studies on seismological questions surrounding Greenland glacier dynamics, we address each of the aforementioned uncertainties. In the second chapter, we perform waveform modeling of five years of glacial earthquakes in order to increase the size of the catalog, and provide a larger number of events for this and future analyses. We establish

connections between glacial earthquakes and changes in glacier dynamics at source glaciers. We then address trends in the occurrence of these events in light of the glacier-dynamic connections we have established and other observations of the Greenland ice sheet over the same time period. We then consider the applicability of the overturning-iceberg model of seismogenesis developed for Helheim Glacier by earlier studies, and the implications for the application of this model to glacial earthquakes across Greenland.

In the third chapter, we address uncertainties in the accuracy of model parameters obtained from waveform modeling of glacial earthquakes by considering changes in glacial-earthquake location and force direction at four important glacial-earthquake producing glaciers in Greenland. We compare these changes to independently determined records of changes in glacier geometry and position, and consider the accuracy of those parameters. Finally, we discuss the implications of our improved understanding of glacial-earthquake source parameters for the use of glacial earthquakes as a tool for remote sensing of glacier dynamics.

Finally, we consider data from a summer 2009 deployment of 6 seismometers around Helheim Glacier. This unique dataset offers us the opportunity to explore the conditions at a glacial-earthquake producing glacier at time scales that were not previously possible. While a wide range of questions may be explored with this dataset, we focus on seismicity that occurs between calving events and the factors controlling the occurrence of that seismicity. In doing so we seek to better understand the short-term drivers of glacier calving, and the effect of calving events on the brittle behaviour of marine-terminating glaciers.

As indicated in the schematic cross-section shown in Figure 1.1, all of the processes discussed in this dissertation occur very near to the terminus of large, marine-terminating glaciers. Understanding of the behaviour of the glacier where it interacts most closely with the ocean is crucial to understand how external forcings influence the dynamics of large tidewater glaciers.

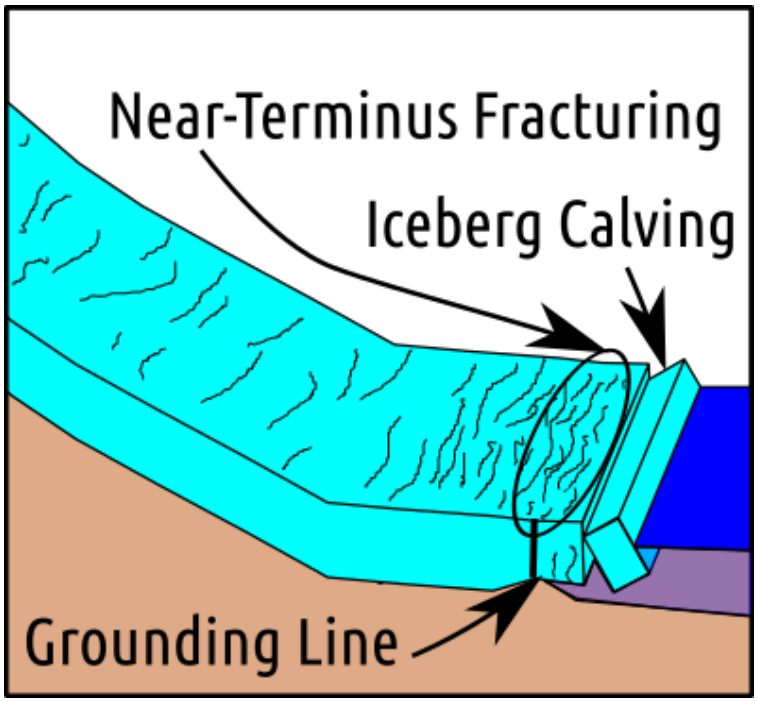

Figure 1.1: A schematic cross section of a large, near-grounded, tidewater glacier. The processes discussed in this dissertation take place in the very lowermost regions of the glacier.

Chapter 2

Glacial Earthquakes in Greenland 1993–2010

NOTE: This chapter has been previously published as:

Veitch, S. A., and M. Nettles (2012), Spatial and temporal variations in Greenland glacial-earthquake activity, 1993–2010, *Journal of Geophysical Research: Earth Surface*, *117*(F4), doi: 10.1029/2012JF002412

2.1 Abstract

Glacial earthquakes are anomalous earthquakes associated with large ice-loss events occurring at marine-terminating glaciers, primarily in Greenland. They are detectable teleseismically, and a proper understanding of the source mechanism may provide a remote-sensing tool to complement glaciological observations of these large outlet glaciers. We model teleseismic surface-wave waveforms to obtain locations and centroid–single-force source parameters for 121 glacial earthquakes occurring in Greenland during the period 2006–2010. We combine these results with those obtained by previous workers [*Tsai and Ekström*, 2007] to analyze spatial and temporal trends in glacial-earthquake occurrence over the 18-year period from 1993–2010. We also examine earthquake occurrence at six individual glaciers, comparing the earthquake record to independently ob-

tained observations of glacier change. Our findings confirm the inference that glacial-earthquake seismogenesis occurs through the capsize of large, newly calved icebergs. We find a close correspondence between episodes of glacier retreat, thinning, and acceleration and the timing of glacial earthquakes, and document the northward progression of glacial earthquakes on Greenland's west coast over the 18-year observing period. Our results also show that glacial earthquakes occur when the termini of the source glaciers are very close to the glacier grounding line, i.e., when the glaciers are grounded or nearly grounded.

2.2 Introduction

Rapid changes in the Greenland Ice Sheet have been documented using a variety of methods over the last decade. Greenland's outlet glaciers have shown large-scale calving-front retreat [e.g., *Joughin et al.*, 2004; *Howat et al.*, 2005; *Luckman et al.*, 2006; *Moon and Joughin*, 2008], trunk acceleration [e.g., *Joughin et al.*, 2004; *Howat et al.*, 2005; *Rignot and Kanagaratnam*, 2006; *Joughin et al.*, 2010], and thinning [e.g., *Thomas et al.*, 2000; *Abdalati et al.*, 2001; *Krabill et al.*, 2004; *Howat et al.*, 2005; *Stearns and Hamilton*, 2007]. Offshore, changes in ocean temperature [e.g., *Holland et al.*, 2008; *Howat et al.*, 2008; *Murray et al.*, 2010; *Straneo et al.*, 2010; *Seale et al.*, 2011], both at the sea surface and at depth, have been observed, and appear to be linked to changes in the ice sheet, primarily through modulation of calving and melt rates at marine-terminating outlet glaciers. These changes coincide with the acceleration of mass loss in Greenland [e.g., *Velicogna and Wahr*, 2005; *Luthcke et al.*, 2006; *Rignot et al.*, 2008; *Khan et al.*, 2010]. Variations in ice discharge at outlet glaciers contribute significantly to changes in Greenland's mass budget [*Rignot et al.*, 2008], and account for roughly half of the total recent mass loss [*van den Broeke et al.*, 2009]. However, the nature of the interaction between processes driving mass loss, including controls on glacier calving and retreat, remains poorly understood.

Glacial earthquakes are globally observable seismic signals associated with large outlet glaciers. Glacial earthquakes were first identified by *Ekström et al.* [2003] through examination of long-

period surface waves. They are located primarily along the coast of Greenland [*Ekström et al.*, 2003], though a few events have also been detected in Antarctica [*Ekström et al.*, 2003; *Nettles and Ekström*, 2010; *Chen et al.*, 2011]. The earthquakes have magnitudes M_{SW} 4.6–5.2, and source durations that are very long (30–60 s) compared with tectonic earthquakes of similar size ($\sim$2 s). The long source durations of these earthquakes, and resultant depletion in high-frequency energy, explains the absence of the glacial earthquakes from standard catalogs of global seismicity, which are based on high-frequency detections. The location of the events in tectonically inactive Greenland and the tight clustering of the earthquakes at large outlet glaciers [*Ekström et al.*, 2006; *Tsai and Ekström*, 2007] suggest an association with glacier motion rather than tectonic activity. Additionally, seismograms from glacial earthquakes are poorly explained by moment-tensor source models appropriate for elastic faulting [*Ekström et al.*, 2003; *Tsai and Ekström*, 2007], but are well explained by a single-force model like that previously used to model seismic emissions from large landslides [e.g., *Kawakatsu*, 1989]. *Ekström et al.* [2006] studied glacial earthquakes in Greenland from 1993–2005, and observed a seasonal pattern in which glacial earthquakes were most frequent in late summer. They also observed an increase in the frequency of earthquake occurrence between 2000 and 2005. *Tsai and Ekström* [2007] conducted a systematic analysis of 184 earthquakes occurring over 13 years (1993–2005) in Greenland. They demonstrated that the long source duration and "landslide" character of the events were consistent throughout the dataset. They also found that the forces active at the earthquake source were predominantly aligned parallel or anti-parallel to glacier flow. Like previous authors [*Ekström et al.*, 2003, 2006], *Tsai and Ekström* [2007] hypothesized that the seismicity resulted from sudden acceleration of a large ice mass at the source glaciers.

The available data did not allow independent determination of the size of the accelerating mass and the distance over which it accelerated, and glacial earthquakes were initially believed to result from sudden sliding of large ($\sim$10 km^3) portions of the glacier trunk over distances of 1–10 m [*Ekström et al.*, 2003, 2006]. A similar phenomenon has since been observed in association with smaller earthquakes at Whillans Ice Stream in Antarctica [*Wiens et al.*, 2008], but recent studies

of individual glaciers have now shown that this mechanism is likely not the cause of the glacial earthquakes observed in Greenland [e.g., *Joughin et al.*, 2008a; *Nettles et al.*, 2008a; *Amundson et al.*, 2008; *Nettles and Ekström*, 2010]. These studies showed that glacial earthquakes are temporally associated with large calving events at the source glaciers, and that no stick-slip sliding of the glacier occurs during the earthquakes. Rather, glacial earthquakes are now understood to result from the capsizing of newly calved icebergs of cubic-km scale, which transfer momentum to the solid earth as their centers of mass accelerate away from the calving front over a distance of 100 m or more. These icebergs typically represent calving through the entire thickness of the glacier, with an along-flow extent of a few hundred meters and a cross-flow extent of several kilometers. Previous authors [*Amundson et al.*, 2008; *Nettles et al.*, 2008a; *Nettles and Ekström*, 2010] have also shown that glacier behaviour during glacial earthquakes is consistent with seismogenesis at the calving front, and *Tsai et al.* [2008] demonstrated that such a mechanism is physically feasible. In addition, variations in the frequency of earthquake occurrence have been linked to variations in the rate of calving-front retreat on both seasonal [*Joughin et al.*, 2008a] and multi-year time scales [*Nettles and Ekström*, 2010].

Much remains unknown about glacial earthquakes, and no systematic study of the earthquakes occurring in Greenland has been undertaken for events after 2005, or in light of the recently developed understanding of the connection between glacial earthquakes and calving processes. Although it has been suggested [*Joughin et al.*, 2008a; *Nettles and Ekström*, 2010] that glacial earthquakes only occur when the calving front is grounded or near grounded, this hypothesis has been based on very limited data, and controls on the occurrence of glacial earthquakes are not well understood. Similarly, the relationship of the earthquakes to other observable changes in the Greenland Ice Sheet has only been documented in a few cases. The glacial-earthquake dataset is limited, with source-parameter solutions currently available only for the period 1993–2005, for the 184 earthquakes studied by *Tsai and Ekström* [2007]. In contrast, the Global CMT project [*Ekström et al.*, 2012] typically publishes $\sim$150 focal-mechanism solutions for tectonic earthquakes each month. An expanded catalog of glacial earthquakes would offer greater insight into their oc-

currence and their link to ice dynamics, and increase the utility of glacial earthquakes as a tool for remote monitoring of the Greenland Ice Sheet.

In this study, we model waveforms for 121 glacial earthquakes occurring in Greenland from 2006–2010 to obtain centroid–single-force source parameters and improved locations, in a manner consistent with the approach of *Tsai and Ekström* [2007]. This allows us to expand the record of well-documented and characterized glacial earthquakes by 65%. We use these results together with the previously published event solutions of *Tsai and Ekström* [2007] to evaluate the extent to which the full glacial-earthquake dataset is consistent with the iceberg-capsize model of glacial-earthquake seismogenesis. We address controls on glacial-earthquake occurrence, including the grounding state of the calving front. Finally, we examine regional and local trends in the occurrence and location of glacial earthquakes in Greenland in the context of ongoing changes in the Greenland Ice Sheet.

2.3 Data & Methods

2.3.1 Event Detection

Because glacial earthquakes have unusually long source durations, the seismograms they generate are depleted in high-frequency energy and lack globally detectable short-period body waves [*Ekström et al.*, 2003]. Teleseismic earthquake monitoring normally relies on the identification of short-period body waves, and glacial earthquakes are not identified by standard earthquake-detection algorithms. However, glacial earthquakes can be detected using surface waves in the manner described by *Ekström et al.* [2003] and *Ekström* [2006].

Intermediate-period (35–150 s) Rayleigh waves recorded at stations of the Global Seismographic Network (GSN) are back-projected to possible earthquake source locations on a global grid of $4^\circ \times 4^\circ$ spacing by deconvolution of a surface-wave propagation operator. Envelope functions for each record are calculated, and detections are identified using a matched-filter approach. Grid points at which a sufficient number of records indicate the presence of an event are identified

as potential earthquake detections. The grid is then further refined, eventually giving a resolution of 0.5° for epicenter locations. The long wavelength of the surface waves used (e.g., ∼200 km for a 50 s Rayleigh wave) and the lack of phase information in the envelope functions result in location uncertainties for these detections that are relatively large (50–80 km).

The surface-wave detection algorithm of *Ekström* [2006] has now been applied to broadband seismic records from the Global Seismographic Network for the period 2006–2010. We use the resulting catalog of event detections (Figure 2.1 and Table 2.1) to provide initial event locations and times for our waveform analysis. For events in 2006–2008, we adopt the published catalog of *Nettles and Ekström* [2010]. The data processing approach used in that study was designed for consistency with the previously published results of *Ekström et al.* [2006]; data for 2009–2010 have been processed in the same way. This consistency allows for direct comparison of event numbers between years, and we refer to events identified in this way as 'standard' detections. For 2009–2010, we also attempt waveform analyses for events identified by a version of the detection algorithm operating in near-real time and using a dataset including a number of additional seismometers in or near Greenland. This results in the identification of several additional events, which we refer to as 'NRT' detections. Additionally, we include two standard detections from 2009 that are of lower quality than those considered in previous studies. The full dataset thus provides times and initial locations for a total of 121 events in Greenland during 2006–2010: 111 standard detections (109 of them high-quality detections) and 10 NRT detections. We present waveform-modeling solutions for all events, but in our analyses of spatio-temporal variations we consider only the standard, high-quality detections in order to to maintain consistency with previously published data from earlier years. For all events, we use the detection locations (shown in Figure 2.1A) and times as inputs for waveform modelling to determine centroid–single-force parameters, including improved locations.

2.3.2 Waveform Inversion

We use a centroid–single-force (CSF) approach to invert seismic waveforms for earthquake source characteristics, including more accurate event locations. This process allows for the inclusion of phase information and manual removal of noisy or bad records. Previous studies [*Ekström et al.*, 2003; *Tsai and Ekström*, 2007] have shown that waveform inversion using a centroid–moment-tensor (CMT) approach [*Dziewonski et al.*, 1981], appropriate for elastic faulting, leads to solutions with a poor fit to the data, while inversions using a momentum transfer or "landslide" model of source physics and the CSF approach [*Kawakatsu*, 1989] reproduce the observed waveforms well. The model parameters determined using the CSF approach are the earthquake centroid location and depth, a time shift of the source centroid from the original detection time, and a three-dimensional vector describing the active force. The CSF amplitude M_{CSF}, a product of mass and distance, is derived by twice integrating the force-time history [*Kawakatsu*, 1989], and is a quantity analogous to the seismic scalar moment. A standard CMT model provides centroid location and depth, time shift, and the six components of the moment tensor, from which the seismic scalar moment is also derived. The improved fit from CSF modelling compared to CMT modelling for glacial earthquakes comes despite a reduction in free parameters, suggesting that the source process represented by the CSF model provides a more appropriate representation of the source physics.

We perform full-waveform inversions using the CSF approach for events initially identified by surface-wave detection, as described in Section 2.1. Our approach follows closely that used for standard CMT analysis by the Global CMT project [*Dziewonski et al.*, 1981; *Ekström et al.*, 2005], with the exception that we invert for CSF rather than CMT parameters. We interactively select records of intermediate-period surface waves in the period band 40–150 s. Records are selected from vertical and horizontal components of stations of the IRIS-USGS GSN, Geoscope, Geofon, and Canadian National seismograph networks located at less than $\sim$110° epicentral distance. Stations are generally well distributed azimuthally. We evaluate the quality of our solutions based on their stability over multiple inversions and the misfit between predicted and observed waveforms,

as for standard CMT solutions [*Ekström et al.*, 2012].

Glacial earthquakes occur at the Earth's surface, but the surface waves we use as data constraints have weak sensitivity to the depth of shallow sources. We calculate excitation functions in the Preliminary Reference Earth Model (PREM) [*Dziewonski and Anderson*, 1981], and the excitation changes little within the PREM upper crust. *Tsai and Ekström* [2007] found that CSF solutions for glacial earthquakes showed little variation when modelled at depths of 3–15 km. Our experience is consistent with this result, and we fix the source depths for the glacial earthquakes at 10 km.

The CSF approach we use also requires us to specify the shape of the force time history (source time function) for each event, similar to the moment-rate function that must be specified for CMT inversion. We choose the time function in a manner consistent with that of *Tsai and Ekström* [2007] so that our results may be directly compared. Because our analysis relies on surface waves at periods near the event source duration, the model source spectrum is sensitive to changes in the source time function, making such consistency important for comparison of CSF amplitudes. *Tsai and Ekström* [2007] used a boxcar source time function with a total duration of 50 s, representing a constant force acting in one direction for 25 s followed by an equal-amplitude force acting in the opposite direction for the following 25 s. We use these same inputs for our waveform inversions to maintain consistency throughout the glacial-earthquake catalog.

2.4 Results

We obtain satisfactory inversion results for all 121 glacial earthquakes identified by global surface-wave detection. Source parameters for the events are listed in Table 2.1 and the improved locations determined by waveform modelling are shown in Figure 2.1B. (Complete source parameters are also available online in electronic format on our website, http://www.globalcmt.org/ .) Waveform modelling improves the accuracy of the earthquake locations and collapses the previously scattered event locations into tight clusters along the Greenland coast at the locations of large

outlet glaciers. Nearly all of the earthquakes occur in the same source regions identified by *Tsai and Ekström* [2007]. However, we observe two events in regions not previously known to produce glacial earthquakes: a standard detection near Rolige Bræ in Scoresby Sound, and an NRT detection in Southeast Greenland between Hornemann Island and the mouth of Sermilik Fjord.

Realistic assessments of the uncertainty in glacial-earthquake locations derived from CSF analysis have previously been hampered by a lack of knowledge of the true source location and limited knowledge of the sources of noise and bias contributing to the true errors. Better knowledge of the glacial-earthquake source process and a larger sample of events allow us to assess both absolute and relative location errors here. *Smith and Ekström* [1997] studied the combined errors in hypocentral and CMT centroid locations for tectonic earthquakes, and found that errors of $\sim$25 km were typical. Because of the similarity in the CMT and CSF approaches, *Tsai and Ekström* [2007] adopted 25 km as an approximate estimate of the likely error in the CSF centroid locations. Nearly all of the events examined by *Smith and Ekström* [1997] were larger than those considered here, and we might expect larger errors for our smaller events; however, the CMT analyses in the *Smith and Ekström* [1997] study did not include the intermediate-period surface-wave constraints that both we and *Tsai and Ekström* [2007] employ, and which are likely to improve the location estimates.

Under the assumption that all of the glacial earthquakes occur at glacier calving fronts, we use the published estimates of ice-front location of *Joughin et al.* [2008a], combined with the estimated earthquake centroids, to evaluate the absolute errors in our earthquake location estimates. *Joughin et al.* [2008a] used MODIS satellite imagery and an edge-detection algorithm, followed by visual verification, to map the locations of the calving fronts of Helheim and Kangerdlugssuaq glaciers as a function of time during 2001–2006. They obtained near-daily estimates from mid-April through early October each year, with less frequent estimates earlier and later in the year. Errors in the ice-front location estimates, which are measured near the center of the fjord, are on the order of the 250-m pixel size of the imagery. These errors are much smaller than the estimated errors in the earthquake centroid locations, as indeed are the total changes in calving-front location during any single season (typically 2–4 km), and we neglect these errors in our

analysis, considering the measured ice-front locations at the times of the earthquakes to represent the true earthquake locations. We combine the results of *Tsai and Ekström* [2007] for 2001–2005 with our results from 2006 at these glaciers, and calculate the distance between the earthquakes and the ice-front locations reported closest in time to each earthquake. Varying the maximum time separation allowed between the earthquake and ice-front estimates changes the results very little, both because the changes in ice-front positions are small compared to the earthquake location errors and because, for most earthquakes, ice-front locations within a few days are available. We are able to make ice-front–earthquake comparisons for 65 events in 2001–2006 at the two glaciers considered. We find a median earthquake mislocation of 12 km and a mean of 15 km, and that 90% of the earthquake locations lie within 24 km of the ice front and 95% within 35 km. The sources of error in the location estimates are unlikely to vary significantly across Greenland, and we believe these estimates of location accuracy can be applied to the full dataset of Greenland glacial earthquakes analyzed here, and previously by *Tsai and Ekström* [2007]. Our results also suggest that, although the glacial earthquakes are small in comparison with the tectonic events studied by *Smith and Ekström* [1997], the inclusion of intermediate-period surface waves in the analysis allows us to achieve similar or slightly better absolute location accuracy.

At many glaciers, the distribution of event locations is asymmetric, with the location distribution elongated approximately along the glacier-flow direction. This is evident in Figure 2.2, which shows glacial earthquakes at three of the most active glaciers in Greenland: Helheim Glacier, Kangerdlugssuaq Glacier, and Kong Oscar Glacier. These glaciers have produced sufficient numbers of events to allow meaningful analysis of patterns in the event locations. We calculate the directions of minimum and maximum variance in the distribution of event locations for each glacier, and fit a Gaussian function to the distribution projected onto each direction. We then calculate the standard deviation in the location distribution in each direction. The standard deviations (σ) in the direction of minimum variance range from $\sim$4.5 km at Kong Oscar to $\sim$7.0 km at Helheim, and in the direction of maximum variance σ ranges from $\sim$8.0 km at Kong Oscar to $\sim$10.0 km at Kangerdlugssuaq. If all of the earthquakes at a given glacier occurred at the same location, the

variance in the event distribution could be taken as a measure of relative location error. The true event locations are unlikely to be identical, in which case the variances we calculate will overestimate the relative location error. Indeed, we find that the direction of maximum variance in the distribution of event locations corresponds to an azimuth subparallel to the fjord walls near the terminus of each glacier as measured from satellite imagery, suggesting a contribution to the variance from motion of the calving front, as described further in section 4. With or without this additional variance, we conclude that the relative location error is smaller than the absolute location error.

The improved accuracy of the earthquake locations we obtain, as well as the clustering of events, allows us to associate each glacial earthquake with a specific glacier with a high degree of confidence. As illustrated in Figure 2.1, it would be difficult to associate many events with a specific source glacier using the initial detection locations. This is particularly true for events located in Northwest Greenland and central East Greenland. In Northwest Greenland, locations derived from surface-wave detection are scattered, and outlet glaciers are closely spaced. In central East Greenland detection locations often lie roughly equidistant from Kangerdlugssuaq Glacier, several glaciers that terminate in Scoresby Sound, and glaciers associated with the Geikie Plateau. In both regions, locations derived from full-waveform inversion are sometimes more than 100 km from the surface-wave-detection locations, and the events are not always found to be associated with the glacier nearest the surface-wave detection location. In most cases, full-waveform inversion provides locations that are sufficiently accurate to eliminate ambiguity as to the source glacier for each event, and we indicate with which glacier we have associated each event in Table 2.1.

Consistent with previous studies, we find that the force vectors for the glacial earthquakes are generally oriented in the glacier-flow direction, perpendicular to the calving front, as illustrated in Figure 2.2 for three very active glaciers. Similar to the results of *Tsai and Ekström* [2007], our solutions show force vectors that are both anti-parallel and parallel to glacier flow. While we report the best-fitting solution for each event, in many cases there also exists a similarly fit solution with a force vector rotated $\sim$180° in azimuth. These secondary solutions show only very small location shifts, but are shifted by $\sim$25 s in time. The combination of the source phase shift and the time

shift results in nearly the same predicted surface-wave phase at the receiver for both solutions at the dominant surface-wave period of $\sim$50 s. Because the difference in the misfit between the two solutions is small, we consider there to be a 180° ambiguity in force direction in our results. We also find that the force vectors are close to horizontal, with a mean plunge angle of less than 10°.

The CSF amplitudes we derive lie between 0.1×10^{14} kg-m and 1.1×10^{14} kg-m, with a median value of 3.5×10^{13} kg-m. This is similar to the amplitudes obtained by *Tsai and Ekström* [2007], with the exception that those authors observed a small number of larger events, with magnitudes in the range 1.1×10^{14} kg-m to 2.0×10^{14} kg-m. As described in Section 2, the amplitudes we obtain are sensitive to the choice of source duration, because the source duration is similar to the shortest-period data included in our analysis. We tested the effect of variations in the chosen source duration by performing additional inversions using a source model with durations 20% shorter (40 s) and 20% longer (60 s) than the 50 s duration used for our final solutions. We find that a 20% decrease in the source duration reduces the CSF amplitude of the glacial earthquakes by $\sim$20%, while a 20% increase in modelled source duration results in an increase in the CSF amplitudes of $\sim$30%. The remaining source parameters and the fit to the data are affected very little by the change in source duration. Like *Tsai and Ekström* [2007], we conclude that a duration of 50 s is appropriate as a general model for glacial earthquakes in Greenland, though individual events may be better explained by shorter or longer durations. Obtaining more detailed constraints on the force time history of glacial earthquakes will likely require the use of recordings at regional distances, where the weak higher-frequency signals will be of higher amplitude.

2.5 Discussion

Previous systematic studies of glacial earthquakes in Greenland [*Tsai and Ekström*, 2007] were made under the operating hypothesis that the earthquakes were caused by sudden sliding of the glacier trunk. More recent studies demonstrating that the toppling and seaward acceleration of newly calved icebergs provides a more likely explanation for the observed seismicity have fo-

cused on small numbers of glacial earthquakes at a handful of individual glaciers [e.g., *Amundson et al.*, 2008; *Joughin et al.*, 2008a; *Nettles et al.*, 2008a]. An initial re-examination of patterns of glacial-earthquake occurrence over time [*Nettles and Ekström*, 2010] supported the iceberg-calving hypothesis, but only employed a full set of glacial-earthquake source parameters through 2005. Here, we combine the 121 source-parameter solutions presented in Section 3 (Table 2.1) with the 184 solutions of *Tsai and Ekström* [2007] to assess the consistency of this larger dataset with the iceberg-calving model. We then examine spatial and temporal patterns of glacial-earthquake occurrence throughout Greenland, and compare observed spatio-temporal patterns to changes observed by satellite remote sensing at several glaciers of particular interest.

2.5.1 Glacial Earthquake Source Characteristics

Current models suggest that glacial earthquakes in Greenland occur at the calving fronts of large marine-terminating glaciers during large calving events [*Nettles et al.*, 2008a; *Joughin et al.*, 2008a; *Amundson et al.*, 2008; *Tsai et al.*, 2008; *Nettles and Ekström*, 2010]. During seismogenic calving events, icebergs the full thickness of the glacier detach from the calving front and overturn due to gravitational instability. Since the iceberg is held against the calving front by resistance from water and floating ice in the fjord, the system is well coupled to the solid earth as the iceberg capsizes. The forces exerted on the calving front by the overturning block are opposite to the motion of the iceberg's center of mass and are roughly perpendicular to the calving front, oriented inland, and approximately horizontal to the surface of the earth. We find that the locations and source parameters for the 1993–2010 glacial-earthquake dataset are consistent with this model.

We observe that the locations of glacial earthquakes throughout Greenland are consistent with earthquake occurrence at glacier calving fronts. Nearly all earthquakes are located within $\sim$35 km of the ice margin, similar to the absolute location uncertainty estimated with and without the assumption that the earthquakes occur at a calving front. As described in Section 3, the distribution of glacial-earthquake locations is asymmetric, with the direction of maximum location variance corresponding to a direction approximately perpendicular to the calving front. That is, scatter in

glacial-earthquake locations is narrowest across each glacier's width, and elongated perpendicular to the glacier calving front. *Tsai and Ekström* [2007] made a similar observation at Kangerdlugssuaq Glacier and, using the now-discarded bed-sliding model, attributed this distribution to event occurrence at different points along the glacier. We interpret the elongation in the glacier-flow direction as resulting from variations in the calving-front location over time.

At the three glaciers with the largest numbers of events recorded — Kangerdlugssuaq Glacier, Helheim Glacier, and Kong Oscar Glacier — we observe that the difference in scatter between the along-flow and cross-flow directions is similar to the amplitude of observed variations in the locations of the glacier calving fronts (3–5 km) over the 18 years considered. In addition, the geometry of changes in mean earthquake location is similar to the change in the calving-front location over time. This correspondence is shown for Helheim Glacier in Figure 2.3, where we compare the mean event locations in three year intervals to the mean late-summer calving-front locations over the same intervals. To determine the late-summer-average front location, we digitized Landsat 7 images taken in early August of each year, and recorded the position of the glacier midway across the fjord. We then averaged these locations in 3-year bins. While the average earthquake locations are offset somewhat from the calving front due to absolute location errors, they show a similar variation in location in both amplitude and direction. Kangerdlugssuaq Glacier and Kong Oscar Glacier show similar trends, and we infer that the greater scatter in locations perpendicular to the glacier calving fronts is related to variation in the location of the calving front over time.

Previous workers [*Ekström et al.*, 2003; *Tsai and Ekström*, 2007] interpreted the orientation of the force vectors to result from sliding at the glacier bed in the glacier flow direction. In contrast, we interpret the orientation of the forces to result from the direction of motion of icebergs as they capsize. As predicted by the iceberg-calving model, most force directions in the 18-year dataset are perpendicular to the calving fronts of the source glaciers. We observe events showing inland-"uphill" and seaward-"downhill" orientations in near-equal numbers. As discussed earlier, we believe this result can be explained by the surface-wave radiation patterns of CSF events, and the spectra of these events, as the data are also fit reasonably well by a solution with the opposite force

direction, shifted $\sim$25 seconds in time. A very small number of earthquakes show force directions rotated $\sim$90° with respect to the calving front (a handful of these events can be seen in Figure 2.2), possibly as the result of complex calving geometry. *Chen et al.* [2011] also detected a small number of glacial-seismic events in Antarctica that share this peculiar geometry, with an unknown physical mechanism. While we believe these events warrant future study, the overwhelming majority of glacial earthquakes show force directions consistent with the iceberg-calving model.

The CSF amplitudes we obtain for the glacial earthquakes are also consistent with the calving model, in which the size of an earthquake must be limited by glacier geometry. Figure 2.4 shows size-frequency distributions for Kangerdlugssuaq Glacier, Helheim Glacier, and the complete glacial-earthquake catalog. The distribution of sizes for glacial earthquakes contrasts strongly with that for tectonic earthquakes, which range in size over more than 10 orders of magnitude and for which the number of earthquakes typically increases by a factor of ten for each one-unit decrease in magnitude [e.g., *Gutenberg and Richter*, 1944; *Ekström et al.*, 2012]. For glacial earthquakes, the range of observed sizes is small, approximately one order of magnitude. For each region, the size distributions show a peak with a rapid decline at larger and smaller sizes. The peak occurs at different sizes in different regions: at Kangerdlugssuaq, the peak occurrence is at 0.7×10^{14} kg-m, while Helheim and the complete catalog are both peaked at a value half as large, 0.3×10^{14} kg-m. The distribution is wider at Kangerdlugssuaq than at Helheim, with a slower fall off towards smaller and larger sizes. These two large glaciers influence the shape of the Greenland-wide distribution, but this distribution retains a similar shape when they are removed. The general shape of the distributions and the range of sizes observed remain very similar to those from the *Tsai and Ekström* [2007] dataset, despite a near doubling in the number of events. The shape of the size-frequency distributions for glacial-earthquakes is likely to reflect a combination of physical bounds on earthquake size and, at the lower end, limitations on detection. Both the differences in the size distribution between glaciers and the fact that the distributions are peaked well above the detection threshold suggest that the decrease in numbers of events at smaller sizes results in part from a true paucity of smaller events, rather than just from the difficulty of detecting smaller

events.

We hypothesize that each glacier will possess a size-frequency distribution with a characteristic shape and peak dependent on its size and geometry, but that the overall variation in these distributions will remain small owing to the limited range of sizes of glaciers producing glacial earthquakes. In order to produce a glacial earthquake, we expect that the calved block must remain substantially intact as it capsizes, in which case, the strength of glacial ice will impose a limit on the minimum size of seismogenic blocks. The upper limit of glacial-earthquake size is likely to be a function of glacier thickness and width, with thicker glaciers producing larger earthquakes [e.g., *Nettles and Ekström*, 2010; *Burton et al.*, 2012]. The glacier thickness controls the along-flow width of seismogenic blocks, because the tendency to capsize depends on the aspect ratio of the block. Blocks that are larger than $\sim$80% of the glacier thickness in the along-flow direction are unlikely to capsize [*MacAyeal et al.*, 2003], though the presence of ice mélange may modify the aspect ratio at which capsize is most likely to occur [*Amundson et al.*, 2010]. The glacier thickness and width are also likely to control the cross-flow dimension of the calved block, which can in any case not exceed the glacier width. The exact relationship between block mass and glacial-earthquake size is unknown, and is likely to depend on additional factors, including hydrodynamic controls [e.g., *Amundson et al.*, 2012]. However, glacier geometry provides a simple and plausible explanation for the small range of observed earthquake sizes, the variation in event sizes between glaciers, and the small sizes of the largest earthquakes observed. Such geometrical control is also consistent with the occurrence of larger earthquakes at Kangerdlugssuaq Glacier than Helheim Glacier, but better information about bed topography at multiple glaciers is required to assess our hypothesis quantitatively.

2.5.2 Spatial and Temporal Changes in Event Distribution

Combining our results for 2006–2010 with those of *Tsai and Ekström* [2007] for 1993–2005 allows us to assess spatial and temporal variability in glacial-earthquake production over an 18-year period, and to compare these changes with other observations of changes in glacier behaviour.

In this section, we provide a brief description of the spatio-temporal patterns we find in the 18-year combined catalog, and in the following section address links to glacier dynamics. We include only those earthquakes from our study (109 events) that were detected in a manner consistent with earlier studies. *Ekström et al.* [2006] demonstrated the lack of a temporal or seasonal trend in the event-detection threshold for earthquakes in 1993–2005, for the same detection procedures we use here. The global seismic network configuration was stable over the period 2005-2010, and we have confirmed that the detection threshold also has remained stable. We are thus able to assess trends over 18 years of glacial-earthquake production, with a total of 293 events. The number of earthquakes occurring in each year is shown in Figure 2.5. Previous studies noted an increase in the number of glacial earthquakes occurring Greenland-wide during the years 1993–2005, peaking at 30 events in 2005 [*Ekström et al.*, 2006]. Since 2005, glacial earthquakes have continued to occur at a high rate, but below this peak level. Earthquake production in 2006–2010 was similar to that in 2003–2004, with the mean annual number of glacial earthquakes during this period more than double that in 1993–2000.

Glacial-earthquake occurrence is also shown for East and West Greenland separately in Figure 2.5. From 1993 to 1999 glacial-earthquake production in both East and West Greenland was low and variable, but with East Greenland producing significantly more glacial earthquakes annually than West Greenland. From 2000 to 2005, trends in earthquake production in East and West Greenland were similar, with annual production increasing rapidly. Both coasts contributed roughly equally to the inter-annual Greenland-wide increases seen during that time, though the fractional increase was greater in West Greenland than East Greenland owing to the former's lower average rate of production prior to 2000. Since 2006 East Greenland and West Greenland have shown different trends.

2.5.2.1 East Greenland

East Greenland produced 6–10 glacial earthquakes per year from 1993–1999, increasing rapidly to a peak of 21 in 2005 (Figure 2.5). A decline of nearly 60% then occurred from 2005 to 2006.

Throughout the entire dataset, glacial-earthquake production in East Greenland has been restricted to a small number of glaciers, with Helheim Glacier and Kangerdlugssuaq Glacier being the most important glacial-earthquake producers in the region (Figure 2.6). Changes in annual numbers of glacial earthquakes in East Greenland are primarily driven by changes at these two glaciers, and the drop after 2005 mainly reflects decreases in glacial-earthquake activity at Helheim and Kangerdlugssuaq. After 2005 we observe a cessation of glacial-earthquake production at Daugaard Jensen Glacier, but this glacier has never produced more than two glacial earthquakes in a single year. We also observe a single glacial earthquake at previously inactive Rolige Bræ. These changes are minor, and did not strongly affect overall glacial-earthquake production in East Greenland. Since 2006 production has been variable, but remains elevated when compared to pre-2000 rates. Kangerdlugssuaq Glacier has shown relatively steady production inter-annually since 2006, while Helheim Glacier has shown large inter-annual changes, leading to the overall variability in annual production in East Greenland since 2006.

2.5.2.2 West Greenland

In West Greenland, glacial-earthquake production was minimal prior to 2000, with only four events recorded prior to 1998 (Figure 2.5). From 2000–2004, production increased steadily, reaching 12 events in 2004 followed by a small decrease in 2005. This period coincides with the Greenland-wide increase in glacial earthquakes. After 2005, in contrast with the sharp decline seen in East Greenland, glacial-earthquake production in West Greenland remained high and continued to show increases following 2005, reaching a peak of 14 in 2010.

The continued increase in West Greenland glacial earthquakes is accompanied by a change in spatial distribution. Prior to 2000, the majority of glacial earthquakes in West Greenland occurred at Jakobshavn Isbræ (Figure 2.6). Jakobshavn is the largest outlet glacier in Greenland, and is responsible for the spike in glacial earthquakes observed in West Greenland during 1998 and 1999. However, during the Greenland-wide rapid increase recorded in 2000-2005, Jakobshavn Isbræ was conspicuously absent from the glacial-earthquake catalog (Figure 2.7, Figure 2.8). Even after

becoming active again in 2005, Jakobshavn accounted for only 28% of West Greenland glacial earthquakes from 2005–2010, contrasting sharply with the 65% of glacial earthquakes in West Greenland for which it accounted prior to 2000.

2.5.2.3 Spread of Glacial-Earthquake Production

Although the dominant source of glacial earthquakes in West Greenland prior to 2000 was Jakobshavn Isbræ, the source of the rapid increase and sustained high rate of glacial-earthquake production in West Greenland during 2000-2010 has been other, smaller, previously inactive glaciers in Northwest Greenland. These glaciers had no significant glacial-earthquake production prior to 2000, and accounted for only one glacial earthquake during the 1990s. Over the last decade, the number of glacial earthquakes at these glaciers has increased dramatically. From 2000–2010, 66 glacial earthquakes occurred at previously quiescent glaciers, representing $>$30% of all glacial-earthquake production since 2000, and $>$40% of glacial earthquakes since 2006. At least four glaciers have produced multiple events during multiple years; Kong Oscar Glacier alone, quiescent prior to 2002, accounts for 30 events from 2002–2010. The onset of glacial-earthquake production at these glaciers represents a major expansion in the number of glaciers producing glacial earthquakes and the geographic range of those glaciers.

We identify three distinct time periods in the glacial-earthquake catalog, characterized by different trends and distributions of production, as shown in Figure 2.6. The first, 1993–1999, is characterized by relatively steady rates of production Greenland wide, dominated by the influence of the three largest glaciers in Greenland, Kangerdlugssuaq, Helheim, and Jakobshavn. The second phase, 2000–2005, corresponds to the Greenland-wide increase in the annual occurrence of glacial earthquakes, showing marked increases in both the number and spatial extent of glacial earthquakes. During this period, glacial earthquakes began to spread into Northwest Greenland, and glaciers there to produce substantial numbers of glacial earthquakes (Figure 2.6). The third phase, lasting from 2006 to at least 2010, is defined by continued high rates of production from glaciers in West Greenland, with East Greenland producing approximately stable numbers of glacial earth-

quakes, but at a rate lower than that seen in 2003–2005. This phase shows the rise in importance of smaller glaciers in Northwest Greenland, and the decline in importance of the large glaciers in both West and East Greenland, with Helheim and Kangerdlugssuaq becoming less active and Jakobshavn Isbræ ceasing to dominate glacial-earthquake activity in West Greenland.

Within West Greenland, the pattern of glacial-earthquake occurrence also shows a northward expansion since 2000. Figure 2.7 shows the latitude of glacial earthquakes in West Greenland plotted versus the time of their occurrence, showing that the onset of glacial-earthquake production has proceeded rapidly northward since 1994. As the West Coast of Greenland is oriented nearly North/South, each horizontal line of events shown in this figure may be taken to represent an individual glacier. During the 2000s, after previous quiescence, multiple glaciers began and have maintained a multi-annual period of regular glacial-earthquake production. The current maximum latitude of observed glacial earthquakes is $\sim$78°N.

2.5.3 Link to Glacier Dynamic Behaviours

The source characteristics of the glacial earthquakes in our dataset, including locations, force directions, and size distributions, are consistent with a physical mechanism of capsize of thick, newly calved icebergs at glacier calving fronts. This interpretation suggests that earthquake production should increase when calving rates increase and glacier fronts retreat, either seasonally or inter-annually, and an initial assessment by *Nettles and Ekström* [2010] found that this relationship holds in at least a general sense. However, it has also been suggested [*Joughin et al.*, 2008a; *Nettles and Ekström*, 2010] that glacial earthquakes occur only when the calving front is near the grounding line. This may be the result of a change in calving style when the calving front is nearly grounded, such that most ice is lost by calving of narrow, gravitationally unstable icebergs, rather than wide, tabular icebergs. Such a change in calving style is often apparent in satellite imagery, an example of which is shown in Figure 2.9. Grounding or near grounding of the glacier calving front may also lead to better coupling to the solid earth, and thus more strongly observable seismic signals. *Amundson et al.* [2010] note, however, that calving fronts that are too strongly grounded are

unlikely to produce icebergs that represent the full thickness of the glacier. By 'grounded or near grounded' in our discussion here, we refer to the situation relevant for many marine-terminating glaciers in Greenland, in which at least several hundred meters of ice can achieve a floatation condition between calving events, but the calving front remains close to the grounding zone.

In several cases studied to date, at Jakobshavn Isbræ and Helheim Glacier [*Amundson et al.*, 2008; *Nettles et al.*, 2008a; *Nettles and Ekström*, 2010], an increase in glacier velocity has been observed to accompany seismogenic calving events. These increases are interpreted as the glacier's response to a decrease in resistive force when calving occurs. *Nettles et al.* [2008a] also observed an increase in the longitudinal strain rate associated with seismogenic calving. If these relationships are general, we expect to see increases in glacier velocity and glacier thinning accompanying increases in glacial-earthquake production. In this section, we compare patterns in the occurrence of glacial earthquakes with dynamic changes in Greenland's glaciers as observed by satellite and airborne remote sensing on a regional, and, in some cases, local, scale.

2.5.3.1 Greenland-Wide and Regional Changes

Greenland-wide, the overall increase in glacial earthquakes from 2000 onward corresponds to a large increase in the number of glaciers in multi-annual retreat [*Howat and Eddy*, 2011]. The increase in East Greenland earthquakes through 2005 coincides with the well-known retreats of Helheim Glacier and Kangerdlugssuaq Glacier [e.g., *Howat et al.*, 2005; *Joughin et al.*, 2008a]. The decrease in East Greenland glacial earthquakes after 2005 coincides with the stabilization, and in some cases, readvance of calving fronts in Southeast Greenland, as documented in surveys by *Moon and Joughin* [2008] and *Seale et al.* [2011]. A decrease in velocity and reduction in the rate of thinning was also observed at the Southeast Greenland glaciers at this time [*Murray et al.*, 2010].

The pattern of expansion of glacial-earthquake production into Northwest Greenland is also similar to trends seen in other observations. Northwest Greenland shows both the highest percentage of glaciers in retreat of any region in Greenland and the largest increase in the number of

glaciers in retreat after 2000 [*Howat and Eddy*, 2011], the same time during which we observe the spread of glacial earthquakes into this region (Figure 2.6). After 2006, the average rate of retreat of glaciers in Northwest Greenland was larger than that in other parts of Greenland, and did not show a reduction in 2006–2007 when compared to 2000–2006 [*Moon and Joughin*, 2008]. Of the glaciers in this region showing the most significant calving-front retreats [*Moon and Joughin*, 2008] and trunk acceleration [*Joughin et al.*, 2010], the majority were responsible for multiple glacial earthquakes.

Satellite gravimetry has also shown mass loss from the northwestern portion of the Greenland Ice Sheet during this time period. Northwest Greenland showed an average net positive change in mass over the 10 years prior to 2002, but a net mass loss from 2003–2005 and in later years [*Luthcke et al.*, 2006; *Wouters et al.*, 2008]. The onset time of this net mass loss is not well constrained, but satellite gravimetry and modelling of GPS-derived uplift data indicate a northward spread of mass loss into Northwest Greenland beginning around 2000 [*Jiang et al.*, 2010] and increasing around 2005 [*Khan et al.*, 2010].

2.5.3.2 Helheim Glacier

Helheim Glacier is one of the largest and fastest-flowing outlet glaciers in Greenland. It has seen significant changes over the last two decades and has been the subject of significant field and remote study since the mid 1990s. Glacial earthquakes have been studied more closely at Helheim than at any other glacier, and combined field and remote-sensing observations there, along with similar observations at Kangerdlugssuaq Glacier and Jakobshavn Isbræ, provide much of the observational basis for our current understanding of the glacial-earthquake seismic source and glacier response. Studies using satellite and time-lapse imagery, field observations, fjord water-pressure monitoring, and seismic and GPS data [*Joughin et al.*, 2008a; *Nettles et al.*, 2008a; *Nettles and Ekström*, 2010; *Hamilton et al.*, 2008] have demonstrated the coincidence of glacial earthquakes with large-scale calving events at Helheim during the summers of 2001–2008. Focused studies of individual earthquakes in 2007 and 2008 have also shown glacier acceleration coincident with

glacial earthquakes [*Nettles et al.*, 2008a,b]. Here, we examine earthquake and glacier behaviour on a broader time scale, over the full range of glacial-earthquake observations, from 1993–2010. Annual and seasonal patterns of glacial-earthquake production at Helheim are shown in Figure 2.8, with event locations shown in Figure 2.2. Helheim is responsible for a glacial earthquake in 1993, the first year of the combined catalog of *Tsai and Ekström* [2007] and this study. No further events occurred until 1996, when there were 5 earthquakes. Since 1996, Helheim has produced earthquakes annually, with 76 events in 1996–2010, for a mean of 5.1 earthquakes/year during that time. Except for 1996, seismicity at Helheim remained low, at 1–3 events yearly, through 2001. In 2002, the number of earthquakes began to increase, with 6, 4, 10, and 12 events in 2002-2005. Seismicity declined dramatically in 2006, to 1 event, and was variable in 2007–2010, ranging from 3–10 events each year.

Satellite observations show that the Helheim calving front advanced slightly between 1992 and 1995, then retreated in 1996, maintaining a similar minimum position until 2000, with seasonal oscillations of $\sim$2 km [*Luckman et al.*, 2006]. During 1993–1998, the Helheim region thinned somewhat [*Krabill et al.*, 1999]. Calving flux appears to have increased slightly in the mid- to late 1990s [*Andresen et al.*, 2012], and the glacier accelerated slightly from mid-1995 to 1997 [*Luckman et al.*, 2006]. The calving front also appears to have been grounded or near grounded in summer during the late 1990s, based on floatation levels and elevation profiles presented by *Howat et al.* [2005]. From 2001 to 2005, Helheim underwent significant retreat and thinning, as well as acceleration [*Howat et al.*, 2005; *Stearns and Hamilton*, 2007; *Joughin et al.*, 2008a], with the largest changes occurring in 2004–2005.

The increases in glacial-earthquake activity in 1996 and 2000–2005 coincide with the observed retreat and acceleration of the glacier at those times. During the 2004–05 retreat and acceleration of Helheim, this glacier was the largest producer of glacial earthquakes in Greenland. The precipitous decrease in glacial-earthquake production at Helheim in 2006 corresponds with a period during which the lowest few km of the glacier appear to have thinned sufficiently to become ungrounded [*Joughin et al.*, 2008a]. During 2006 calving at Helheim was observed [*Joughin et al.*, 2008a] to

be dominated by tabular icebergs >1 km wide (similar to the tabular icebergs shown in the top panel of Figure 2.9). Tabular icebergs do not capsize as they calve, and thus do not produce glacial earthquakes. During this time, GPS observations show a vertical tidal signal on the lower glacier [*de Juan et al.*, 2010], indicating that a short section of the glacier was indeed floating. The lone glacial earthquake recorded at Helheim in 2006 occurred in late August, when the calving front was closest to the grounding line. The increased earthquake production in 2007 at Helheim coincides with a small retreat and regrounding of the glacier; the glacier was also grounded in summer of 2008 [*de Juan et al.*, 2010], and the current authors' field observations suggest Helheim remained grounded in 2009 and 2010, consistent with ongoing glacial-earthquake activity in those years.

As shown in Figure 2.3, changes in earthquake locations over time at Helheim are consistent with the pattern of calving-front changes described above. We note here that force directions for glacial earthquakes at Helheim, in addition to being generally consistent with the orientation of the calving front, also show a gradual clockwise rotation since the late 1990s. This rotation is consistent with changes in the calving-front geometry over the same time period, as observed from late-summer Landsat imagery, suggesting a very close link between glacier and earthquake characteristics. However, more detailed comparisons will be needed to validate and interpret this observation.

2.5.3.3 Kangerdlugssuaq Glacier

Kangerdlugssuaq Glacier is the largest outlet glacier in East Greenland [*Rignot and Kanagaratnam*, 2006], and has produced a greater number of glacial earthquakes since 1993 than any other glacier. A close correspondence between large-scale calving events and glacial earthquakes at Kangerdlugssuaq during the summers of 2001–2006 was shown by *Joughin et al.* [2008a] and some characteristics of earthquake size and seasonality at this glacier were discussed by *Tsai and Ekström* [2007]. Kangerdlugssuaq Glacier has consistently generated multiple earthquakes every year since 1993 (Figure 2.8), for a total of 79 events and an average of 4.4 earthquakes/year. Locations of the earthquakes are shown in Figure 2.2. Variations in glacial-earthquake activity at Kangerd-

lugssuaq over the last 18 years are lower in amplitude than at the other glaciers discussed here, but we identify two periods of increased activity, one from 1995–1997, with 5.7 earthquakes/year, and another from 2003–2005, with 6.0 earthquakes/year. Three-year running averages otherwise range from 4.0–4.7 events/year in 1993–2002 and from 2.3–5.3 events/year in 2001–2010. Since 2005, Kangerdlugssuaq's annual rate of glacial-earthquake production has declined, to an average of 3.0 earthquakes/year during 2006–2010.

Altimetry observations at Kangerdlugssuaq Glacier showed large thinning between repeat measurements made in 1993 and 1998 [*Thomas et al.*, 2000]. Based on the low flow velocities they determined for 1995–96 and faster speeds in 1999, *Thomas et al.* [2000] concluded that the thinning began in or after 1995. *Luckman et al.* [2006] observed a 1–2 km advance of the calving front from 1992–1994, followed by a 2–3 km retreat in 1995–1997, at which time the glacier velocity also increased. By 2000, a pattern of seasonal advance and retreat of the calving front had established itself [*Seale et al.*, 2011], but the mean position remained nearly constant until 2004. During 2004–2005, the calving front retreated $\sim$5 km [*Luckman et al.*, 2006; *Seale et al.*, 2011]. The glacier flow speed also increased dramatically at this time [*Luckman et al.*, 2006; *Howat et al.*, 2007], and the lower reaches of the glacier thinned by $>$100 m compared with 2001 [*Howat et al.*, 2007; *Stearns and Hamilton*, 2007]. From 2006 onward, the mean annual position of the Kangerdlugssuaq calving front has been steady, at a position slightly advanced from the 2005 minimum but several km behind the pre-retreat position. Seasonal variation in the front position is of similar amplitude to that observed in the early 2000s [*Seale et al.*, 2011].

Although the changes in earthquake numbers are small, the increase in glacial earthquakes in 1995–1997 corresponds in time to the thinning, small front retreat, and acceleration observed by *Thomas et al.* [2000] and *Luckman et al.* [2006] at that time. The 2003–2005 increase in glacial-earthquake activity corresponds to the large-scale increases in velocity, thinning, and retreat observed then. The decrease in earthquakes in 2006–2010 compared with 2003–2005, returning the seismicity to levels slightly below that observed in the early 2000s, corresponds to the restabilization of front behaviour at Kangerdlugssuaq. We note also that the 1993–2010 earthquake

dataset shows the greatest frequency of earthquake occurrence at Kangerdlugssuaq in September–November, later than at other glaciers, as also observed by *Tsai and Ekström* [2007], but consistent with Kangerdlugssuaq's delayed seasonal retreat cycle [*Joughin et al.*, 2008a; *Nettles and Ekström*, 2010; *Seale et al.*, 2011].

2.5.3.4 Jakobshavn Isbræ

Jakobshavn Isbræ is the largest outlet glacier in Greenland, and one of the best-studied glaciers in the world. Seismic signals of a variety of types have been studied at Jakobshavn by multiple authors [e.g., *Ekström et al.*, 2003, 2006; *Amundson et al.*, 2008, 2010; *Tsai and Ekström*, 2007; *Rial et al.*, 2009; *Walter et al.*, 2012a]. Jakobshavn is one of the two field locations, together with Helheim Glacier, at which the correspondence of large-scale calving events and glacial earthquakes has been documented and the velocity response of the glacier demonstrated [*Amundson et al.*, 2008; *Nettles and Ekström*, 2010; *Walter et al.*, 2012a]. We restrict our attention here to the long-period glacial earthquakes analyzed throughout this study.

Jakobshavn has produced glacial earthquakes since 1998 (Figure 2.6, Figure 2.8), but production was sporadic prior to 2005. The first glacial earthquakes at Jakobshavn were observed during summer of 1998, when 6 events occurred. An additional 5 earthquakes occurred in summer of 1999. No further events occurred until 2005, when annual earthquake production commenced, with 1–2 earthquakes per year in 2005–2008, increasing to 6 and 4 events in 2009 and 2010.

Jakobshavn maintained a long, floating tongue for several decades prior to the mid-1990s, with relatively little inter-annual variation in the position of the ice front during that time [*Sohn et al.*, 1998]. The glacier thickened slightly from 1991–1997, then began a period of rapid thinning, retreat, and acceleration [e.g., *Thomas et al.*, 2003; *Joughin et al.*, 2004, 2008b]. *Tsai and Ekström* [2007] noted the correspondence of the 1998–1999 period of earthquake activity with a $\sim$4 km retreat of Jakobshavn's tongue [*Luckman and Murray*, 2005], and the beginning of a multi-year period of acceleration [e.g., *Joughin et al.*, 2004]. *Joughin et al.* [2008b] examined the correspondence between the 1998–99 events and glacier behaviour in more detail, pointing out that the 1998

earthquakes, which occurred in June and July, correspond very closely in time to the initial dramatic speedup at Jakobshavn, constrained by *Luckman and Murray* [2005] to the period between satellite images taken in May and August, 1998. During June and July, the glacier retreated $\sim$2 km to what was then a record-minimum position. *Joughin et al.* [2008b] note that the calving front was at this time close to the 'rumples', rifts associated with a pinning point likely due to bedrock highs on the north [*Thomas et al.*, 2003] and south [*Echelmeyer et al.*, 1991] sides of the fjord. The 1999 earthquakes occurred during a period (April–August) without good satellite coverage, but sometime between April 1999 and February 2000 the glacier speed again increased significantly [*Luckman and Murray*, 2005], suggesting that these earthquakes occurred under a similar set of circumstances to the 1998 glacial earthquakes. During both the 1998 and 1999 earthquake sequences, the glacier appears to have been partially grounded at the north and south sides. In 2000, the calving front retreated past this pinning point [*Joughin et al.*, 2004, 2008b; *Luckman and Murray*, 2005], and was again floating.

The disintegration of most of the remaining floating tongue occurred by 2003 [*Joughin et al.*, 2008b], at which time the glacier began a cycle of seasonal advance and retreat, with the minimum ice-front position typically reached in late August, and a short (6–8 km) floating tongue growing during the winter. *Dietrich et al.* [2007] observed vertical tidal motion close to the calving front in summer, 2004, with the calving front retreating behind their inferred grounding line in 2005. Earthquakes did not resume at Jakobshavn until 2005 (Figure 2.7), when the calving-front reached a new summer minimum position; summer calving fronts were then at or behind this position through 2010 [*Joughin et al.*, 2008b; *Seale et al.*, 2011; *Truffer et al.*, 2011]. The glacier appears to have been grounded in summer since 2005 [*Dietrich et al.*, 2007; *Amundson et al.*, 2008, 2010].

In 2005–2008, Jakobshavn averaged fewer than 2 earthquakes/year, with all events occurring during May–August, during the retreat phase of seasonal fluctuations in the calving-front position. In 2009, a marked increase to 6 earthquakes was seen, as the calving front again reached a record minimum position [e.g *Seale et al.*, 2011]. In 2010, for the first time, a glacial earthquake was recorded as early as February at Jakobshavn. This early onset of glacial earthquakes is consistent

with the observation that, although the glacier began to grow a floating tongue in the early winter of 2009, this tongue was lost following the resumption of calving activity in December, 2009 [*Truffer et al.*, 2011]. Retreat of the calving front to the grounding line thus occurred several months earlier than normal.

One of the 2009 earthquakes bears special mention, having been studied in detail by *Walter et al.* [2012a]. Two distinct calving events, and two corresponding earthquakes, occurred on August 21, 2009; we present results only for the first earthquake (event number 82 in Table 2.1). The second earthquake is visible in inspection of the back-projected seismograms used for event detection, but presents a much weaker signal than the first. We find an azimuth of 299° (or 119°, due to our 180° ambiguity), plunge of 11°, and CSF amplitude of 4.4×10^{13} kg-m; *Walter et al.* [2012a] find corresponding values of 149° (329°), 12°, and 1.2×10^{13} kg-m. The perpendicular to the calving front at the source location identified by Walter et al. (2012) was ∼303° (123°) prior to the calving events and ∼296° (116°) afterwards. We believe the two sets of seismological results to be in good agreement, particularly considering the different methodologies and datasets used for the two analyses.

Finally, we note that Jakobshavn provides a clear example of glacial earthquakes that are missed by the 'standard' detection procedure used here to provide consistency across the 18-year dataset, which relies on a particular baseline set of seismic networks. An additional four events were detected at Jakobshavn in 2010 by the near-real-time (NRT) version of the detector discussed in Section 2.1; these are clearly real earthquakes, not false detections, and waveform-modelling results for these events are included in Table 2.1, along with an additional lower-quality detection for 2009. The complexity of many events occurring at Jakobshavn (see also *Walter et al.* [2012a]) may contribute to difficulty of detection, but there is clearly room for improvement in identification of these events on a global and regional scale.

2.5.3.5 Kong Oscar Glacier

Kong Oscar Glacier began producing glacial earthquakes in 2002. Since that time 30 glacial earthquakes have occurred at Kong Oscar, with a peak of 6 during 2004 (Figure 2.2, Figure 2.8). Glacial-earthquake production has been fairly steady at ∼3–4 earthquakes/year since 2004, making Kong Oscar one of the most active producers of glacial earthquakes in recent years.

The calving front of Kong Oscar Glacier retreated ∼1.5 km between 1992 and 2000 [*Moon and Joughin*, 2008], with an additional retreat of more than 3 km from 2000–2008 [*Moon and Joughin*, 2008; *McFadden et al.*, 2011]. More than 1 km of this retreat occurred in 2002, with little change in 2003 and a return to retreat of several hundred meters per year in the following years [*McFadden et al.*, 2011]. The glacier thinned by 4–28 m/yr over this time [*McFadden et al.*, 2011], and accelerated by a small amount in the interval 2000–2005 [*Joughin et al.*, 2010]. A review of imagery obtained from the Landsat program shows a floating tongue prior to 2002. This tongue was heavily crevassed and fractured, lacking a distinct calving front and gradually becoming less and less consolidated as it progressed seaward, eventually separating into distinct tabular icebergs. These icebergs are readily identifiable in satellite imagery as large, intact blocks, whose surface maintains the textural characteristics of the intact glacier tongue (Figure 2.9, top), much like the tabular icebergs that calved from the floating terminus of Helheim Glacier in 2006 [*Joughin et al.*, 2008a]. The ice tongue at Kong Oscar Glacier disintegrated completely during the period 2001–2002, and the glacier had retreated to the mouth of its fjord by summer of 2003. From 2004 onwards, Kong Oscar shows a clearly delineated calving front, and the ice mélange is nearly devoid of large, upright icebergs, being dominated by smaller, overturned blocks and broken ice (Figure 2.9, bottom). These observations suggest a transition from a floating to a grounded or near-grounded terminus, with the transition beginning or occurring in 2002.

The onset of glacial-earthquake production at Kong Oscar Glacier in 2002 coincides with the transition from floating to grounded ice at the glacier terminus. The reason for the increase in glacial-earthquake production in 2004 is not obvious from the available data, but the calving front appears to be very close to the likely grounding line from this time onward. The steady rate of

continued earthquake production since 2004 is consistent with the grounded style of calving we infer from the Landsat imagery. As discussed in Section 3, a few earthquakes at Kong Oscar Glacier show unusual force directions (Figure 2.2), and these events are obvious targets for more detailed future study.

2.5.3.6 Alison Glacier

Alison Glacier lies at the southern end of Melville Bay. Over the last decade, Alison has nearly doubled its flow speed and has experienced one of the largest calving-front retreats in Greenland [*Moon and Joughin*, 2008; *Joughin et al.*, 2008a, 2010; *McFadden et al.*, 2011]. During this time, Alison Glacier produced 9 glacial earthquakes: the first 3 earthquakes were observed in 2003, 2005, and 2006, followed by 4 earthquakes in 2007 and 2 in 2008; no events were observed in 2009–2010.

Little change in ice-front position occurred at Alison Glacier between 1992 and 2000 [*Moon and Joughin*, 2008]. The work of *McFadden et al.* [2011] shows that Alison retreated $\sim$2 km from 2000 to late 2002, followed by $\sim$7 km of retreat from mid 2003 to early 2006. An additional $\sim$1 km of ice was lost between late summer 2006 and the beginning of 2007. From 2007–2009, the front was relatively stable, retreating a total of $\sim$0.5 km. The glacier flow speed increased fairly steadily from 2000–2005, to a level $\sim$80% higher than in 2000 [*McFadden et al.*, 2011]. The mean speed then appears to have leveled off, though with significant scatter possibly related to seasonal variability. We do not have good knowledge of the floatation level at Alison Glacier, but the elevation profiles of *McFadden et al.* [2011] show a transition from very low and flat ice near the calving front in 2002 and early 2003 to marginally higher-standing frontal ice in 2004–2005 and onwards. The front of the glacier stands particularly high in 2007, $\sim$90 m above sea level, suggesting the front is likely to have been grounded. Satellite imagery from 2007 also shows small, capsized icebergs in the fjord (Figure 2 of *Moon and Joughin* [2008]). By 2009, the ice surface had lowered by 20–30 m, and our inspection of Landsat imagery from summer 2009 shows an ice mélange dominated by tabular icebergs (similar to the top panel of Figure 2.9), suggesting a

floating front.

The earthquakes in 2003–2005 occurred during the glacier's most rapid retreat phase, but it is difficult to assess the level of grounding of any part of the front during this time, especially since the mapped calving fronts [*McFadden et al.*, 2011] suggest somewhat different behaviour on the north and south sides of the glacier. The 2006 earthquake, in December, coincides with the late retreat of the glacier that year. Most of the earthquakes observed at Alison occurred in 2007, when the glacier front appears to have been grounded based on both iceberg character and elevation profiles. The cessation of earthquakes in 2009 appears to correspond to a return to floatation at the glacier front.

2.5.3.7 Tracy Glacier

Tracy Glacier and its near neighbour Heilprin Glacier, which lies immediately to the south, terminate in Inglefield Bredning and together drain $\sim$10,000 km^2 of the Northern Greenland Icesheet [*Rignot and Kanagaratnam*, 2006]. Although the termini of these glaciers are separated by only 15 km, the geometry and location of the observed glacial earthquakes in this region suggest Tracy as the source. While not one of the most active producers of glacial earthquakes, Tracy Glacier is of interest due to its current position as the northernmost producer of glacial earthquakes, and the most recent glacier to become active in Northwest Greenland. Tracy began to produce glacial earthquakes in August of 2005 (Figure 2.8), and produced a single glacial earthquake annually through 2008, since which time it has not produced an observed glacial earthquake.

Tracy Glacier has been in recession for at least 90 years [*Dawes and van As*, 2010]. During much of this time it possessed a significant floating tongue, which extended beyond Tracy's fjord by several km and was also fed by additional glaciers to the north [*Kollmeyer*, 1980; *Dawes and van As*, 2010]. Based on observations made in 1968–1978, *Kollmeyer* [1980] describes calving at Tracy Glacier as producing "large flat icebergs", suggesting continued floatation. This mode of calving is seen as late as 2002, in a Landsat image captured in July of that year. By 2005, Landsat imagery shows that the calving front had retreated to the mouth of the fjord. In contrast

to the large tabular bergs observed in July of 2002, a June, 2005, image shows the waters beyond the calving front filled with small, overturned blocks. This change in calving mode from stable, tabular icebergs to unstable, capsized icebergs suggests that Tracy was grounded or near grounded at this time. Between 2000 and 2005, flow speeds at Tracy Glacier increased by 40% [*Rignot and Kanagaratnam*, 2006; *Joughin et al.*, 2010], and dynamic thinning was observed to elevations of at least 900 m [*Pritchard et al.*, 2009].

The change in calving style observed in 2005 and the inferred transition to a grounded or near-grounded calving front are consistent with the onset of glacial earthquakes in that year. The calving front remained at a similar position through at least 2009 [*Dawes and van As*, 2010], and earthquakes were produced in each year through 2008. The lack of earthquakes in 2009 and 2010 may indicate that the front of the glacier has thinned to floatation, as at Helheim in 2006, or may reflect the statistics of small numbers of glacial earthquakes at this glacier. Further knowledge of the evolution of Tracy Glacier, and further assessment of the seismic record, will be needed to evaluate the causes of the recent apparent cessation of glacial earthquakes after 2008.

2.5.3.8 Major Glaciers Not Producing Glacial Earthquakes

Using the combined catalog of *Tsai and Ekström* [2007] and this study, we have documented glacial earthquakes at more than 15 individual glaciers in Greenland. However, *Moon and Joughin* [2008] identified more than 200 outlet glaciers in Greenland with termini at least 2 km wide. Clearly, the majority of Greenland's outlet glaciers do not produce teleseismically observable glacial earthquakes. Many of these glaciers may simply not be thick enough to produce sufficiently massive icebergs to excite globally detectable seismic signals. As knowledge of bedrock topography increases across Greenland, we expect it will be possible to identify particular cases of geometrically similar glaciers that differ in earthquake productivity and to use these to improve our understanding of the conditions that are necessary for glacial earthquakes to occur. At some glaciers, glacial earthquakes may occur at sizes below our 'standard' detection threshold of M_{SW} $\sim$4.6, and regional observations will be required to identify these cases. At other glaciers, the

lack of glacial-earthquake activity is unlikely to be an artifact of our detection threshold, but rather the result of differing dynamic conditions. We observe no glacial earthquakes at land-terminating glaciers like those that dominate in southwest Greenland, consistent with our interpretation that the earthquakes result from calving of large icebergs. We also do not observe glacial earthquakes at some of Greenland's largest outlet glaciers, including Petermann Glacier, Nioghalvfjerdsbræ (79 North), and Zachariae Isstrøm, despite significant losses of ice at these glaciers in recent years [e.g., *Moon and Joughin*, 2008]. All of these glaciers still terminate in long, floating ice tongues or ice shelves [*Moon and Joughin*, 2008; *Thomas et al.*, 2009; *Rignot and Steffen*, 2008], and calve tabular icebergs far from the grounding line. The lack of glacial earthquakes at these large glaciers is thus also consistent with the collapsing-iceberg model of glacial-earthquake seismogenesis, and earthquakes are not expected to occur at these or similar glaciers unless the ice margin retreats to within a few km or less of the grounding line.

2.6 Conclusions

We obtained estimates of centroid–single-force source parameters for 121 glacial earthquakes occurring in Greenland during 2006–2010, extending the time span for which such estimates are available to 18 years (1993–2010) and expanding the total number of available solutions by 65%. These earthquakes include all of the events identified using the surface-wave detection approach of *Ekström* [2006], applied in a manner consistent with previous studies [*Ekström et al.*, 2003, 2006; *Tsai and Ekström*, 2007; *Nettles and Ekström*, 2010], as well as several additional events identified using the same detection procedure and data from additional seismic stations. An error assessment using satellite-remote-sensing data finds a median centroid mislocation of 12 km, with relative mislocation about half as large.

All of the detected events are explained well by centroid–single-force (CSF) solutions. We find that the improved locations, force-direction estimates, and earthquake size distributions we retrieve are consistent with an explanation of the earthquake source process in which large, newly calved

icebergs capsize against the calving front at marine-terminating outlet glaciers. We do not find any evidence for seismogenesis by basal sliding in this dataset, suggesting that the seismic amplitudes of any such events occurring in Greenland are likely to be smaller than M$\sim$4.5, consistent with the small sizes of basal-sliding seismic events observed in Antarctica (M_S 3.6–4.2; *Wiens et al.* [2008]).

Spatio-temporal patterns of glacial-earthquake occurrence in Greenland correlate well with independently observed changes in glacier dynamics, both at the regional scale and at individual glaciers. Where data quality and quantity are sufficient, we observe that glacial-earthquake locations track the motion of the ice front over time. Earthquake occurrence tends to increase during periods of rapid glacier retreat, and correlates with periods of glacier thinning and acceleration. Detailed examination of the earthquake-occurrence history at individual glaciers shows that earthquakes occur when the glacier calving front is at or very near the grounding line. This inference is also supported by the lack of glacial earthquakes at large glaciers draining into floating ice tongues or ice shelves, as in northern Greenland.

At the regional scale, we document the northward propagation of earthquake occurrence in western Greenland over the observational period, with many previously inactive glaciers beginning to generate glacial earthquakes between 2000 and 2005. Most of these glaciers have remained seismically active since the onset of glacial-earthquake production. Earlier workers found little change in flow speed at glaciers in northwest Greenland between 2000 and 2005 [*Rignot and Kanagaratnam*, 2006]; more recent work has identified changes in flow speed, thinning rates, and calving-front position during that time [*Moon and Joughin*, 2008; *Joughin et al.*, 2010; *Howat and Eddy*, 2011; *McFadden et al.*, 2011]. The onset of changes in ice-front position in the cases we have examined often precedes the onset of the glacial earthquakes, both seasonally and interannually; in some cases, the onset of glacier thinning and acceleration also precede the onset of earthquake occurrence. *Rignot and Kanagaratnam* [2006] noted that, although they did not find significant dynamic changes in the northwest Greenland glaciers, the mass balance for these glaciers was generally negative, and suggested that any related changes in ice dynamics must have occurred

decades earlier. The correspondence between glacial-earthquake occurrence and the calving of grounded ice leads us to suggest that, indeed, an important change in ice dynamics took place in northwest Greenland in the early 2000s, with many glaciers transitioning from floating to grounded termini.

Although much remains to be learned about the glacial-earthquake source process, analysis of these events provides information about glacier behavior and dynamics complementary to that obtained from other forms of remote sensing, including providing an additional means to assess the grounding state of the calving front. It is clear that patterns of glacial-earthquake occurrence respond to both local and regional-scale forcings, and further study combining seismological and glaciological observations will help to clarify additional controls on the generation of glacial earthquakes, providing both better tools for investigation of glacier dynamics and better explanations of a little-explored part of the seismic wavefield.

2.7 Acknowledgements

The GSN data analyzed in this study were collected and distributed by the Incorporated Research Institutions for Seismology (IRIS), the USGS, the CNSN, and the Geoscope, Geofon and Mednet projects; additional data were provided by the GLISN project and the Lamont Cooperative Seismographic Network. We thank I. Joughin for providing calving-front locations for Helheim and Kangerdlugssuaq Glaciers in digital form. We appreciate constructive comments from associate editor M. Truffer and reviewers D. Wiens, F. Walter, and J. Amundson, which improved the manuscript. This research was supported by NSF Grants ARC-07-13970 and EAR-09-44055.

2.8 Table

Table 2.1 Centroid–single-force solutions for 121 earthquakes of this study.

No.	Centroid Parameters											Scale Factor	M	CSF Vector					
	Date			Time			Latitude		Longitude										
	Y	M	D	h	m	sec	δt_0	λ	$\delta\lambda_0$	ϕ	$\delta\phi_0$	10^{ex}	CSF	V_r	V_θ	V_ϕ	pl.	azim.	reg.
1	2006	2	13	20	29	36.2±0.4	-15.8	68.76±.03	-1.49	-33.19±.05	-2.44	13	5.5	0.37±0.19	-5.35±0.20	-1.06±0.24	-4	349	1
2	2006	2	28	22	45	2.2±0.3	30.2	68.72±.02	-0.28	-33.19±.02	-0.19	13	5.6	0.64±0.15	-5.24±0.17	-1.80±0.19	-7	341	1
3	2006	3	4	23	5	33.5±0.4	13.5	65.28±.03	-0.47	-41.47±.04	-0.22	13	2.7	0.16±0.11	-1.84±0.14	-1.92±0.13	-3	314	3
4	2006	4	29	11	39	29.1±0.4	17.1	65.26±.00	0.01	-41.28±.01	-0.03	13	3.6	0.37±0.11	-2.26±0.19	-2.73±0.16	-6	310	3
5	2006	5	1	6	44	36.2±0.3	4.2	71.81±.02	-0.44	-51.98±.07	0.77	13	4.1	-1.35±0.14	1.78±0.16	-3.40±0.16	19	242	6
6	2006	6	24	10	48	28.3±0.4	-3.7	69.31±.01	0.06	-49.89±.04	-0.14	13	2.4	-0.63±0.08	-0.64±0.12	-2.21±0.10	15	286	7
7	2006	7	10	18	13	35.4±0.3	-0.6	65.32±.01	0.07	-41.27±.05	-0.52	13	3.6	-0.19±0.15	0.67±0.16	3.58±0.14	3	101	3
8	2006	7	16	3	15	45.4±0.5	17.4	68.75±.02	-0.25	-33.21±.11	-2.21	13	1.5	0.32±0.10	0.11±0.10	-1.43±0.09	-13	266	1
9	2006	7	16	6	42	11.4±0.4	19.4	71.86±.03	-1.39	-51.56±.09	1.69	13	2.5	-0.12±0.12	1.44±0.12	-2.03±0.11	3	235	6
10	2006	7	25	4	52	1.3±0.4	17.3	69.22±.02	0.47	-49.55±.08	0.20	13	3.0	-0.15±0.14	-1.05±0.13	-2.77±0.11	3	291	7
11	2006	8	10	18	45	32.0±0.4	12.0	77.49±.00	-0.01	-66.11±.07	-0.61	13	2.7	0.16±0.10	0.04±0.15	2.70±0.11	-3	91	4a
12	2006	8	23	17	19	31.2±0.4	3.2	66.48±.03	0.73	-38.19±.04	-0.44	13	3.2	-1.29±0.12	2.24±0.14	1.81±0.15	24	141	2
13	2006	8	28	7	55	0.3±0.4	-3.7	70.56±.03	1.06	-28.44±.07	-2.94	13	3.1	0.34±0.14	2.38±0.14	-1.96±0.16	-6	219	8
14	2006	9	10	4	19	23.0±0.4	-53.0	76.05±.03	-1.70	-59.78±.07	-2.53	13	7.2	-0.60±0.28	5.18±0.27	-4.91±0.31	5	223	4b
15	2006	10	9	4	3	27.5±0.5	15.5	76.07±.03	-0.43	-59.41±.10	1.09	13	3.7	-0.47±0.17	-2.56±0.16	2.66±0.19	7	46	4b
16	2006	10	14	7	23	15.5±0.4	-4.5	76.10±.01	0.10	-59.49±.11	-1.49	13	3.5	0.03±0.15	1.37±0.15	-3.19±0.15	0	247	4b
17	2006	11	5	9	13	3.5±0.5	-0.5	75.55±.02	-0.20	-58.11±.11	0.14	13	2.8	-0.26±0.15	1.20±0.18	-2.52±0.15	5	245	4c
18	2006	11	28	10	55	59.6±0.3	15.6	68.64±.01	-0.11	-33.12±.04	-0.37	13	5.8	1.62±0.19	-3.76±0.23	-4.04±0.24	-16	313	1
19	2006	12	19	16	57	43.6±0.6	-0.4	74.60±.01	-0.15	-56.39±.13	1.36	13	2.0	-0.78±0.12	0.85±0.16	-1.68±0.13	22	243	4e
20	2007	4	22	8	54	47.9±0.4	-16.1	66.31±.01	0.06	-38.09±.03	0.16	13	3.1	1.02±0.10	-1.46±0.15	-2.57±0.15	-19	300	2
21	2007	4	23	21	57	12.6±0.4	16.6	76.06±.02	0.81	-59.91±.14	-1.66	13	4.5	0.33±0.22	0.04±0.22	4.53±0.18	-4	91	4b
22	2007	5	30	2	57	5.1±0.4	-6.9	77.71±.01	0.21	-66.28±.12	-2.78	13	2.6	-0.45±0.10	1.27±0.11	-2.22±0.11	10	240	4b
23	2007	6	9	5	16	57.7±0.4	1.7	76.01±.03	0.26	-59.81±.10	0.94	13	3.8	-0.01±0.17	-2.49±0.17	-2.83±0.19	0	311	4a
24	2007	7	4	16	55	13.1±0.4	-6.9	69.35±.01	0.10	-49.78±.03	-0.03	13	4.8	-1.10±0.15	1.14±0.21	-4.49±0.18	13	256	7
25	2007	7	9	1	8	33.1±0.3	17.1	66.36±.01	0.11	-38.35±.06	-1.10	13	4.8	1.14±0.19	-0.12±0.18	-4.69±0.16	-14	271	2
26	2007	7	9	2	42	28.0±0.4	20.0	66.44±.02	-0.31	-38.29±.06	-0.04	13	2.8	0.80±0.12	-1.10±0.14	-2.48±0.13	-16	294	2
27	2007	7	9	5	31	25.8±0.4	13.8	74.61±.03	-0.39	-56.08±.12	0.92	13	1.8	-0.23±0.10	0.83±0.09	-1.55±0.09	8	242	4e
28	2007	7	20	0	36	19.9±0.4	3.9	68.65±.02	-0.60	-33.17±.07	0.08	13	3.5	-0.79±0.15	0.25±0.15	3.43±0.14	13	94	1
29	2007	7	24	23	3	35.1±0.4	23.1	75.94±.02	-1.31	-59.86±.14	0.89	13	6.3	0.80±0.31	-0.09±0.29	6.23±0.25	-7	89	4b
30	2007	7	26	22	42	50.7±0.4	2.7	66.47±.00	-0.03	-38.49±.01	0.01	13	3.5	-0.44±0.12	2.71±0.16	2.18±0.17	7	141	2
31	2007	8	3	19	25	18.7±0.6	6.7	71.83±.03	-0.42	-51.55±.11	0.70	13	2.4	-0.75±0.14	0.82±0.14	-2.08±0.16	18	248	6
32	2007	8	13	20	37	53.4±0.4	1.4	66.40±.02	0.15	-38.34±.05	0.41	13	4.4	-1.00±0.18	2.48±0.22	3.49±0.21	13	125	2
33	2007	8	25	9	19	3.8±0.4	-0.2	74.63±.02	-0.62	-56.21±.09	0.54	13	4.3	-0.61±0.17	2.19±0.16	-3.61±0.17	8	239	4e
34	2007	9	11	22	42	8.6±0.5	8.6	71.83±.03	1.58	-51.13±.11	-0.38	13	1.8	-0.35±0.10	0.69±0.12	1.58±0.11	12	114	6
35	2007	10	13	5	55	7.1±0.5	-4.9	74.62±.02	-0.13	-56.19±.09	0.56	13	2.9	-0.50±0.13	1.26±0.15	-2.58±0.16	10	244	4e
36	2007	11	21	18	4	56.1±0.4	0.1	66.49±.02	0.24	-38.33±.05	0.42	13	7.3	0.81±0.29	-3.75±0.30	-6.19±0.30	-6	301	2
37	2007	11	24	0	9	1.5±0.4	5.5	68.72±.02	0.22	-33.41±.07	0.09	13	3.6	0.17±0.17	-0.33±0.16	-3.63±0.15	-3	275	1
38	2007	11	24	12	54	31.1±0.3	-0.9	66.33±.01	-0.17	-38.33±.02	0.17	13	9.6	-2.26±0.23	4.35±0.33	8.22±0.31	14	118	2
39	2007	11	24	13	29	42.9±0.3	-9.1	66.39±.03	-0.86	-38.34±.06	-0.09	13	4.2	-0.77±0.18	1.68±0.18	3.81±0.17	10	114	2
40	2007	12	14	6	39	47.4±0.3	11.4	74.65±.02	-0.60	-56.01±.09	0.74	13	4.1	0.14±0.17	-1.48±0.15	3.86±0.15	-2	69	4e

Table 2.1 (continued)

No.	Centroid Parameters											Scale Factor	M	CSF Vector					
	Date			Time				Latitude		Longitude									
	Y	M	D	h	m	sec	δt_0	λ	$\delta\lambda_0$	ϕ	$\delta\phi_0$	10^{ex}	$_{CSF}$	V_r	V_θ	V_ϕ	pl.	azim.	reg.
41	2007	12	31	14	40	57.3±0.4	1.3	66.44±.01	0.19	-38.21±.04	0.54	13	5.4	-1.27±0.17	2.56±0.23	4.55±0.22	14	119	2
42	2008	2	14	5	11	56.3±0.6	-27.7	72.92±.02	0.17	-54.54±.13	1.21	13	2.6	0.70±0.18	-1.52±0.18	1.98±0.19	-16	52	5b
43	2008	4	5	21	6	29.5±0.4	21.5	76.13±.03	0.63	-59.65±.11	-3.15	13	4.0	0.05±0.17	-2.60±0.16	3.01±0.17	-1	49	4b
44	2008	4	7	13	58	13.7±0.6	13.7	74.76±.03	0.51	-55.99±.10	0.76	13	1.9	0.05±0.11	0.48±0.13	-1.81±0.11	-2	255	4e
45	2008	5	4	12	52	55.1±0.4	15.1	65.38±.01	-0.12	-40.98±.05	0.52	13	2.8	0.43±0.11	-2.11±0.15	-1.80±0.15	-9	320	3
46	2008	5	28	21	6	31.6±0.5	-8.4	69.18±.03	-1.57	-49.41±.11	-0.16	13	4.3	0.12±0.25	-1.69±0.26	-3.93±0.20	-2	293	7
47	2008	6	12	17	20	27.7±0.5	19.7	69.28±.02	0.28	-49.39±.11	-0.39	13	2.3	0.29±0.14	0.44±0.17	2.29±0.13	-7	101	7
48	2008	6	13	15	40	51.7±0.5	11.7	75.94±.04	0.19	-59.97±.11	-2.22	13	3.2	-0.85±0.18	2.73±0.16	-1.35±0.20	16	206	4b
49	2008	6	19	15	20	3.5±0.4	3.5	74.75±.01	0.00	-55.84±.12	2.41	13	3.1	0.03±0.14	1.96±0.17	-2.44±0.14	-1	231	4e
50	2008	7	13	5	0	9.2±0.6	25.2	69.25±.03	-0.25	-49.52±.08	-0.02	13	2.3	-0.44±0.14	1.37±0.17	-1.84±0.15	11	233	7
51	2008	8	1	14	43	19.4±0.4	-0.6	66.53±.00	0.03	-38.22±.04	0.28	13	2.9	-0.51±0.11	0.88±0.16	2.75±0.14	10	108	2
52	2008	8	1	23	0	35.4±0.3	-4.6	66.33±.02	-0.42	-38.58±.06	0.67	13	4.1	-0.26±0.16	1.22±0.17	3.95±0.15	4	107	2
53	2008	8	14	20	58	32.6±0.3	8.6	76.03±.02	-1.72	-59.80±.09	-1.05	14	1.1	0.14±0.03	-0.42±0.04	1.00±0.03	-7	67	4b
54	2008	8	19	21	5	24.0±0.4	-4.0	66.48±.02	0.23	-38.34±.01	-0.09	13	3.4	-0.66±0.14	2.14±0.16	2.60±0.16	11	129	2
55	2008	11	3	16	44	9.1±0.5	-38.9	68.66±.01	-0.09	-32.89±.07	0.86	13	5.9	1.51±0.25	-4.44±0.29	-3.50±0.34	-15	322	1
56	2008	11	7	13	44	11.1±0.5	-12.9	77.80±.02	0.30	-66.40±.06	0.10	13	2.8	-0.73±0.12	0.60±0.17	-2.66±0.14	15	257	4a
57	2008	11	21	20	31	49.2±0.4	-2.8	75.98±.01	-0.02	-59.68±.10	-1.68	13	7.2	-0.24±0.28	5.05±0.32	5.17±0.32	2	134	4b
58	2008	11	25	4	10	47.4±0.5	7.4	68.69±.02	0.19	-33.28±.04	0.22	13	5.5	1.16±0.21	-2.45±0.27	-4.75±0.28	-12	297	1
59	2008	12	13	14	48	1.3±0.4	9.3	68.67±.02	0.67	-33.19±.05	0.81	13	8.8	1.94±0.29	-5.24±0.38	-6.80±0.36	-13	308	1
60	2009	1	8	16	11	19.1±0.4	15.1	71.80±.03	-0.70	-51.82±.05	0.68	13	5.8	-0.75±0.23	5.47±0.23	-1.74±0.28	7	198	6
61	2009	2	6	18	51	24.9±0.5	-11.1	66.40±.03	0.65	-38.22±.07	0.03	13	1.8	-0.47±0.10	0.70±0.12	1.61±0.10	15	113	2
62	2009	2	6	18	59	7.1±0.4	3.1	66.49±.02	0.24	-38.31±.02	-0.06	13	4.0	-0.89±0.12	2.06±0.17	3.33±0.15	13	122	2
○ 63	2009	2	7	19	14	54.2±0.4	22.2	73.08±.03	-1.17	-54.18±.11	3.07	13	2.9	-0.23±0.15	-0.99±0.14	2.68±0.12	5	70	5b
64	2009	2	11	13	13	9.6±0.3	-2.4	66.45±.02	0.20	-38.33±.01	-0.08	13	5.1	-0.94±0.15	3.22±0.20	3.78±0.19	11	130	2
65	2009	4	19	19	7	32.4±0.4	12.4	66.41±.02	-0.34	-38.22±.04	0.53	13	5.6	-1.18±0.19	4.34±0.23	3.32±0.24	12	143	2
66	2009	4	26	9	55	25.0±0.3	-3.0	66.39±.02	-0.36	-38.46±.04	-0.71	13	7.0	-0.66±0.20	3.96±0.25	5.75±0.24	5	125	2
67	2009	4	27	10	54	34.8±0.4	-5.2	66.48±.01	0.23	-38.11±.04	0.64	13	3.2	-0.92±0.10	0.96±0.16	2.93±0.13	17	108	2
68	2009	5	11	21	56	4.8±0.4	12.8	66.44±.01	-0.06	-38.04±.05	-0.54	13	2.5	0.83±0.11	-1.36±0.15	-1.89±0.13	-20	306	2
69	2009	5	13	2	11	13.8±0.3	-14.2	66.45±.02	-0.30	-38.45±.05	-2.20	13	7.7	-0.56±0.23	4.41±0.25	6.29±0.25	4	125	2
70	2009	5	23	10	41	40.9±0.4	-11.1	69.34±.02	-0.41	-49.84±.07	0.41	13	2.6	-0.51±0.11	1.44±0.12	-2.08±0.12	11	235	7
• 71	2009	5	23	10	53	17.8±0.5	29.8	69.18±.01	-0.07	-49.70±.07	-1.45	13	3.4	0.11±0.13	3.03±0.17	1.48±0.18	-2	154	7
72	2009	5	25	12	42	51.6±0.5	11.6	69.17±.01	-0.08	-49.37±.08	-1.12	13	2.5	-0.20±0.13	-1.63±0.14	1.90±0.15	4	49	7
73	2009	5	26	21	7	41.2±0.3	-2.8	66.44±.01	-0.06	-38.47±.01	0.03	13	3.8	-0.33±0.10	1.96±0.14	3.25±0.14	5	121	2
74	2009	6	14	0	2	16.4±0.4	-7.6	76.11±.03	-0.39	-59.37±.08	2.13	13	3.5	0.22±0.15	3.20±0.12	-1.29±0.16	-4	202	4b
75	2009	6	18	16	24	43.7±0.3	-4.3	69.25±.02	-0.50	-49.60±.03	0.15	13	4.5	-0.79±0.15	-2.74±0.19	-3.46±0.17	10	308	7
76	2009	6	26	13	27	53.8±0.4	17.8	69.24±.02	0.49	-49.49±.06	0.76	13	9.0	0.00±0.32	6.75±0.34	5.99±0.33	0	138	7
77	2009	7	3	7	19	51.3±0.6	-8.7	73.09±.01	0.09	-54.25±.10	0.75	13	1.9	-0.11±0.11	0.78±0.12	-1.76±0.11	3	246	5b
78	2009	7	22	0	19	54.5±0.4	-5.5	75.00±.02	-1.00	-56.75±.10	-2.75	13	4.4	-0.17±0.17	-2.60±0.17	-3.52±0.16	2	306	4d
79	2009	7	22	21	16	27.2±0.5	3.2	65.32±.03	0.32	-41.24±.04	-0.24	13	2.5	-0.39±0.12	1.94±0.12	1.47±0.13	9	143	3
80	2009	8	11	20	12	17.1±0.4	9.1	69.18±.00	-0.07	-49.52±.08	1.73	13	3.8	-0.47±0.17	-2.46±0.18	-2.92±0.17	7	310	7

Table 2.1 (continued)

No.	Centroid Parameters											Scale Factor	M	CSF Vector					
	Date			Time				Latitude		Longitude									
	Y	M	D	h	m	sec	δt_0	λ	$\delta\lambda_0$	ϕ	$\delta\phi_0$	10^{ex}	$_{CSF}$	V_r	V_θ	V_ϕ	pl.	azim.	reg.
○ 81	2009	8	20	0	16	21.3±0.5	-18.7	75.61±.01	0.11	-58.32±.08	-0.82	13	2.8	0.76±0.10	-1.19±0.14	2.39±0.14	-16	64	4c
82	2009	8	21	7	2	18.8±0.4	-5.2	69.20±.03	-0.55	-49.55±.02	0.20	13	4.4	-0.88±0.15	-2.14±0.21	-3.80±0.19	11	299	7
83	2009	8	23	7	24	9.8±0.5	9.8	75.71±.03	0.21	-58.08±.06	0.42	13	2.7	-0.17±0.12	1.45±0.14	-2.25±0.15	4	237	4c
○ 84	2009	8	26	22	59	14.5±0.4	-5.5	66.41±.02	0.16	-38.33±.05	0.42	13	3.6	-1.01±0.16	2.63±0.18	2.28±0.19	16	139	2
• 85	2009	9	19	22	30	58.7±0.4	-5.3	76.06±.00	0.06	-59.58±.09	2.42	13	4.4	-0.23±0.16	3.65±0.17	-2.39±0.22	3	213	4b
86	2009	11	5	21	7	45.4±0.4	1.4	66.52±.02	0.27	-38.50±.02	-0.25	13	4.6	-0.17±0.16	2.24±0.22	4.01±0.19	2	119	2
87	2009	11	22	17	15	35.7±0.4	15.7	75.97±.02	-0.28	-59.55±.09	1.20	13	5.6	-0.17±0.22	3.29±0.24	4.55±0.23	2	126	4b
88	2009	11	27	8	52	50.3±0.4	18.3	68.57±.02	-0.43	-33.12±.06	-0.12	13	7.5	2.24±0.25	-2.67±0.34	-6.66±0.31	-17	292	1
89	2009	12	2	10	31	1.1±0.4	-10.9	76.04±.02	0.79	-59.44±.10	-1.19	13	5.5	-0.17±0.20	3.03±0.20	-4.59±0.20	2	237	4b
90	2009	12	5	5	0	38.3±0.4	14.3	68.65±.03	-1.10	-33.81±.10	0.44	13	2.3	0.46±0.13	-0.04±0.13	2.27±0.11	-12	89	1
91	2009	12	28	2	50	32.2±0.4	0.2	68.63±.02	-0.87	-33.08±.04	0.42	13	5.1	-1.17±0.17	2.60±0.22	4.26±0.21	13	121	1
92	2010	1	26	10	52	48.4±0.3	-7.6	68.73±.00	-0.02	-33.10±.04	0.65	13	5.1	-1.08±0.14	2.61±0.19	4.23±0.19	12	122	1
93	2010	1	27	15	38	2.7±0.5	18.7	76.05±.03	0.55	-59.87±.09	-0.37	13	2.8	0.47±0.15	-2.00±0.15	1.85±0.17	-10	43	4b
94	2010	2	4	0	16	50.5±0.6	-5.5	68.69±.04	-0.31	-33.30±.10	-0.30	13	1.9	-0.17±0.14	1.33±0.12	1.36±0.14	5	134	1
95	2010	2	11	1	16	41.6±0.4	-22.4	66.41±.02	-0.84	-38.37±.03	-0.12	13	2.9	-0.56±0.09	1.75±0.12	2.19±0.12	11	129	2
96	2010	2	21	4	12	20.6±0.3	-3.4	69.19±.01	-0.06	-49.52±.05	-1.27	13	2.9	-0.47±0.09	-0.53±0.11	-2.80±0.10	9	281	7
○ 97	2010	3	19	1	13	1.8±0.4	13.8	69.27±.02	-0.23	-49.50±.08	1.00	13	3.0	0.56±0.14	1.17±0.16	2.72±0.14	-11	113	7
98	2010	3	22	5	55	15.1±0.4	3.1	76.14±.02	0.39	-59.65±.07	1.10	13	2.3	-0.10±0.10	1.45±0.09	-1.75±0.10	3	230	4b
○ 99	2010	4	14	14	10	14.0±0.4	-26.0	69.25±.03	0.75	-49.38±.07	-0.88	13	2.8	-0.20±0.12	-2.28±0.13	-1.60±0.14	4	325	7
100	2010	5	21	3	56	8.7±0.3	-7.3	69.34±.02	0.59	-49.69±.02	0.56	13	4.4	-0.70±0.12	-3.73±0.15	-2.14±0.16	9	330	7
101	2010	5	27	11	23	41.2±0.4	-2.8	69.30±.02	0.05	-49.52±.07	-3.77	13	8.5	0.59±0.30	6.40±0.33	5.60±0.33	-4	139	7
○ 102	2010	6	17	9	23	33.5±0.3	-50.5	69.27±.02	1.02	-49.40±.05	-3.15	13	3.6	0.19±0.13	3.22±0.14	1.56±0.15	-3	154	7
103	2010	6	21	9	34	46.0±0.4	-10.0	66.39±.03	-0.86	-38.29±.07	-0.54	13	2.9	0.75±0.12	-0.94±0.16	-2.59±0.14	-15	290	2
104	2010	7	12	17	49	43.5±0.5	-0.5	66.46±.01	-0.04	-38.32±.07	-0.82	13	5.8	-1.24±0.26	2.76±0.30	4.98±0.26	12	119	2
105	2010	7	15	8	53	29.6±0.4	-6.4	66.41±.01	-0.09	-38.48±.02	0.02	13	3.6	-0.66±0.12	1.45±0.18	3.22±0.16	11	114	2
106	2010	7	15	11	20	22.1±0.3	-9.9	69.28±.02	0.28	-49.24±.02	-0.24	13	4.4	-0.56±0.13	-3.41±0.16	-2.72±0.17	7	321	7
107	2010	7	17	3	50	53.6±0.5	-18.4	75.97±.03	0.72	-60.01±.10	-1.76	13	4.3	-0.92±0.18	2.85±0.22	-3.10±0.23	12	227	4b
108	2010	7	27	15	7	36.2±0.3	-7.8	75.96±.01	-0.29	-59.81±.07	2.94	13	7.4	-1.35±0.20	4.06±0.26	-6.01±0.24	11	236	4b
109	2010	8	4	2	27	15.3±0.4	-4.7	66.45±.02	0.70	-38.34±.04	1.41	13	7.0	-1.28±0.21	3.17±0.27	6.06±0.26	11	118	2
○ 110	2010	8	19	16	0	34.8±0.4	-5.2	69.17±.01	0.17	-49.24±.07	1.76	13	7.5	-0.10±0.28	-5.92±0.34	-4.58±0.34	1	322	7
111	2010	9	5	11	57	5.0±0.5	9.0	73.11±.01	0.11	-54.30±.08	0.70	13	3.6	0.20±0.17	-2.31±0.19	2.71±0.18	-3	50	5b
112	2010	10	10	3	13	13.6±0.5	9.6	73.13±.02	0.38	-54.30±.06	0.45	13	5.4	0.22±0.23	-0.21±0.28	5.43±0.25	-2	88	5b
113	2010	10	24	13	13	48.4±0.5	4.4	75.99±.02	0.24	-59.80±.11	0.95	13	4.7	-0.65±0.25	1.77±0.27	-4.30±0.25	8	248	4b
114	2010	10	27	1	44	8.5±0.5	-7.5	71.84±.02	0.09	-51.78±.01	-0.03	13	2.2	0.23±0.10	-1.52±0.12	1.61±0.14	-6	47	6
115	2010	11	7	8	18	50.9±0.5	2.9	73.14±.02	0.14	-54.66±.04	0.34	13	3.7	0.52±0.16	-1.81±0.19	3.15±0.20	-8	60	5b
116	2010	11	22	13	16	15.7±0.5	15.7	68.69±.03	0.44	-32.99±.08	1.26	13	4.0	0.95±0.21	-2.35±0.23	-3.11±0.22	-14	307	1
○ 117	2010	11	24	12	58	5.1±0.5	5.1	68.68±.03	-0.82	-33.26±.12	0.24	13	2.6	0.16±0.18	-0.92±0.18	-2.43±0.14	-4	291	1
○ 118	2010	11	24	20	50	59.6±0.4	-12.4	76.02±.02	-0.23	-59.59±.11	0.66	13	4.8	-0.21±0.20	2.27±0.22	-4.19±0.19	2	242	4b
○ 119	2010	12	5	17	40	54.4±0.4	-1.6	65.80±.03	-0.70	-39.64±.07	-0.14	13	3.5	-0.36±0.18	-1.50±0.18	3.19±0.17	6	65	3
120	2010	12	14	23	49	39.1±0.5	19.1	68.72±.03	0.72	-33.02±.06	0.98	13	4.9	1.07±0.22	-3.47±0.25	-3.34±0.27	-13	316	1
121	2010	12	29	0	56	45.5±0.4	5.5	73.04±.02	-0.21	-54.53±.09	1.22	13	3.6	0.57±0.15	-1.98±0.18	2.98±0.17	-9	56	5b

Table 2.1: Centroid–single-force solutions for 121 glacial earthquakes in 2006–2010. NRT detection events are indicated by empty dots (○), and poorer-quality standard detections are indicated by solid dots (•). Columns give earthquake number, centroid time (year, month, day, hour, minute, second) with standard error; centroid time shift from detection time (δt_0); centroid latitude with standard error, and shift in latitude from detection location ($\delta\lambda_0$); centroid longitude with standard error, and shift in longitude from detection location ($\delta\phi_0$); scaling exponent for CSF amplitude and vector; CSF amplitude M_{CSF}, in units of kg-m, to be scaled by exponent given in the previous column (for event 1, $M_{CSF} = 5.5 \times 10^{13}$ kg-m); CSF vector in geographic coordinates r, θ, ϕ (up, south, east), with standard errors, to be scaled by the Scale Factor; plunge of CSF vector with respect to horizontal; azimuth of CSF vector with respect to north; and glacial-earthquake source glacier or region. Region definitions are consistent with Tsai and Ekström [2007], but have been subdivided in some cases: 0: Daugaard-Jensen Glacier; 1: Kangerdlugssuaq Glacier; 2: Helheim Glacier; 3: Southeast Greenland (multiple glaciers); 4a: Tracy Glacier; 4b: Kong Oscar Glacier; 4c: Sverdrup Glacier; 4d: Hayes Glacier; 4e: Alison Glacier; 5a: Giesecke Bræer; 5b: Upernavik Isstrøm; 6: Rinks Glacier; 7: Jakobshavn Isbræ; 8: Rolige Bræ.

2.9 Figures

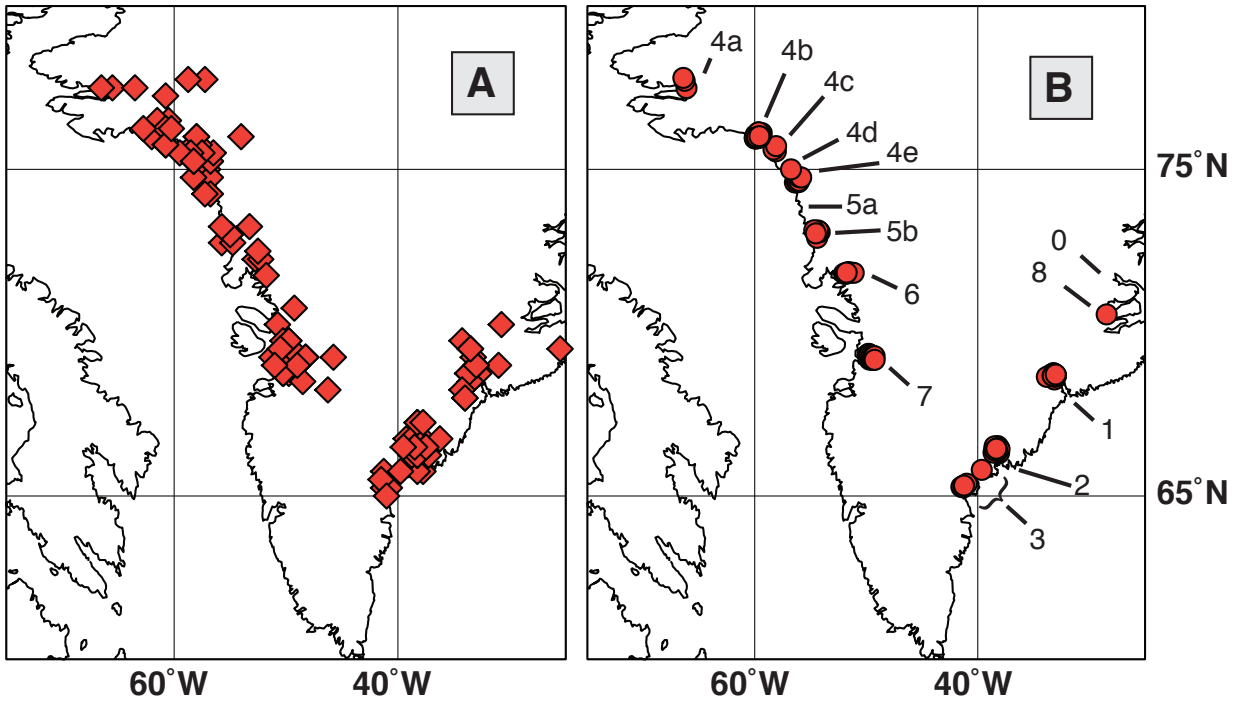

Figure 2.1: Locations of 121 glacial earthquakes, 2006–2010. A: locations of all events as determined by surface-wave detection. B: locations of the same events as determined by waveform inversion. Glaciers are labeled as in Table 1: 0: Daugaard-Jensen Glacier; 1: Kangerdlugssuaq Glacier; 2: Helheim Glacier; 3: Southeast Greenland (multiple glaciers); 4a: Tracy Glacier; 4b: Kong Oscar Glacier; 4c: Sverdrup Glacier; 4d: Hayes Glacier; 4e: Alison Glacier; 5a: Giesecke Bræer; 5b: Upernavik Isstrøm; 6: Rinks Glacier; 7: Jakobshavn Isbræ; 8: Rolige Bræ. While included on this figure for completeness, we that note neither Region 0 nor Region 5a produced glacial earthquakes during the period 2006–2010.

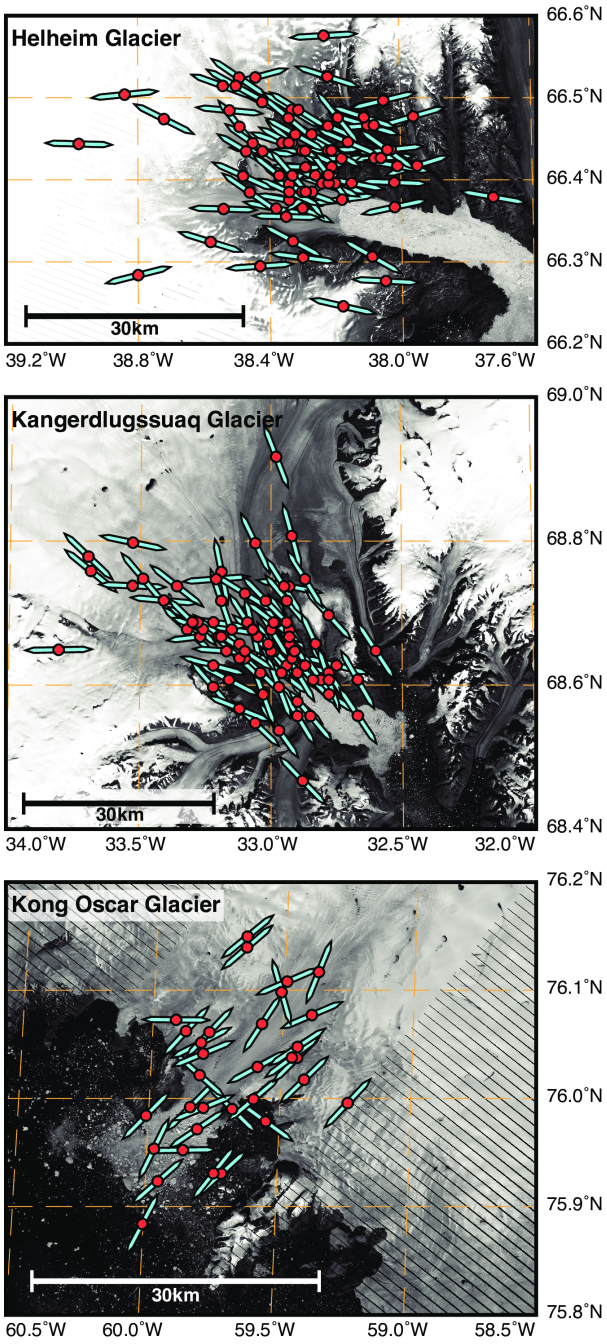

Figure 2.2: Distribution of glacial earthquakes, 1993–2010, at three glaciers: Helheim Glacier (top), Kangerdlugssuaq Glacier (middle), and Kong Oscar Glacier (bottom). In each map, the locations of glacial earthquakes are shown as red dots, and the orientations of the force vectors associated with each event as blue bars. Because we consider the force directions to have a 180° ambiguity for a given event (see text), we plot only the vector orientation here. The background images for each map are Landsat images obtained during August 2005, on the 4th, 15th, and 22nd, respectively.

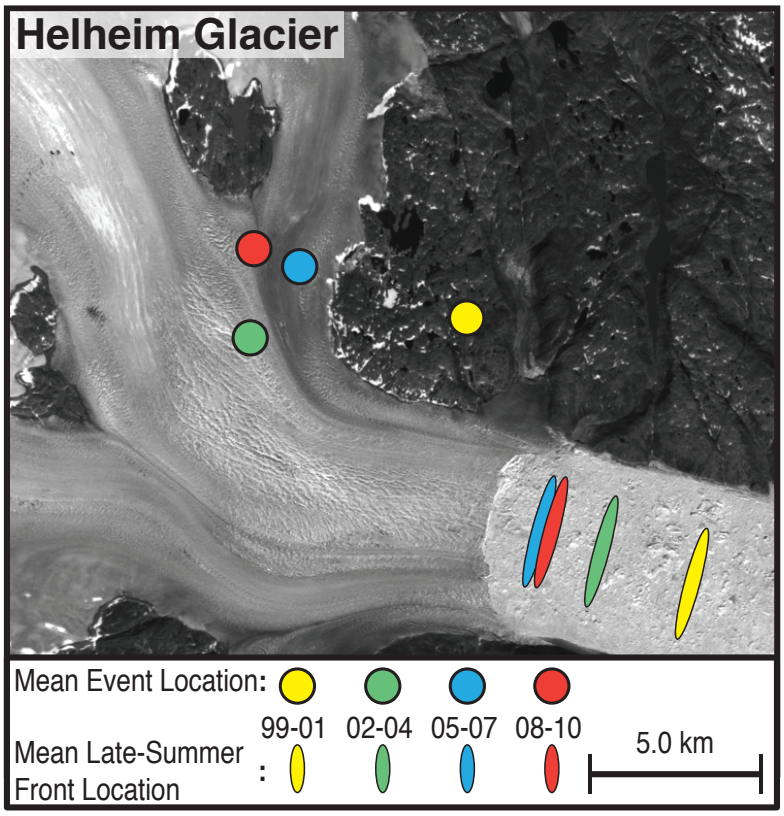

Figure 2.3: Comparison of changes in locations of glacial earthquakes and glacier calving front at Helheim Glacier, 1999–2010. Circles indicate the mean location of glacial earthquakes during each three-year time period; ellipses indicate the mean mid-August calving-front location as measured from Landsat imagery. The range and orientation of changes in event location are similar to changes in the position of the calving front. The mean earthquake location for 2002–2004 is dominated by events in 2004; the calving-front location averages are not weighted. Background is a Landsat image from 4 August, 2005.

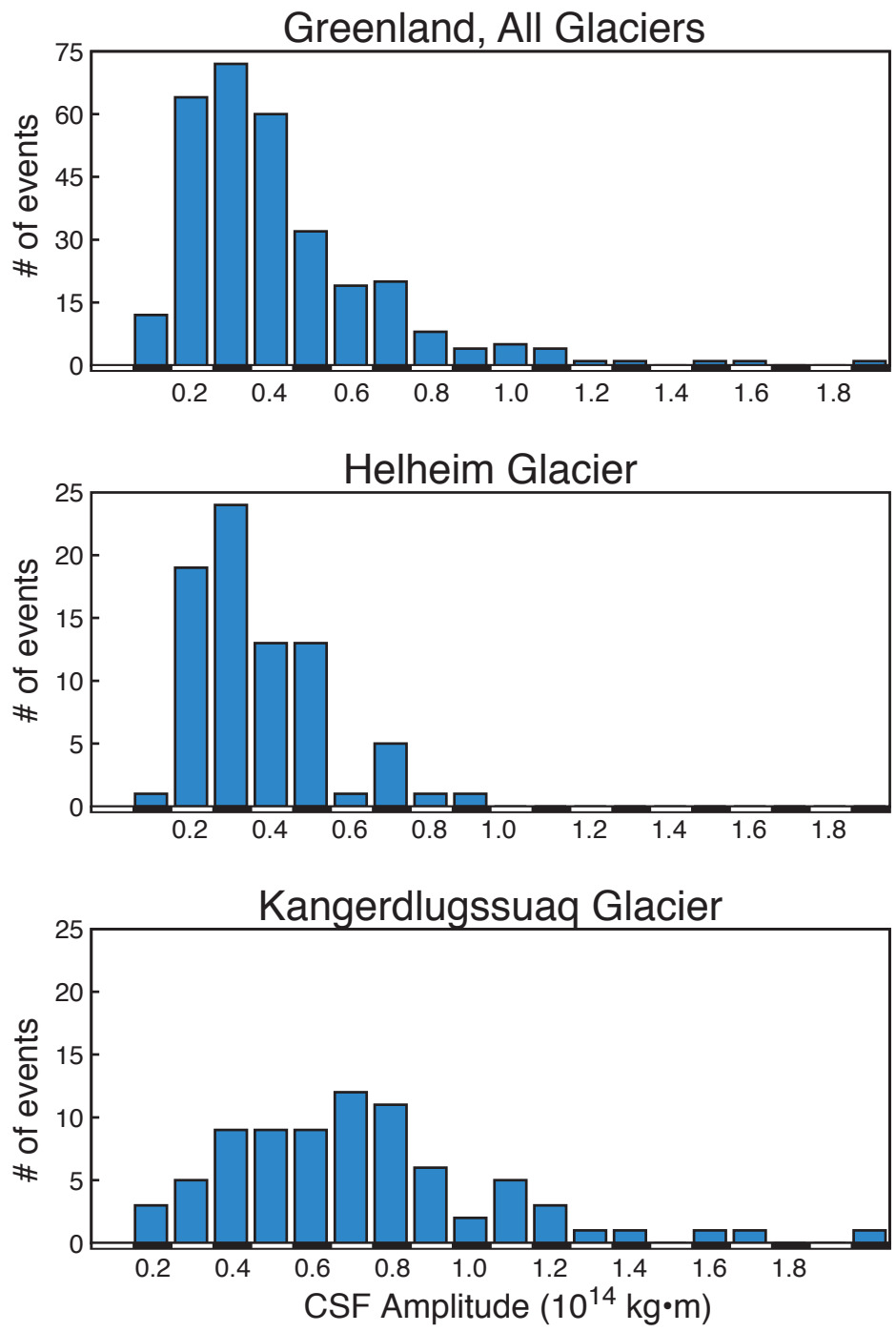

Figure 2.4: Size distribution for all Greenland glacial earthquakes (top), Helheim Glacier (middle) and Kangerdlugssuaq Glacier (bottom) from 1993–2010. We observe a narrow range of event sizes, with a peak at a value that is twice as large at Kangerdlugssuaq as at Helheim. Kangerdlugssuaq produced 79 events during this time period, Helheim produced 78 events, and Greenland a total of 305 events.

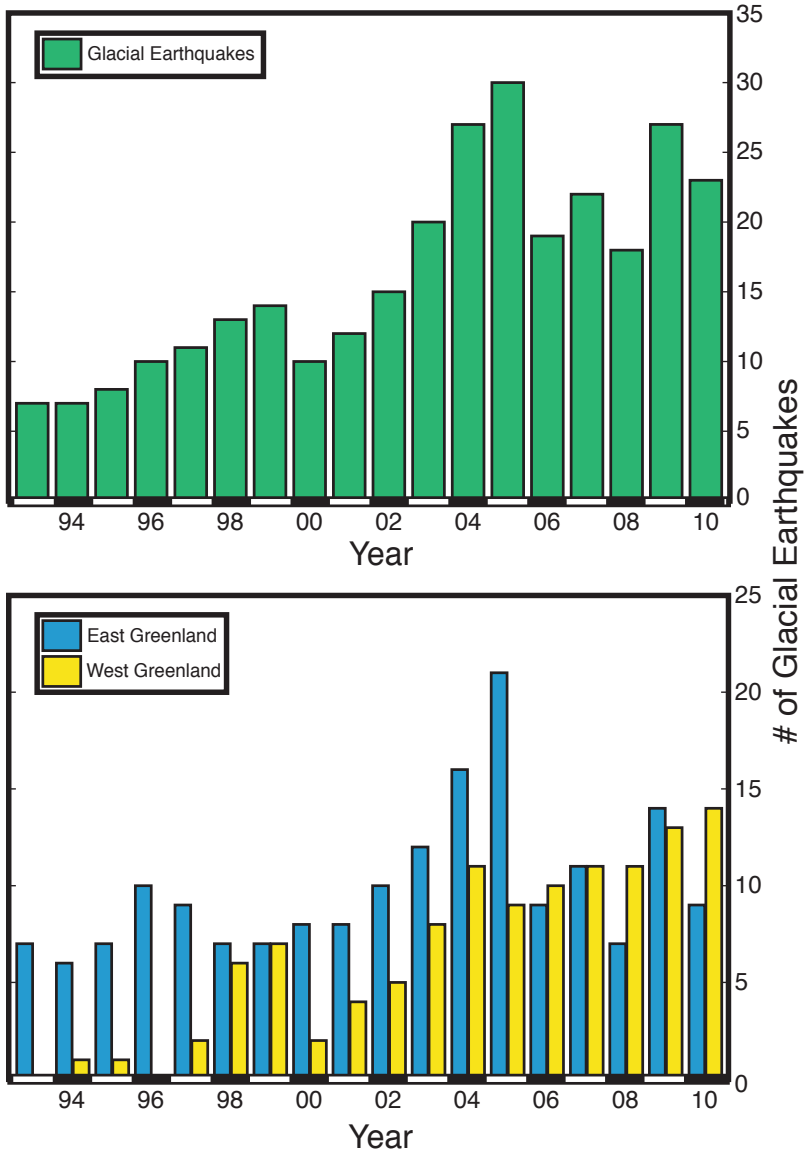

Figure 2.5: Glacial-earthquake production in Greenland, 1993–2010. The top panel shows the yearly occurrence of glacial earthquakes across Greenland. Note the decline in events from 2005 to 2006, with subsequent production at levels similar to 2003–2004. The lower panel shows the yearly occurrence of glacial earthquakes in West Greenland and East Greenland. Note the differing trends after 2005, as production in West Greenland continues to rise, while production in East Greenland is more variable.

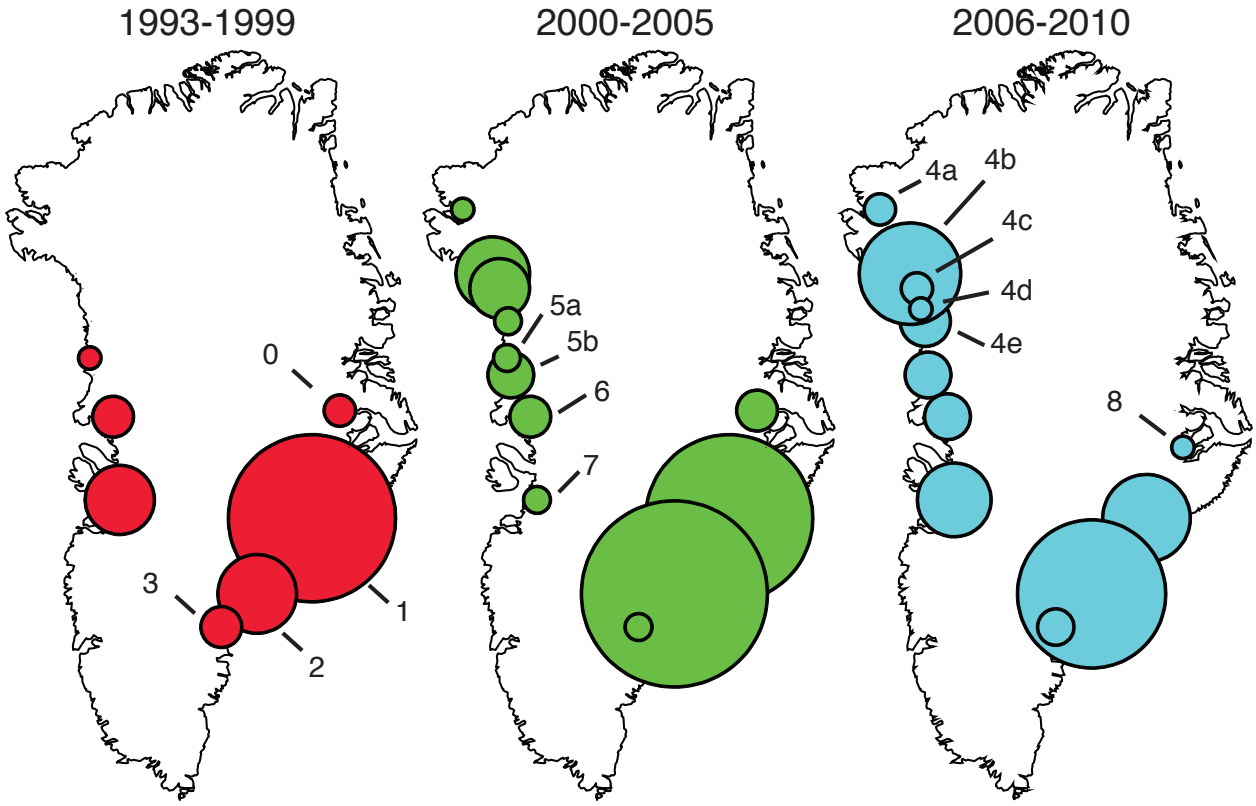

Figure 2.6: Three phases of glacial-earthquake production in Greenland. Each glacier is represented by a single dot, with sizes scaled linearly by the number of glacial earthquakes occurring at the glacier during each time period. The scaling is consistent between time periods; numbers range from 1 earthquake at Rolige Bræ (region 8) during 2006–2010 to 36 earthquakes at Helheim Glacier (region 2) during 2000–2005. From 1993–1999, production was relatively steady and concentrated in Southeast Greenland, with some production at a handful of larger glaciers in central West Greenland. From 2000–2005, glacial-earthquake production increased Greenland-wide, as many previously inactive glaciers in Northwest Greenland began to produce glacial earthquakes regularly. From 2006–2010, production declined in East Greenland, but continued to rise in West and Northwest Greenland. Glaciers are labeled as in Table 1: 0: Daugaard-Jensen Glacier; 1: Kangerdlugssuaq Glacier; 2: Helheim Glacier; 3: Southeast Greenland (multiple glaciers); 4a: Tracy Glacier; 4b: Kong Oscar Glacier; 4c: Sverdrup Glacier; 4d: Hayes Glacier; 4e: Alison Glacier; 5a: Giesecke Bræer; 5b: Upernavik Isstrøm; 6: Rinks Glacier; 7: Jakobshavn Isbræ; 8: Rolige Bræ.

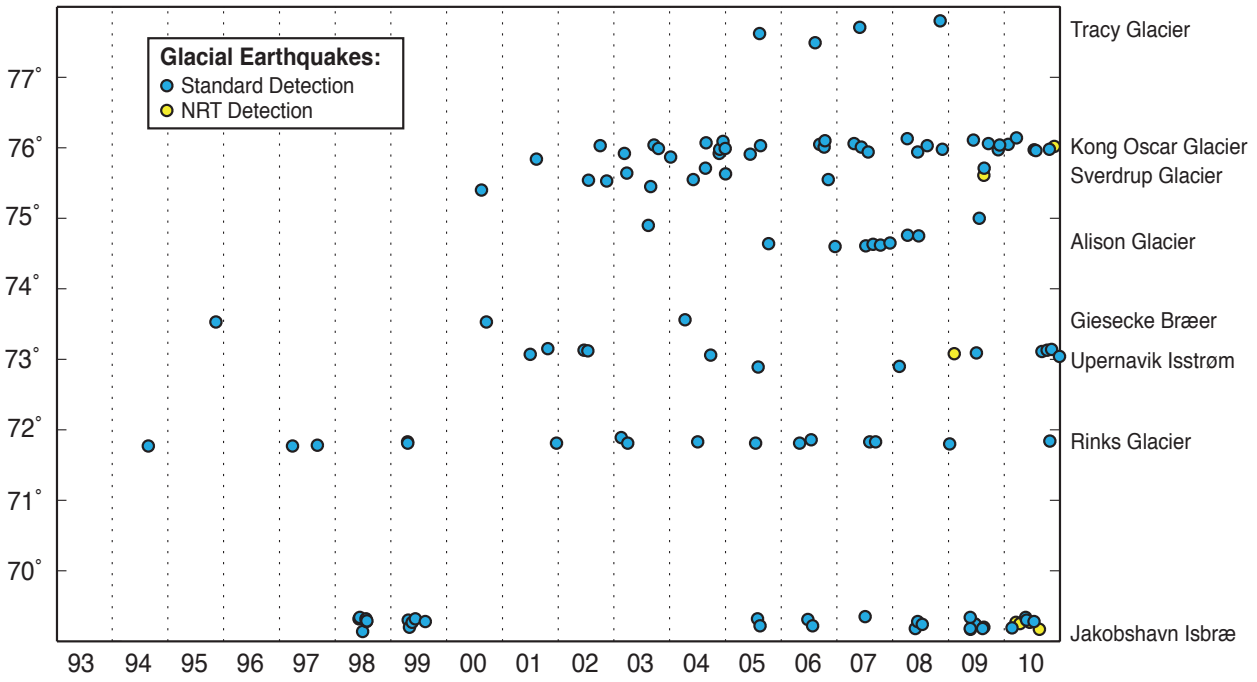

Figure 2.7: Latitude of glacial earthquakes in West Greenland vs. time of occurrence. Standard detections are indicated in blue, NRT detections are indicated in yellow; source glaciers are labeled on the right. The coast of West Greenland is oriented approximately North/South, thus glaciers are separated by latitude. Production of glacial earthquakes has spread northward over time, with multiple glaciers producing glacial earthquakes after previous quiescence.

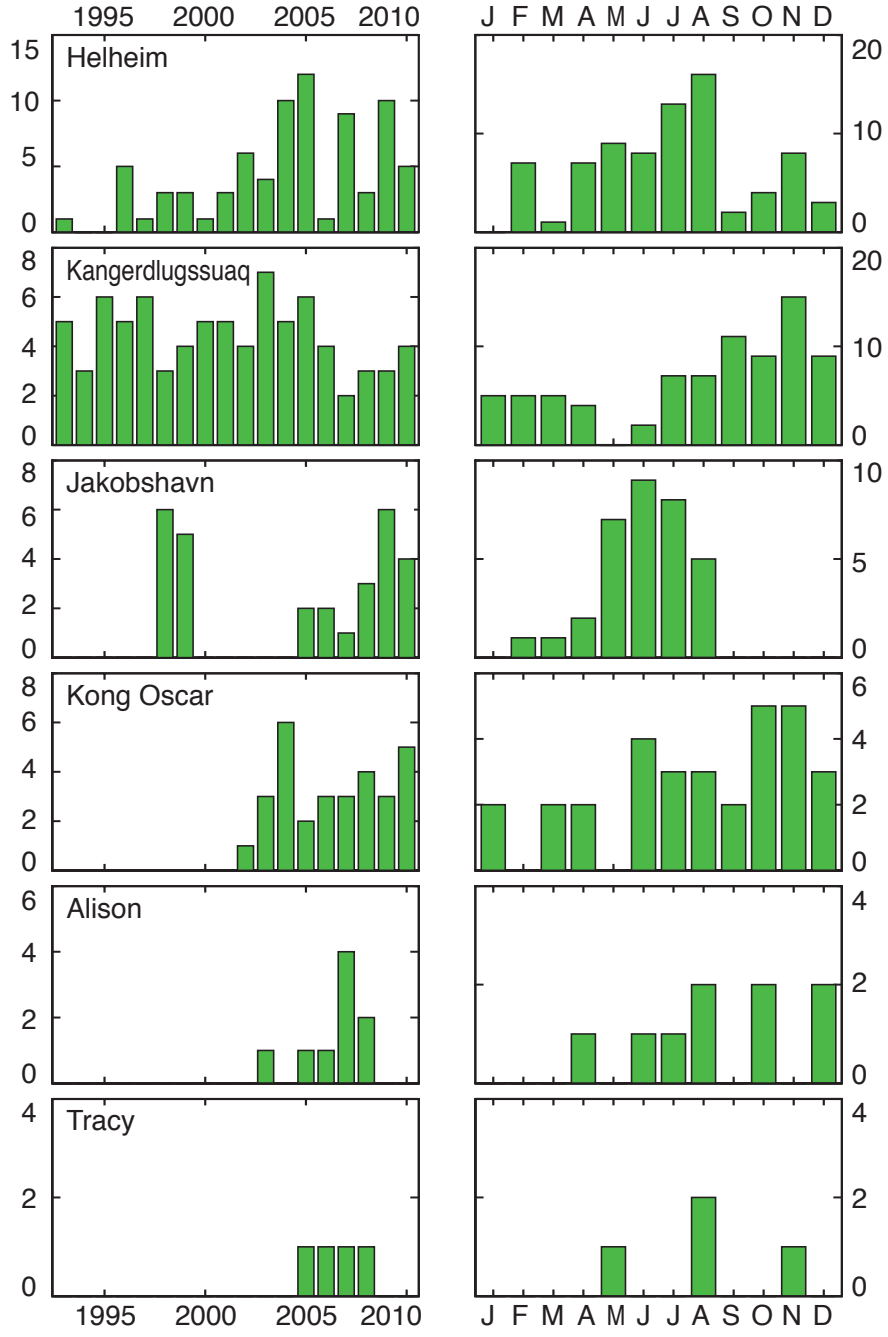

Figure 2.8: Yearly (left column) and monthly (right column) distributions of glacial earthquakes at the six glaciers discussed in detail in Section 4.3.

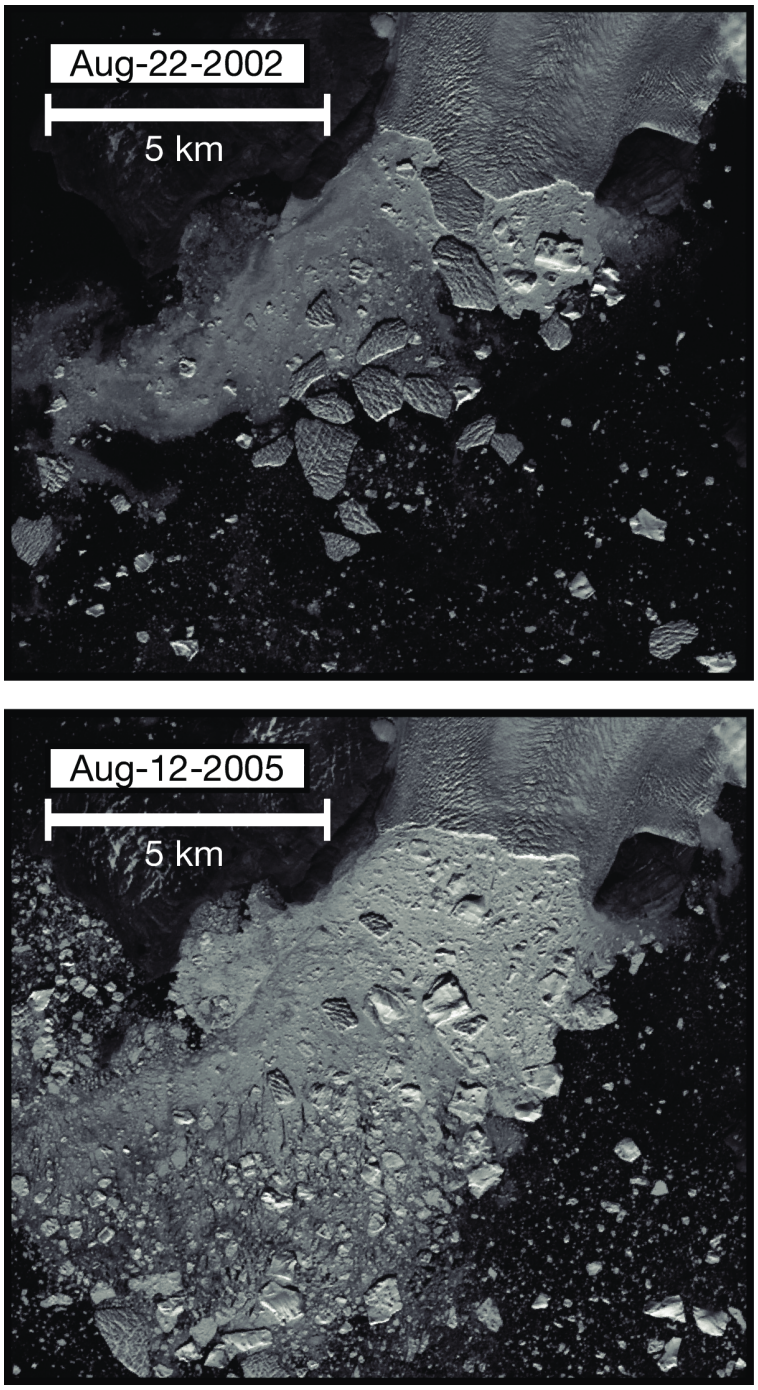

Figure 2.9: Two images of Kong Oscar Glacier demonstrating the visual difference between calving of tabular (top) and capsizing (bottom) icebergs. Tabular icebergs are typically larger and show the same surface texture as the source glacier. Capsized icebergs are typically smaller, appear brighter, and show a smooth surface texture. The top image was captured a few months prior to the inferred transition to grounded calving, and the onset of glacial-earthquake production. Though one large capsized iceberg is visible, the proglacial mélange is dominated by tabular bergs. The bottom image, showing calving close to the grounding line, is dominated by capsized icebergs, though several smaller tabular icebergs are also present.

Chapter 3

Assessment of Glacial-Earthquake Source Parameters

3.1 Introduction

Glacial earthquakes are moderate earthquakes with globally observable intermediate-period surface waves [*Ekström et al.*, 2003] that are associated with major marine-terminating glaciers in Greenland [e.g. *Ekström et al.*, 2003] and Antarctica [*Nettles and Ekström*, 2010; *Chen et al.*, 2011]. Glacial earthquakes in Greenland occur at glaciers with near-grounded calving fronts [*Veitch and Nettles*, 2012] when large icebergs comprising the full thickness of the glacier detach and capsize against the glacier's calving front [e.g., *Tsai et al.*, 2008; *Amundson et al.*, 2008; *Veitch and Nettles*, 2012; *Murray et al.*, 2015a]. Since first detected, glacial earthquakes have shown promise as a tool to monitor large outlet glaciers in Greenland, and focused, multidisciplinary studies of glacial-earthquake producing glaciers have resulted in a rapid refinement of our understanding of the source mechanism of glacial earthquakes. During calving, the accelerating iceberg [*Tsai et al.*, 2008; *Nettles et al.*, 2008a; *Nettles and Ekström*, 2010; *Veitch and Nettles*, 2012] and hydrodynamic interaction between the rapidly rotating iceberg and the fjord water [*Murray et al.*, 2015a] exert a seismogenic force on the solid earth. The resulting seismic surface waves are glob-

ally detectable, and may be used to determine source-parameters describing the glacial earthquake [*Ekström et al.*, 2003; *Nettles and Ekström*, 2010]. Waveform analysis using a centroid-single-force (CSF) model [*Kawakatsu*, 1989] has been applied systematically for events in Greenland, and complete catalogs for all events in Greenland are currently published for the years 1993–2010 [*Tsai and Ekström*, 2007; *Veitch and Nettles*, 2012]. However, the use of glacial earthquakes as a monitoring tool has been somewhat limited by an imprecise understanding of both the physics of their source, and of the physical meaning of the glacial-earthquake source parameters obtained through waveform modeling.

The CSF source modeling performed by *Tsai and Ekström* [2007] and *Veitch and Nettles* [2012] utilizes intermediate-period surface waves and an assumed source-time function in order to provide information on each glacial earthquake's source. This information consists of a centroid time and centroid location as well as a three-dimensional source vector describing each event's active force; this vector is expressed as two angles, one describing the force's direction with respect to the Earth's surface (plunge), and the other describing the force's direction with respect to north (azimuth). The physical meaning of the azimuth has been a particular point of uncertainty. As modeled, this parameter should represent the direction of the force acting on the solid earth, opposite to the direction of the capsizing iceberg [*Nettles and Ekström*, 2010]. However, the orientations of these forces vary widely at individual glaciers, leading to uncertainty about the accuracy of this parameter. An ideal means of addressing this uncertainty would be to measure the calving fronts of source glaciers immediately before and after a number of calving events and then compare them to force-orientations estimated from seismic data, unfortunately this is not possible due to limitations imposed by the availability of the required satellite imagery. However, a previous study [*Walter et al.*, 2012a] was able to precisely identify the source region of a glacial earthquake that occurred at Jakobshavn Isbræ. The source region, the measured calving-front orientation, and the active-force orientation for that event are shown in Figure 3.1. The orientation of the source region very closely matches the active-force orientation of the event published by *Veitch and Nettles* [2012], a promising result. Here, in order to asses the accuracy of published force-orientations estimates for

a large number of glacial earthquakes, we compare the range of calving-front orientations observed at glaciers over time, and consider their relationship to glacial-earthquake active-force orientations for the same glacier.

At three of the four glaciers we address here, there also exists a particular question with regard to force orientation that is specific to that glacier. In the case of Helheim Glacier, variations in force orientation have a clear temporal signal; *Veitch and Nettles* [2012] noted that active-force orientations have shown a generally clock-wise trend since approximately 2000 (Figure 3.2). Helheim has undergone significant dynamic changes over this time period, including accelerating, thinning, retreating, slightly readvancing, and slightly slowing [e.g *Howat et al.*, 2005; *Murray et al.*, 2015b], and we wish to establish whether the trends in force orientation reflect physical changes at the glacier or are simply representative of uncertainty in force orientations obtained by waveform inversion. At Jakobshavn Isbræ the calving front retreated significantly over the period we consider here (1993–2010), changing from a rock-bounded fjord to a wider terminus with at least two rapidly flowing ice streams separated by slower ice [*Joughin et al.*, 2008b]. As these two ice streams are quite different in their orientation, but fairly close spatially, we investigate whether active-force orientation will allow us to more specifically determine the source of glacial earthquakes at Jakobshavn. At Kong Oscar Glacier, *Veitch and Nettles* [2012] noted a number of 'anomalous' glacial earthquakes where the active-force orientation was nearly parallel to the orientation of the calving front and perpendicular to the expected active-force orientation. We consider whether these results may be explained using a higher-temporal-resolution analysis of the geometry of the calving front at Kong Oscar Glacier.

In this paper, we obtain estimates of glacier geometry from satellite remote sensing products and compare these with previously published glacial-earthquake source parameters in an effort to better understand the physical meaning of model parameters obtained from waveform inversion of glacial-earthquake seismograms, as well as the errors associated with those parameters.

3.2 Data & Methods

We characterize the angle and position of the calving fronts of several glaciers over a multi-year time period using satellite imagery and relate those physical characteristics to changes in earthquake source parameters using published earthquake data. We consider glacial-earthquake solutions and remote-sensing imagery from the four glaciers that have contributed the greatest number of glacial earthquakes to the combined catalog of events recorded by *Tsai and Ekström* [2007] and *Veitch and Nettles* [2012] (Chapter 2 of this dissertation): Helheim Glacier, Kangerdlugssuaq Glacier, Jakobshavn Isbræ, and Kong Oscar Glacier.

3.2.1 Earthquake Source Parameters

We use glacial-earthquake locations and active-force orientations from 179 glacial earthquakes occurring in 1999–2010 as the basis of our analysis. We obtain these parameters from the previously published solutions of *Tsai and Ekström* [2007] and *Veitch and Nettles* [2012]. Both studies use intermediate-period surface waves obtained from globally distributed stations and invert for centroid-single-force source parameters [*Kawakatsu*, 1989] using a methodology similar to that routinely employed for tectonic earthquakes of similar magnitudes [*Ekström et al.*, 2012].

Glacial-earthquake active-force orientations are reported in the source publications with azimuths ranging from -180° to $+180^\circ$ east of north. *Veitch and Nettles* [2012] identified an 180° degree ambiguity in the active-force orientations. We therefore simplify the published results and express all angles as positive, ranging from 0° to $+180^\circ$ i.e., glacial earthquakes with a reported active-force azimuth of -45° may be expressed as 135°.

The glacial-earthquake locations we use have a mean error of 15 km [*Veitch and Nettles*, 2012], which is large in comparison to the glaciers' dimensions. We therefore consider multi-year mean glacial-earthquake locations in our analysis. We first determine annual mean earthquake locations at each glacier for each year of our study period, we then calculate a multi-year mean location, weighting the annual means by the number of glacial earthquakes occurring in each year. We

compute the multi-year mean locations for four, non-overlapping time periods consisting of the years 1999–2001, 2002–2004, 2005–2007, and 2008–2010.

The locations show systematic offsets from their true locations because of inaccuracies in the earth model utilized for the seismic inversion [*Smith and Ekström*, 1997; *Veitch and Nettles*, 2012]; this is visible in Figure 3.3 for Helheim Glacier, where event locations are systematically biased to the northwest. As we are only interested in variations in glacial-earthquake source location in the direction of each glacier's retreat or advance, we wish to eliminate the systematic location bias before proceeding with our analysis. We determine the geographic center line of each glacier from satellite imagery and project the mean locations onto this line. We then describe these projected positions as relative positions along that line. We define the origin (0 km) as the multi-year mean location for the years 1999–2001, with inland motion (the direction of glacier retreat) defined as positive, and seaward motion (the direction of glacier advance) defined as negative.

The steps in this processing are shown graphically in Figure 3.3 for one of the four glaciers we consider in this study (Helheim Glacier). The upper panel shows the source location of each event associated with Helheim Glacier and considered in this study. The active-force orientation for each event is indicated by sticks. The locations shown in the upper panel are colour-coded by their year of occurrence; in the lower panel, the weighted mean locations for those same time periods are coloured correspondingly. Also shown in the lower panel (dashed orange line) is the center line of the glacier. The projection of the multi-year mean locations onto that line are indicated by arrows plotted from each mean location to its projection onto the center line.

3.2.2 Calving-Front Orientation

We measure the glacier calving front from Landsat 7 imagery, which is available starting in 1999 and remains available for the duration of our study period. We use the pan-chromatic band, which has a ground resolution of 15 m. We selected Landsat 7 imagery because of its high resolution, good temporal coverage throughout the year, and ease of access. While other satellites, notably MODIS, provide imagery with higher temporal resolution, and with spatial resolution

sufficient to accurately determine calving-front position, the higher spatial resolution offered by Landsat 7 is required in order to obtain measurements of sufficient precision for accurate determination of calving-front orientation. The temporal resolution offered by Landsat 7 is sufficient for our primary purpose of establishing trends and assessing variability in calving-front orientation. Imagery obtained by Landsat 7 after May 31, 2003 contains unimaged sections due to the failure of the instrument's scan-line-corrector (SLC). The presence of unimaged sections affects our ability to obtain measurements in some cases, which will be discussed in more detail as they arise.

For each glacier, we select the time period for which we estimate the calving-front geometry based on a combination of image availability and the timing of glacial-earthquake occurrence. The latest date for which published glacial-earthquake source parameters are available is 2010. For Helheim Glacier and Kangerdlugssuaq Glacier, we consider all available imagery from 1999–2010. At Kong Oscar Glacier, the onset of glacial-earthquake production occurred in 2002 [*Veitch and Nettles*, 2012] and we consider imagery from 2002–2010. Earthquake occurrence at Jakobshavn Isbræ has been sporadic, and for this glacier we restrict our analysis to years after 1999 in which glacial earthquakes were recorded, and we analyze imagery only from months during which glacial earthquakes occurred, along with the preceding and following months.

We begin by selecting Landsat 7 scenes that completely contain the calving front and are relatively free of cloud cover (an example of which can be seen in Figure 3.4A). We then manually digitize the calving front in each image, selecting as many points as necessary to capture the shape and position of the front, leaving generally not more than 100 m between points. We exclude portions of the calving front that are obscured by scan-line-corrector errors, rather than interpolating across them, and we exclude sections of the calving front within 500 m of the fjord walls. An example of a digitized calving front is shown in Figure 3.4B; Figure 3.3 shows all of the calving fronts digitized at Helheim Glacier for this study.

We chose to exclude the marginal sections of the calving front (within 500 m of the fjord walls) because we believe that slow, thin ice is unlikely to play an important role in glacial-earthquake seismogenesis. Additionally, these portions of the calving front often lack a clearly identifiable

transition from glacier ice to ice mélange, making it difficult to precisely digitize the calving front. However, in the case of Kong Oscar Glacier, we include sections of the glacier closer to the south-eastern edge of the calving front. The far-southeast portion of Kong Oscar's calving front does not appear to be stagnant, is one of the most variable sections of the glacier's calving front, and may be precisely digitized.

Scan-line-corrector errors are of particular concern in imagery of Kong Oscar Glacier and the Northern Ice Stream of Jakobshavn Isbræ. In these locations, scan-line errors are nearly parallel to the calving fronts in images where they occur, and may obscure considerable portions of the calving front. In some such cases, the position of the calving front can be reasonably determined to within the width of the scan-line error, but it is not possible to accurately assess the orientation of the calving front, and we exclude these images from our analysis. In imagery of Helheim, Kangerdlugssuaq, and the Southern Ice Stream of Jakobshavn, scan-line errors are nearly perpendicular to the calving fronts (as seen in Figures 3.4E,F). Thus, while imagery at these fronts may have multiple errors impinging on the calving fronts, their effect on our ability to accurately access the calving-front orientation is small.

The digitized calving fronts are initially collected and recorded as a series of segments defined by start and end points, such that more complex sections of the calving front are recorded with a greater number of points, and would bias our fit toward these sections without interpolation. To measure the orientation of each digitized calving front we first interpolate the digitized sections of the calving front, excluding sections affected by scan-line corrector errors, so that the digitized calving front is recorded as a series of X, Y coordinates with 1 m separation between each point. We then fit a small number of straight lines to the interpolated calving front using an orthogonal linear regression in order to quantify the orientation of the calving front in each image, as shown in Figure 3.4C. We then report the orientation of the calving front as the normals of the lines fit to the calving front.

The calving fronts of Helheim, Kangerdlugssuaq, and Kong Oscar Glaciers are commonly more retreated in the center than at the margins, resulting in a calving front that is concave

downglacier. This shape makes it difficult to fit a single line to the calving front in most cases. After a series of trials, we found that fitting a maximum of two lines to the calving front provided the best compromise between completeness and simplicity in characterizing the orientation of the calving fronts. In cases where two lines were used, the point separating those two lines was first automatically determined as the most retreated point along the calving front. This selection was then reviewed, and shifted slightly in some cases (for example, if a small 'bite' out of the calving front that is generally not representative of the broader shape of the calving front was automatically selected). This point is not fixed between scenes, and varies in cross-flow position as the shape of the glacier changes, as seen in Figures 3.4C & E. We thus report two angles, one for the northern or western section of the calving front, and one for the southern or eastern section. In a small number of cases, the calving front was better characterized by a single line or returned two orientations that were nearly identical. In those cases, we report a single value for the calving-front orientation.

The calving front of Jakobshavn Isbræ can also be broadly described as having a concave downglacier shape. However, Jakobshavn is significantly wider and more complicated than the calving fronts of the other glaciers discussed in this study, particularly after the calving front retreated inward of it's fjord. There are two clearly identifiable regions of high-velocity ice flow at Jakobshavn, terminating at distinct calving fronts. This makes it possible to identify two separate regions of probable high calving flux at Jakobshavn. Thus, after 2005, we treat Jakobshavn as having two distinct calving fronts, and fit each section of Jakobshavn separately.

3.2.3 Calving-Front Position

We consider temporal trends in calving-front position using the same digitized calving fronts from which we obtained information on calving-front orientation. To simplify the analysis, we estimate a single, representative position for each measured calving front. We first find all points that lie within 1.5 km of the geographic center line (Section 3.2.1) of the glacier. We then find the mean position of those points. Due to asymmetry in the calving front, in many cases the mean position lies slightly off the geographic center line. In order to correct for this we project the mean

position onto the geographic center line, and record this as the position of that digitized calving front. This correction is nearly always less than a few 10s of meters in the along flow direction.

After determining the position of each measured calving front, we compute annual and multi-annual means of these positions. The annual mean is calculated as a simple arithmetic mean. In order to calculate the multi-annual mean, we weight the annual mean positions by the number of glacial earthquakes occurring in each year for a direct comparison with the mean earthquakes locations. We use the same four non-overlapping time periods that we use for glacial-earthquake source locations (1999–2001, 2002–2004, 2005–2007, and 2008–2010). An example of mean calving-front positions are shown for Helheim Glacier in the upper panel of Figure 3.3. We express the calving front positions to relative distances along the geographic center line, as for the earthquake locations, and define the 1999–2001 mean calving-front position as 0 km. Calving-front retreat results in positive positions, and advance in negative positions, following the sign conventions adopted earlier.

3.3 Results

We measured calving-front orientation and position at four glaciers during the time period 1999–2010, obtaining observations from more than 250 images at both Helheim Glacier and Kangerdlugssuaq Glacier, $\sim$100 images of Kong Oscar Glacier, and $\sim$70 images of Jakobshavn Isbræ. The results of our calving-front measurements are plotted in Figure 3.5, and our position measurements are plotted in Figure 3.6.

3.3.1 Calving-Front Orientations

At Kangerdlugssuaq Glacier, (lower-left panel of Figure 3.5), we observe calving-front orientations between 60° and 180°, with most of the measurements in the range of $80^\circ - 180^\circ$. There is no observable trend in the calving-front orientations at Kangerdlugssuaq. The annual range is consistently $\sim 100^\circ$, with little variation from year to year.

At Helheim Glacier (upper-left panel of Figure 3.5) the measured calving-front orientations range from 60° to 160°, with most falling between 80° and 140°. The orientations show a temporal trend, with the median calving-front orientation increasing by ∼10° between 1999 and 2007, and then remaining nearly constant from 2007 to the end of the study period. The nature of the change is different between the northern and southern sections of the calving front. The northern portion increases smoothly in both range and maximum orientation angle. The southern also shows an increase in maximum angle, but as a sharp increase in 2003. During most years, the measured calving-front orientations are fairly tightly clustered with annual ranges of between 40° and 50°. The range is notably larger, reaching as much as 90°, during several years in the early-2000s, most notably in 2005.

At Kong Oscar Glacier (upper-right panel of Figure 3.5), we observe orientations ranging from -20°(160°) to 70°, with an annual range of ∼60° degrees. The shape of the calving front remained notably stable throughout the study period, and there is no clearly observable trend in the calving-front orientations at Kong Oscar glacier.

Jakobshavn Isbræ (bottom-right panel of Figure 3.5) has a complicated calving-front geometry, with at least two highly active regions of calving. These two regions are measured independently and represented with different symbols in Figure 3.5. The two regions of Jakobshavn we measured result in calving-front orientations that span nearly the full 180° of possible orientations, but which fall into two distinct ranges separated by gaps of ∼40° & ∼20°. The group containing orientations between 60° and 160° represents the southern section of the glacier. The group containing orientations predominantly between 0° and 40° represents the northern section of the glacier. Neither calving front shows an identifiable trend in its orientations during the study period.

3.3.2 Calving-Front Position

In Figure 3.6, we plot the weighted-mean calving-front position for each time period examined at each glacier as well as the range of positions measured over that time period. For Helheim Glacier, Kangerdlugssuaq Glacier and Jakobshavn Isbræ we define the weighted-mean position

for 1999–2001 as 0 km, and for Kong Oscar Glacier we define the weighted-mean position from 2002–2004 as 0 km.

Kangerdlugssuaq and Helheim Glaciers, shown in the top two panels of Figure 3.6, exhibit very similar position records in our analysis. Both glaciers reached to a maximum retreat of $\sim$5 km in the 2005–2007 time period, and then advanced again slightly in the 2008–2010 time period. Helheim shows very little variation in its position in the first time period (1999–2001), while Kangerdlugssuaq shows more; both glaciers also show 3–5 km of variation in their position in each of the time periods after 1999–2001. For Helheim Glacier, the individual calving fronts as well as the multi-annual means are also shown in Figure 3.3.

Kong Oscar Glacier, shown in the third panel of Figure 3.6, shows the least variability of the four glaciers we considered, both in multi-annual mean position and in multi-annual range. Kong Oscar was at its most advanced during the earliest period we studied (2002–2004). Prior to 2002, the terminus of Kong Oscar was a diffuse floating tongue, unconstrained by a fjord. Consistent with the presence of a floating tongue, the glacier did not produce glacial earthquakes during that time. The terminus of Kong Oscar retreated steadily by $\sim$1.5 km during the study period, a small variation compared to the other glaciers in this study, and indeed to many other glaciers in Greenland [*Moon and Joughin*, 2008]. The range of observed positions was also consistently less than $\sim$1.5 km.

Jakobshavn Isbræ, shown in the bottom panel of Figure 3.6 exhibits the largest retreat — greater than 10 km — of the four glaciers we study here. Much of that retreat took place during the 2002–2004 time period, which is not addressed here due to the lack of glacial earthquakes during that time period. The very small range of positions during the 1999–2001 time period is due to the comparatively small number of measurements from that time period, and does not necessarily represent an immobile calving-front position during those years. During the later two time periods of this study Jakobshavn continued to retreat, with a $\sim$3 km annual range in observed positions.

3.4 Discussion

3.4.1 Calving-Front Orientation

3.4.1.1 Kangerdlugssuaq Glacier

Kangerdlugssuaq Glacier presents the simplest case of the glaciers considered in this study. The range of active-force orientations from the earthquake data and the calving-front orientations are similar throughout the study period. This consistency encompasses a period of rapid retreat [*Joughin et al.*, 2008a] and increased glacial-earthquake activity [*Tsai and Ekström*, 2007; *Veitch and Nettles*, 2012]. Despite some potential complexities in the shape of the fjord, we see no effect of the retreat on the calving-front or active-force orientations. As Kangerdlugssuaq retreats, its fjord widens and the calving front grows to include ice from an embayment on the northern side of the glacier, increasing the length and range of potential orientations of the calving front. The retreat of the glacier also exposed two small former tributary glaciers to the ocean on the southern side of the fjord, potentially altering the glacier's flow field, and also potentially creating a new, independent source of calving events.

Both of these glaciers, if responsible for glacial earthquakes, would be expected to produce events with active-force orientations of $\sim 20^{\circ}$. However, no events with that orientation are recorded (and we have not measured the calving-front orientations of these glaciers). We conclude that none of the glacial earthquakes were generated by these smaller glaciers simply because of their small size, thus their calving events are simply too small to generate globally observable glacial earthquakes.

Any glacial earthquake from the portion of Kangerdlugssuaq's calving front contained within the northern embayment would also be expected to produce active-force orientations of $\sim 20^{\circ}$. The lack of glacial earthquakes from that section of the calving front is not unexpected after our review of many satellite images; the ice in the embayment appears stagnant, and the position and orientation of the portion of Kangerdlugssuaq's calving front contained within the embayment barely change over many months.

Thus, our analysis shows that variations in the geometry of the central portion of Kangerdlugssuaq's calving front are sufficient to explain the range of observed glacial-earthquake active-force orientations throughout the study period. Kangerdlugssuaq's calving front does not show a change in orientation in response to the rapid retreat that transpired during the study period.

3.4.1.2 Helheim Glacier

One of the catalysts for this study was the observation by *Veitch and Nettles* [2012] of a trend in the active-force orientations of the CSF source parameters at Helheim Glacier (Figure 3.2, upper-left panel of Figure 3.5). The observed force azimuths increase from 1999 to 2005, and level off after 2005. Nearly all of the active-force orientations prior to 2005 are less than the 1999–2010 average orientation of $\sim$105° while nearly all of the active-force orientations after 2005 are larger than this value. The year of 2005 itself shows an atypically large range of active-force orientations. These changes coincide with a calving-front retreat [*Joughin et al.*, 2008a] and increase in glacial-earthquake production [*Tsai and Ekström*, 2007; *Veitch and Nettles*, 2012]. As can be seen in Figure 3.5, the temporal trend in the calving-front orientations we measure is similar to the trend in active-force orientations. This suggests that changes in glacial-earthquake active-force orientations represent true physical changes at the glacier.

However, the trend in calving-front orientations is less pronounced and the change in orientations around 2005 is less abrupt than the trend in the earthquake data. The gradual increase in the angle of the active-force orientations prior to 2005 is mirrored by a gradual increase in the angle of the calving-front orientations. Prior to 2005, the active-force orientations at Helheim agree well with the range of calving-front orientations measured from the southern portion of the calving front. After 2005 the active-force orientations fall almost exclusively within the range of calving-front orientations measured from the northern portion of Helheim's calving front. Our data therefore suggest that the primary source of seismogenic calving events shifted from the southern to the northern section of the glacier following 2005.

Several important changes in Helheim's behaviour occurred in 2005. Between 2000 and 2005,

Helheim retreated nearly 10 km and accelerated significantly [*Howat et al.*, 2005; *Joughin et al.*, 2008a], while the number of glacial earthquakes nearly doubled annually [*Tsai and Ekström*, 2007]. However, in 2006, the glacier showed dramatic reduction in the number of glacial earthquakes [*Veitch and Nettles*, 2012] and the calving front readvanced somewhat [*Joughin et al.*, 2008a]. The full range of dynamic changes which must have been required to affect a change in the source of seismogenic calving events is beyond the scope of this paper, but we note that the variations in the cross-flow grounding state of Helheim's terminus were observed by *Murray et al.* [2015b] during the summer of 2013. *Murray et al.* [2015b] observed that south of a mid-glacier medial moraine, the glacier was securely grounded while north of this moraine the lowest several hundred meters of the glacier was ungrounded. The observation of differing states north and south of a glacier dynamic feature (a medial moraine) support the idea that dynamic differences may exist between two regions of the same calving front; such a difference may have led to the apparently preferential occurrence of glacial-earthquakes from the northern section of Helheim's terminus following 2005.

3.4.1.3 Kong Oscar Glacier

At Kong Oscar Glacier (upper-right of panel of Figure 3.5) the overall agreement between the calving-front orientations and the glacial-earthquake force orientations is good. However, we note a feature that warrants further discussion: the presence of two distinct groups of active-force orientations that appear to be outliers with respect to the majority of the active-force orientations at Kong Oscar, and are not well explained by any of the calving-front orientations we measured.

The glacial earthquakes with outlier active-force orientations fall into two distinct groups. The first group is comprised of two events with active-force orientations of $\sim$90° that occurred in 2007. The second group is comprised of three events with active-force orientations of $\sim$120° with one event occurring each year from 2007 to 2009. Both of these groups events fall well outside the range of calving-front orientations we measured at Kong Oscar Glacier, and are evident as outliers in the earthquake data [*Veitch and Nettles*, 2012]. *Veitch and Nettles* [2012] reviewed these events

and found them to be unremarkable from a seismological standpoint. The quality of fit of the observed waveforms to synthetic waveforms generated using the event source parameters is typical of the events located at Kong Oscar in that study, as are the event sizes and locations.

The first group of events, with the $\sim$90° active-force orientations, are less problematic. These two events do lie outside the range of observed calving-front orientations at Kong Oscar, but are only $\sim$20° from calving-front orientations observed during the years preceding and subsequent to their occurrence. Scan-line-corrector errors pose a larger problem at Kong Oscar than at any of the other glaciers we consider, and in 2007 in particular, there were a large number of images in which only the western portion of the glacier's calving front were measurable. The eastern portion of the calving front appears to be responsible for most of the glacial earthquakes at Kong Oscar glacier, and has shown the orientations closest to those observed ($\sim$90°) for these events. It is therefore possible that the calving front may have achieved such an angle, and that we simply did not observe it in any of the usable imagery.

However, in the case of the second group of events — those with orientations of $\sim$120° — the preceding explanation cannot be reasonably invoked. These three events have angles that are nearly perpendicular to the median orientation ($\sim$50°) of the calving front, and lie more than 60° from any observed calving-front orientation in the years prior to or following their occurrence. The only identifiable feature associated with Kong Oscar Glacier that shows an orientation similar to what would be expected for these events is a small secondary calving front on the south-east side of Kong Oscar Glacier, which meets a bay to the east of Kong Oscar roughly 2 km from the glacier's calving front. This small secondary front is slow flowing and disconnected from the glacier's main flow field [*Ahn and Howat*, 2011], and is therefore unlikely to be the source of any glacial earthquakes. Our investigation shows no evidence to suggest that secondary front plays any significant role in ice loss at Kong Oscar Glacier. We have to, therefore, consider the possibility that the source parameters for these events are incorrect. While the CSF inversion scheme as applied by *Tsai and Ekström* [2007] and *Veitch and Nettles* [2012] appears to be robust in the vast majority of cases, it is possible that some combination of factors has resulted in erroneous active-

force orientations for these few events at Kong Oscar Glacier. In particular, if these earthquakes are complex or involve multiple subsequent calving events, the simple CSF representation used by *Tsai and Ekström* [2007] and *Veitch and Nettles* [2012] may be inadequate for capturing the earthquake source parameters accurately. We note also that Kong Oscar is not a particularly well studied glacier, and the limited literature that is available suggests several other unique characteristics of the glacier. *Bevan et al.* [2012] found that Kong Oscar's flow speed remained remarkably stable over a more than 20 year period, despite experiencing thinning and retreat, which are strongly correlated elsewhere with increases in flow speed. They attribute this to a front-geometry that led to an atypical stress response of the glacier to ice loss at the calving front. *Enderlin and Howat* [2013] found that Kong Oscar's rate of submarine melting at the calving front was higher than that of its neighbours, and increasing more rapidly. We believe continued investigation of Kong Oscar's dynamics would be fruitful and warranted, and might provide further insights into the dynamics of calving there, possibly elucidating the cause of the force orientations of these events.

3.4.1.4 Jakobshavn Isbræ

The geometry of Jakobshavn Isbræ (lower-right panel of Figure 3.5) is the most complicated of the four glaciers discussed here. In the late 1990's, when Jakobshavn first produced glacial earthquakes, its calving front consisted of a single, wide terminus contained within a fjord, similar to the morphology of the other glaciers discussed here. The glacier then ceased to produce glacial earthquakes for a number of years, during which time the glacier retreated beyond its simple fjord. The terminus geometry evolved into a complex and very broad region where calving occurs primarily at regions of fast flow which are separated from the rest of the terminus by shear margins. We identified and analyzed the two sections of Jakobshavn's terminus that appear most active, and most likely to produce seismogenic calving events. The southern section, which is also shown in Figure 3.4, typically exhibits calving front orientations of $\sim$110°, while the northern section (not shown in Figure 3.4) exhibits azimuths of $\sim$30°.

We have only a handful of images from 1999, the time period during which Jakobshavn was

defined by a single wide calving front. However, the orientations we measure from those images are consistent with the active-force orientations of glacial earthquakes occurring during that period (Figure 3.5). Two earthquakes in 1999 show azimuths $\sim 20^{\circ}$ different from the measured calving fronts, but occurred more than a month before Landsat 7 imagery became available, during which time the shape of the calving front is likely to have changed.

When Jakobshavn began producing glacial earthquakes again in 2005, the glacier's complex terminus allowed the possibility of seismogenic calving from calving fronts with a wide range of orientations. Most of the active-force orientations observed at Jakobshavn Isbræ fall within the range of calving-front orientations measured on the southern terminus region of the glacier. No force orientations fall within the range of measured orientations for the northern terminus region, suggesting that no glacial earthquakes occur at the northern terminus. This observation is consistent our qualitative assessment of the northern terminus calving front: the northern region exhibits much slower changes in position than does the southern section and it often lacks the sharp, clearly defined calving front that is present at other glacial-earthquake producing glaciers.

A small number of events recorded in 2008 and 2009 fall between the two groups of calving-front orientations from the two distinct calving fronts. We believe there are two possible explanations for these events. Firstly, as Jakobshavn's terminus has continued to retreat, the central sections of the calving front have retreated faster than the margins. As a result the central, most-active region of the calving front is bordered by only slightly less active-appearing regions of ice, that might also produce seismogenic calving events. We were able to accurately measure the central and most active-appearing regions of the calving front, but not the regions bordering it. It is possible that one of these regions may have been the source of these three glacial earthquakes.

Secondly, field observations of large calving events at Jakobshavn Isbræ [*Amundson et al.*, 2008] shows that calving events of the scale expected to produce glacial earthquakes often involve the capsize of multiple icebergs along large sections of Jakobshavn's calving front. The seismic analysis of glacial earthquakes [*Tsai and Ekström*, 2007; *Veitch and Nettles*, 2012] assumes a single source, and in the case of a source comprised of multiple capsizing icebergs, it is probable that the

source parameters obtained from seismic analysis contain larger errors than they otherwise would. As these events are only $\sim 30^{\circ}$ outside of the range of observed calving-front orientations, we believe it is most likely that the three events occurred at the southern terminus, like the other events for which the force azimuths closely match the measured terminus orientations. The southern section of Jakobshavn Isbræ is clearly the source of the majority of glacial earthquakes occurring at the glacier.

3.4.2 Position

Based on a preliminary comparison, *Veitch and Nettles* [2012] noted that changes in multi-year averages of glacial-earthquake position seemed to correspond to changes in the position of the source glacier's calving front. Using the calving-front positions that are a by-product of our orientation analysis, we confirm that initial finding for the four glaciers studied here. Figure 3.6 shows the multi-annual mean position of the glacial earthquakes for each glacier and time period, as well as the standard deviations for those mean positions.

Changes in the position of the calving front are reflected well in changes in the position of the mean glacial-earthquake locations. Retreats in the calving-front position correspond to retreats in the mean earthquake locations at all glaciers, and the range of observed positions overlaps within standard deviations in the earthquake positions. Even very limited retreats, such as those seen at Kong Oscar Glacier, are reflected in changes in the mean position of the glacial-earthquakes. In general the scale of the changes in location of the glacial earthquakes is consistent with the true changes in the positions of the calving fronts.

Our purpose in discussion of this finding is not to advocate the use of glacial-earthquake source locations as a primary means to track the position of glacier calving fronts; clearly existing satellite remote-sensing datastreams are vastly superior for such a task. Rather, we believe that the fact that glacial-earthquake source locations are sensitive to kilometer-scale changes in the location of their source supports the reliability of the use of these locations to associate glacial earthquakes with their source glaciers. Because the occurrence of glacial earthquakes at a glacier does provide

otherwise-difficult-to-obtain information on that glacier's dynamic behaviour at the time of the glacial earthquake, it is important to confirm the validity of the practice of determining the source glacier base primarily on the event's source location.

3.5 Conclusions

We have compared estimates of calving-front geometry from satellite imagery with glacial-earthquake source parameters obtained from seismic analysis using a centroid-single-force approach. We find good agreement between earthquake force azimuths and the measured orientations of the calving fronts, consistent with the interpretation that calving events transferring momentum to the calving fronts are the source of glacial earthquakes. Changes in the earthquake force orientations track changes in calving-front orientations over time. Observed variations in active-force orientation in glacial-earthquake source parameters thus appear to represent true variability in geometry at the source glaciers rather than errors in the seismic analysis.

Despite its simplicity, the CSF source model allows for accurate estimation of calving-front orientation at the time of glacial earthquakes. The distribution of calving-front and active-force orientations also indicates that glacial earthquakes typically emanate from the central, most active, section of the glacier calving front. At the glaciers we examined, there is a preferred section of the calving front for production of seismogenic calving events. In some cases, as at Helheim Glacier, the preferred region changes over time. In a small number of cases, inferred force orientations differ substantially from observed calving front geometries. The simple CSF source model may not be adequate in these cases, and such events warrant further study.

Location estimates for individual glacial earthquakes contain both systematic and random errors, but are good enough to allow correct verification of the source glacier. When the same glacial-earthquake centroid locations are averaged over multiple events to reduce location errors, we find that true changes in earthquake location due to movement of the calving front over time explain a large portion of the variability present in glacial-earthquake locations.

Our results show that variations in estimates of glacial-earthquake source parameters derived from centroid-single-force analysis reflect true variability in the geometry of the calving front at the source glacier. This finding represents an important step forwards in out understanding of glacial-earthquakes. It allows us to better apply glacial-earthquakes as a tool for remote study of marine-terminating glaciers in Greenland, and improves our understanding of the physical processes underlying glacial-earthquake seismogenesis.

3.6 Figures

Figure 3.1: An example of a glacial earthquake with the source region identified by *Walter et al.* [2012a]. This image shows the calving front of Jakobshavn Isbræ after a seismogenic calving event, while the prior calving front is indicated in yellow. The angle perpendicular to the prior calving front is indicated by the blue arrow, while the force orientation as determined by *Veitch and Nettles* [2012] is indicated in orange. This image contains only the southern portion of Jakobshavn Isbræ discussed in this study.

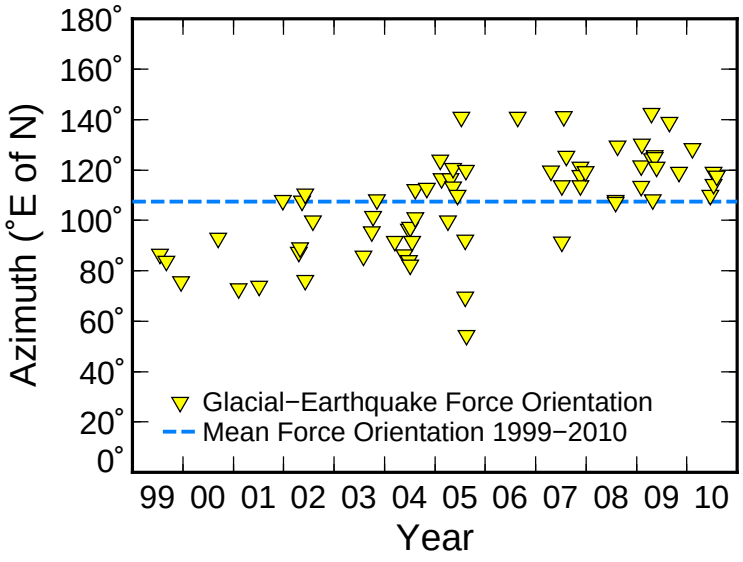

Figure 3.2: Glacial-earthquake active-force orientations as determined by teleseismic waveform inversion for events at Helheim Glacier 1999–2010 [*Tsai and Ekström*, 2007; *Veitch and Nettles*, 2012]. Dashed line shows mean force orientation for this time period.

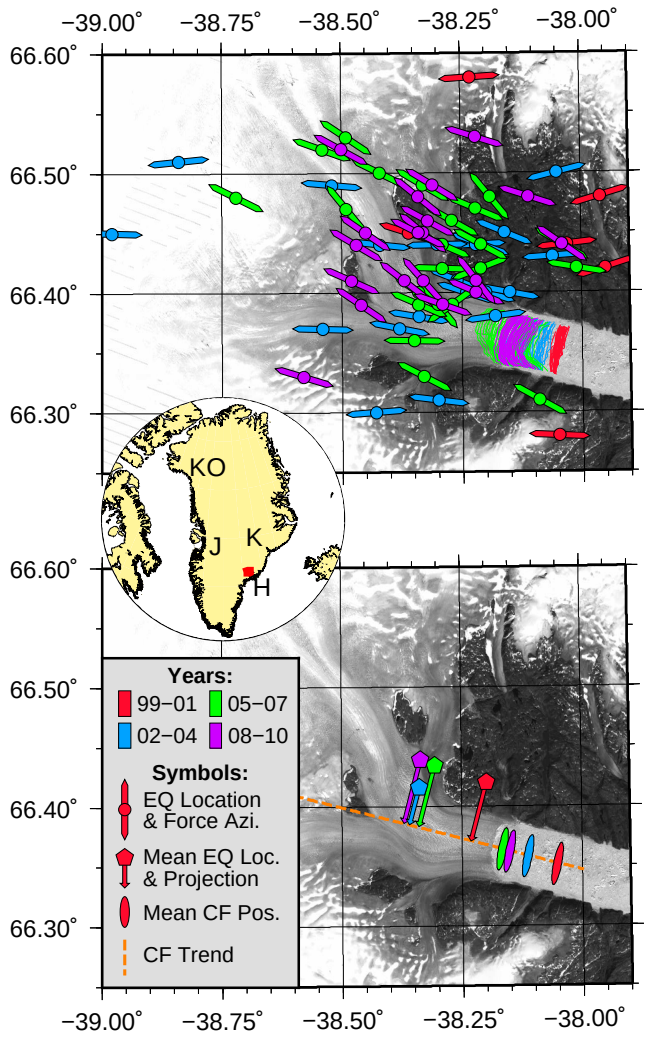

Figure 3.3: (Top) Glacial-earthquake locations, active-force orientations and calving-front positions for Helheim Glacier 1999–2010, colour coded by year. (Bottom) Mean earthquake locations and calving-front positions for the four three-year periods discussed in this paper (1999–2001, 2002–2004, 2005–2007, and 2008–2010). The dashed line represents the approximate center line, and arrows show the projections of the mean earthquake locations onto that line. (Middle) Location of map area shown in the top and bottom panels in Greenland (Helheim Glacier (H)), as well as the locations of the other glaciers discussed in this study: Kong Oscar Glacier (KO), Kangerdlugssuaq Glacier (K) and Jakobshavn Isbræ (J).

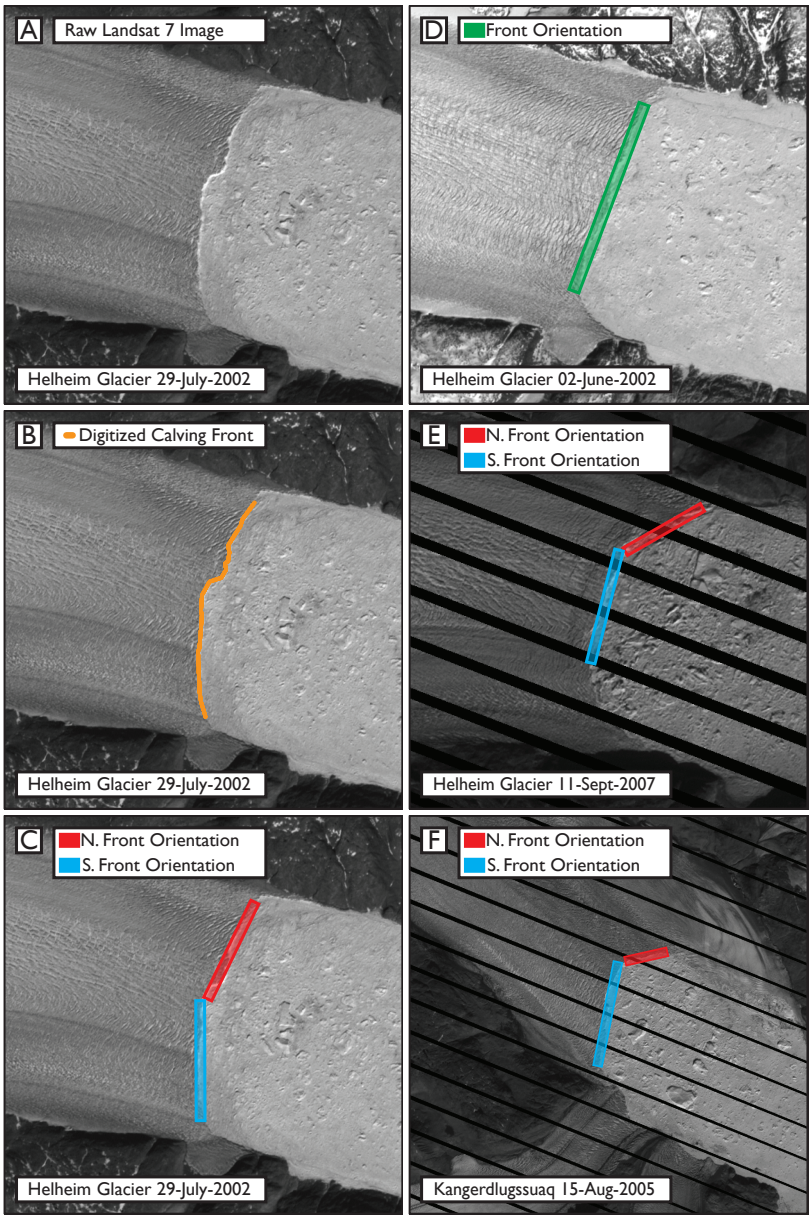

Figure 3.4: The process of digitizing a calving front and calculating its orientation are shown in A–C, and additional examples are shown in D–F. (A) The base image prior to processing. (B) The digitized calving front. (C) Two sections of the calving front for which we calculated orientation separately. (D) A calving front well-described by a single angle. (E) In this image, the southernmost sections of the calving front lack a clear transition from glacier to mélange and have been excluded from the analysis. Scan-line-corrector errors are present in this image. (F) An example from Kangerdlugssuaq Glacier showing the exclusion of slow ice from the embayment to the north of the glacier. The scale of images A–E is consistent, where the highlighted portion of the calving front in C is $\sim$5.5 km, and the highlighted segment in F is $\sim$5.0 km.

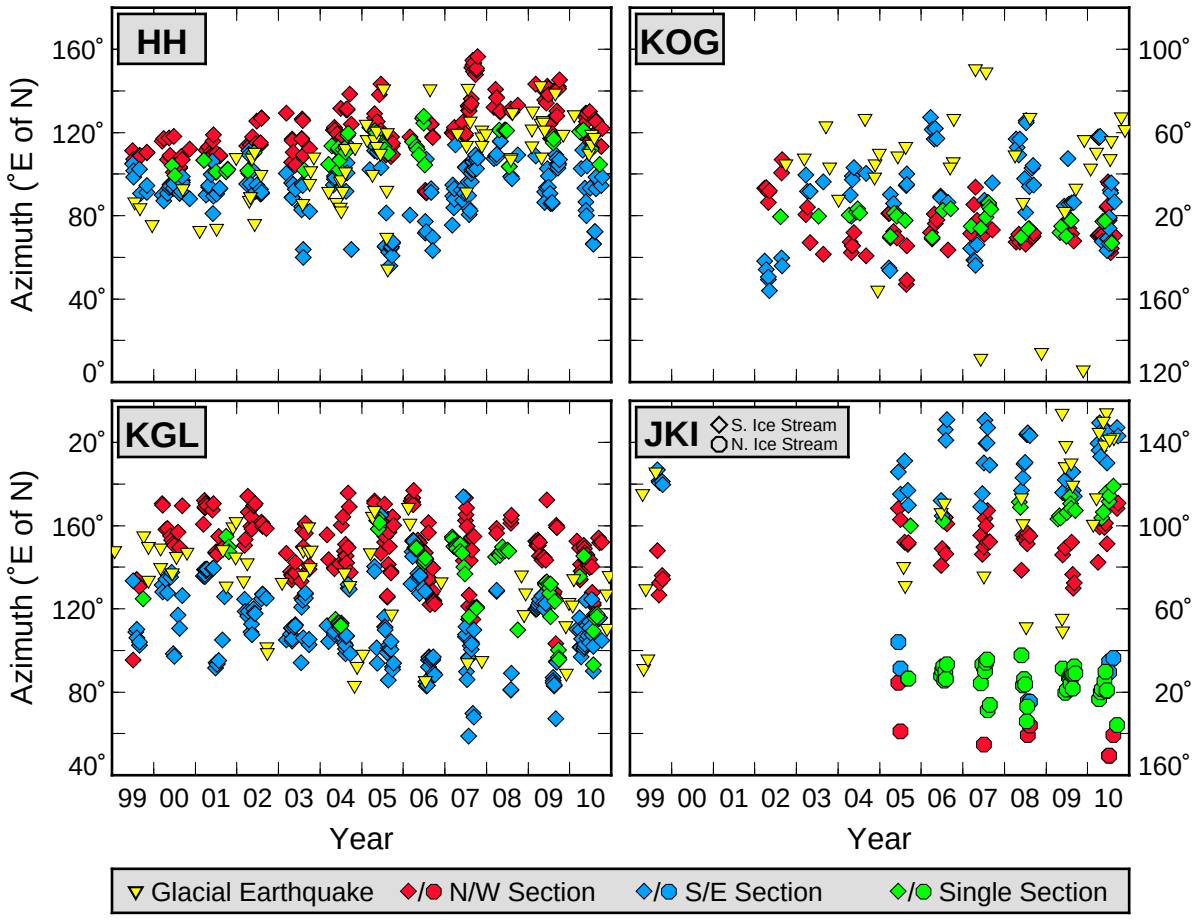

Figure 3.5: Comparison of glacial-earthquake active-force orientations and measured calving-front orientations for four glaciers: Kangerdlugssuaq Glacier (KGL), Helheim Glacier (HH), Kong Oscar Glacier (KOG) and Jakobshavn Isbræ (JKI). The calving-front orientation is given as the normal to the calving front, as discussed in the text.

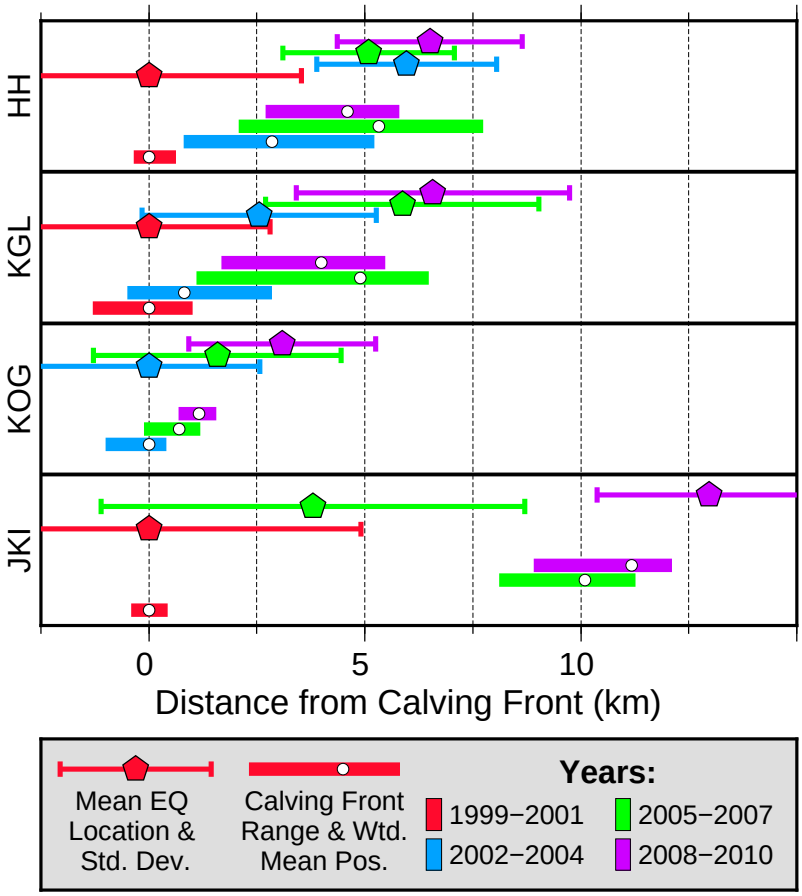

Figure 3.6: Comparison of changes in mean earthquake location and weighted mean calving-front position. Positions are relative, with the mean for the first time period set to zero. Mean earthquake locations are projected onto the glacier center line.

Chapter 4

Local Seismicity of Helheim Glacier

4.1 Introduction

The Greenland Ice Sheet is the second largest body of fresh-water ice on Earth and has been losing mass at an increasing rate [e.g., *Rignot et al.*, 2008; *Velicogna*, 2009; *Zwally et al.*, 2011; *Shepherd et al.*, 2012; *Enderlin et al.*, 2014]. A significant portion of this mass is lost through dynamic processes at the ice sheet's many marine-terminating outlet glaciers [*van den Broeke et al.*, 2009], where calving accounts for the majority of mass loss [*Enderlin and Howat*, 2013]. As these glaciers have retreated due to atmospheric [*Box and Cohen*, 2006; *Hanna et al.*, 2008] and oceanic [e.g., *Howat et al.*, 2008; *Straneo et al.*, 2010] warming, an increasing number have lost floating tongues and now have near-grounded or grounded termini [*Howat et al.*, 2007; *Joughin et al.*, 2008a; *Veitch and Nettles*, 2012; *Walter et al.*, 2012a]. At near-grounded glaciers, calving is dominated by full-glacier-thickness icebergs several ice-thicknesses wide [*Amundson et al.*, 2008; *Veitch and Nettles*, 2012; *Bassis and Jacobs*, 2013]. These icebergs are larger in height than along-flow length, and capsize due to their gravitationally unstable shape [*MacAyeal et al.*, 2003; *Amundson et al.*, 2010]. Understanding the factors that influence and drive these calving events is crucial for understanding the future behaviour of the outlet glaciers of the Greenland Ice Sheet [e.g., *Benn et al.*, 2007; *Nick et al.*, 2009].

The importance of understanding the dynamics of the calving process in Greenland and elsewhere has led to a wide range of techniques, utilizing both remote-sensing and *in situ* data, being applied to the study of calving glaciers. In this study, we report observations of high-frequency seismicity from a major outlet glacier in Greenland. Seismology is not a new tool to glacier researchers [e.g., *Neave and Savage*, 1970; *Wolf and Davies*, 1986; *Qamar*, 1988], but recent years have seen increasing application of seismology to questions of glacier behaviour [e.g., *Smith*, 2006; *Bassis et al.*, 2007; *O'Neel et al.*, 2007; *Walter et al.*, 2009; *West et al.*, 2010; *Dalban Canassy et al.*, 2013]. At many glaciers, capsizing-type calving events produce globally observable surface waves in seismic events known as glacial earthquakes [*Ekström et al.*, 2003; *Tsai and Ekström*, 2007; *Nettles and Ekström*, 2010; *Veitch and Nettles*, 2012]. Observation and study of these moderate magnitude ($M_S \sim 5$) glacial earthquakes has produced advances in our understanding of the dynamics of the calving process and illustrated ongoing changes in the dynamics of Greenland outlet glaciers over intermediate time scales [e.g., *Ekström et al.*, 2006; *Tsai and Ekström*, 2007; *Amundson et al.*, 2008; *Joughin et al.*, 2008a; *Nettles et al.*, 2008a; *Veitch and Nettles*, 2012; *Murray et al.*, 2015b], and questions posed by the study of these events have helped to motivate local non-seismic observations that have provided insight into the details of the calving process and its effect on the glacier [e.g., *Nettles et al.*, 2008a; *Amundson et al.*, 2008; *Murray et al.*, 2015a].

However, there are limitations to the use of global seismology in the study of Greenland's glaciers. Global seismic observations only capture large seismic events from the largest glaciers. In order to study smaller-scale seismogenic behaviour, a more localized approach is needed. Local seismic deployments on glaciers in environments ranging from the Alps to Antarctica have proven useful in increasing understanding glacier dynamics. In Antarctica, seismic studies have addressed inland basal seismicity [e.g., *Anandakrishnan and Bentley*, 1993; *Wiens et al.*, 2008; *Winberry et al.*, 2011] and ice-shelf rift propagation [e.g., *Bassis et al.*, 2007, 2008; *Heeszel et al.*, 2014]. Seismology has also been used to study the stability of hanging glaciers in the Alps [e.g., *Faillettaz et al.*, 2008; *Dalban Canassy et al.*, 2012], and calving dynamics at marine-terminating glaciers in Alaska [e.g., *O'Neel et al.*, 2007; *Walter et al.*, 2010; *Bartholomaus et al.*, 2012]. In Greenland,

recent studies have used small networks to explore sub-glacial hydrology [e.g., *Doyle et al.*, 2013; *Röösli et al.*, 2014]. However, the seismic environment of outlet glaciers in Greenland remains relatively unexplored, particularly at higher frequencies. Local or regional studies have considered high-frequency seismicity that occurs in conjunction with calving at Jakobshavn Isbræ [*Amundson et al.*, 2008, 2010; *Walter et al.*, 2012a] and Store Glacier [*Walter et al.*, 2012b], but do not address seismicity that does not occur as part of calving or its immediate aftermath.

In this study, we consider data from a small, temporary seismic network deployed during the summer of 2009 around Helheim Glacier, a major outlet glacier in East Greenland and a prodigious producer of glacial earthquakes [*Tsai and Ekström*, 2007; *Veitch and Nettles*, 2012]. Helheim is a relatively well studied glacier, and has been the site of a significant amount of research into the dynamics of marine-terminating glaciers [e.g., *Howat et al.*, 2005; *Joughin et al.*, 2008a; *Hamilton et al.*, 2008; *Nettles et al.*, 2008a; *Murray et al.*, 2010], including several field studies that have helped to clarify the seismogenic mechanism of glacial earthquakes [*Nettles et al.*, 2008a; *Joughin et al.*, 2008a; *Murray et al.*, 2015a], and the influence of tides on glacier flow [*de Juan et al.*, 2010; *Davis et al.*, 2014]. During the period of the seismic deployment in 2009, Helheim remained near-grounded at the calving front [*Veitch and Nettles*, 2012], typical behaviour for the glacier in the years following its slight readvance in 2006 [*Joughin et al.*, 2008a] that followed several years of retreat [*Howat et al.*, 2005; *Luckman et al.*, 2006; *Stearns and Hamilton*, 2007]. Ten glacial earthquakes were reported at Helheim Glacier in 2009 [*Veitch and Nettles*, 2012], but none during our study period. We report one additional event, which occurred in the middle of our study period, here. We investigate abundant small icequakes recorded on our temporary network, and assess their relationship to calving and other processes active near the terminus of the glacier, including ocean tides.

4.2 Data

We deployed six seismometers in a temporary ($\sim$7 week) network around Helheim Glacier in Southeast Greenland (Figure 4.1, Table 4.1). The seismometers were installed at bedrock sites located on the walls of the glacial fjord or on nunataks (outcroppings of bedrock surrounded completely by glacial ice) in above-ground temporary vaults. The remote location of the study area and the expense of the helicopter transport required to access the sites necessitated a station design that was lightweight and rapidly deployable by a single individual. The stations made use of "MEVO" power and enclosure systems provided by IRIS-PASSCAL, consisting of a combined solar and battery system packed in a single suitcase-sized Hardigg case. The instrumentation at each station consisted of a CMG40T seismometer recording on a Reftek RT130 datalogger sampling at 100 Hz. Station HM03, shown in Figure 4.2, is representative of the installation of all six stations.

The stations were deployed on July 8, 2009 (day of year 189) and recovered on August 25, 2009 (day of year 237), for a total deployment period of 49 days. The data are nearly continuous through the entire deployment, with the only data gap occurring on station HM01 between August 14 (day 226) and August 24 (day 236) due to a power failure. Additionally, one of the horizontal components (HH2) of HM01 contained a large number of abrupt, high-amplitude, regularly occurring signals that are not visible on other components, and that we believe associated with an instrument problem. We exclude this component from our analysis. We limit our analysis to complete days only, using data recorded between July 9 (day 190), 00:00:00 and August 24 (day 236), 23:59:59, leaving us with 47 days of data from all stations but HM01, where we have 36 days of data.

4.3 Signal Detection and Analysis

The recorded seismograms reveal abundant seismic events, which often occur one or more times per minute. These signals appear moderately self-similar, are often emergent, have a moderate signal-to-noise ratio, and are most clearly evident at frequencies higher than $\sim$10 Hz. Examples

of the recorded seismograms are shown in Figure 4.3. We develop an automated event detector to identify such seismic signals, and apply it to generate an event catalog. We then analyze patterns observed in the catalog.

4.3.1 Detection

The first goal of our study is to develop a catalog of high-frequency seismic signals occurring during our study period at Helheim Glacier. Given the large number of signals contained in the seismograms, an automated method is required. We attempted to apply the commonly used short-term-average to long-term-average (STA/LTA) detection method, using a variety of detection parameters, to determine arrival times of seismic phases. However, the resulting catalogs of detections were unsatisfactory based on visual comparisons of the seismograms and events detected using the STA/LTA approach.

We instead developed a detection method drawing on our observations of the characteristics of the signals of interest. Our approach relies on identifying peaks in a smoothed version of the envelope of the seismogram. Our simple detection method searches for sections of the smoothed envelope with an amplitude that is higher than a particular threshold for a minimum amount of time. The method thus requires only two input parameters: amplitude threshold (A) and a minimum signal duration (t). Our method is illustrated schematically in Figure 4.4, and shown applied to example seismograms in Figure 4.5. Envelope-based detection methods similar to ours have been used previously in a variety of environments. For example, *Bassis et al.* [2007] used envelope functions as the basis for their STA/LTA-like detection methodology in a study of ice-shelf rift propagation in Antarctica, and *Husebye et al.* [1998] applied a smoothed-envelope approach to signals generated by mining explosions in Norway.

We applied the detection method we developed as follows: We first bandpass filtered the seismograms at 5 Hz – 25 Hz. We used the seismograms as recorded in instrumental units (digital counts), as the frequency band we are interested in lies within the range of flat velocity response for these instruments. After filtering, we computed the envelope functions of the filtered seismo-

grams. We then smoothed the envelope functions over approximately one second (99 samples) and applied our detection scheme to the smoothed envelopes.

Our detection method produces similar results for a reasonable range of detection parameters. However, there are trade-offs in varying the amplitude threshold (A) and minimum signal duration (t). For example, decreasing A or t will increase the number of detections. In some sections of the seismograms, the increased number of detections may lead to a more complete record of detections, while in other sections it may lead to a larger number of false detections. We explored the results of employing a wide range of values for A and t, and after manual inspection of the quality of detections produced, we chose a value for t of 3.5 seconds, for all stations and components. We found that no single value of A produced satisfactory results for all stations and components. We therefore chose the value of A to be the mean amplitude of the smoothed envelope over the entire deployment for each component of each station. The value we use for A are given in Table 4.2.

4.3.2 Analysis

Applying our smoothed-envelope detection scheme to the Helheim data allows us to identify hundreds of detections per hour on each component of each station, resulting in a catalog consisting of tens of thousands of seismic detections on each station and component over the course of the seven-week deployment. These detections are shown for the vertical (Z) components of each station in Figure 4.6 for the duration of the study period. We found similar detection patterns for the horizontal components of each station; an example showing all three components of HM03 is plotted in Figure 4.7.

From Figure 4.6, it is apparent that the detection time series can be divided into two groups, consisting of stations that show a regular, periodic variation in the number of events detected (HM01, HM02, and HM03), and those stations that do not show such a pattern (HM04, HM05, and HM06). The stations showing these two different patterns of detections are representative of distinct geographic areas of the glacier: HM01–03, the stations showing periodic variations, are located downglacier, near the calving front, while HM04–06, the stations lacking clear periodic

variations, are all located >10 km upglacier from the calving front.

4.3.2.1 Upglacier Stations

Seismicity upglacier (Figure 4.6) generally occurs at a lower background rate compared to the downglacier stations, though the upglacier stations (HM04–06) show large short-term spikes in activity at irregular intervals, the peaks of which can be higher than the levels we see at the downglacier stations. In general, individual seismic events are recorded at only one of the upglacier stations, and we are unable to consistently associate arrivals at one station with arrivals at the other stations. The lack of association is likely due in part to the relatively large distances between the upglacier stations. We therefore do not present any locations for these events.

In some cases, short-term changes in the rate of seismicity at two or more of the upglacier stations appear to be temporally correlated. In particular, the large spikes in seismicity that characterize the detections at these stations often occur at similar times. However, the onset times and peaks of the spikes in seismicity may differ by several tens of minutes to hours between the different upglacier stations, and thus we do not believe these spikes are records of the same events on different stations. We believe it is likely that the spikes in seismicity are due to transient changes in glacier behaviour that cause perturbations to the seismic environment at slightly different times in different locations. These spikes in seismicity present an intriguing target for further study, but we do not address them further here. Instead, we focus on the seismicity we observe at the downglacier seismic stations.

4.3.2.2 Downglacier Stations

At the downglacier stations (HM01–03) we see similar trends and characteristics in all of the stations' detection rates (Figure 4.6), and we are regularly able to associate arrivals between all three stations. The vast number of detections makes manual inspection of all arrivals impractical, but we have inspected a subset of the detections for quality and completeness. A large fraction of the arrivals at a given station can be convincingly associated with arrivals at the other downglacier

stations. For the subset of events we manually associated between stations, the largest number showed arrivals at HM03 first, then at HM02, and finally HM01. The delay between the first and last arriving signals is typically less than 4 seconds.

The individual signals we detect are often emergent, complicated signals lacking in identifiable phases (left panel of Figure 4.3). Prior studies in a diverse range of cryoseismic environments have also described signals as either emergent or lacking obvious or easily identifiable body waves [e.g., *Wolf and Davies*, 1986; *Bassis et al.*, 2007; *Walter et al.*, 2009; *Thelen et al.*, 2013], though a few authors describe identifiable body phases in at least some of the signals they record [*Stuart et al.*, 2005; *Walter et al.*, 2009, 2013; *Röösli et al.*, 2014]. The complicated nature of the signals, and the lack of clear P or S phases, is likely due to the small size of the events we identify and the complicated seismic velocity structure of the glacier-terminus region.

At all three stations, the rate of seismic detections is dominated by a periodic variation, which modulates a slowly varying background level of seismicity. Throughout the study period, we see the rate of detections at the downglacier stations vary with a period of $\sim$12 hours (Figure 4.6, Figure 4.7). This pattern is especially clear in the first several weeks of data, but remains present throughout the entire study period. The semi-diurnal highs and lows at the three downglacier stations occur simultaneously, with no observable lag between the stations.

4.4 Event Identification and Location

The process of associating arrivals and locating the detected seismic events is complicated by the characteristics of the signals themselves. As discussed previously, the vast majority of the signals we detect on both the vertical and horizontal components are lacking in identifiable body phases, making traditional earthquake-location techniques impossible for most of the events we identify. Instead, we use the time of the peak of each envelope as the arrival time. We believe these peaks are representative of near-simultaneous arrival of multiple refracted and scattered phases, similar to Lg or Rg phases.

The difference in arrival times between associated detections at the three downglacier stations is typically much smaller than the difference in arrival times between prior or subsequent detections at a given station. Thus, we use temporal proximity as a means of identifying associated arrivals at different stations. We search for signals that arrive within 5 seconds of arrivals at other stations. We are able to associate 31% of the detected arrivals, allowing us to identify $\sim$28,000 icequakes. The large number of detections and identified events prevents us from reviewing every association, but for quality assurance we inspected a subset of the associations we generated and found them to be satisfactory.

For a handful of identified events, we are able to identify examples of what we believe to be body-wave arrivals within the signals. These are most commonly visible on HM03, but we are able to identify several events for which we are able to pick at least one body-wave arrival at each station with a reasonable degree of confidence. Using these picks, we obtain event epicenters using a simple, two-layer (ice and bedrock) velocity model and a grid-search approach. Since we were only able to identify three arrivals for some of these events, we did not attempt to determine their depths, but assumed a depth of 0 km within our simplified model. The results (Figure 4.8) show that this small subset of events for which we were able to pick arrivals has epicenters distributed across the near-terminus region of the glacier. While these locations are useful for a guide to inform our further exploration of the data, we believe that these locations are, individually, of poor quality, given the uncertainties in our phase picks and our velocity model.

While our ability to establish locations for this small number of events provides some insight into the likely distribution of events we detect, they represent a tiny percentage of the event catalog. In order to estimate source locations for a larger number of events, we use the prominent, high-amplitude peak of the signal that we used for event association to provide seismic arrival times. This peak occurs after the body waves in the small number of cases in which they are identifiable. We have already established the timing of this peak automatically, and we attempt to use these arrival times to locate the sources of the signals. The phase represented by these sections of the signals is unclear, but their relatively large amplitudes and slow horizontal velocities when com-

pared to body waves suggest that they represent Rayleigh or quasi-Rayleigh waves on the vertical component of the seismogram, and a combination of Rayleigh and Love waves of the horizontal components. We assume a direct (surface) travel path from the origin to the receiver for these sections of the signal.

Published values for shear-wave velocity in ice vary, but are typically in the range of $\sim$1.9 km s^{-1} [e.g. *Anandakrishnan and Bentley*, 1993; *Deichmann et al.*, 2000]. We tested a range of seismic velocities slower than the shear-wave velocity in ice for these phases, and found the icequake locations to vary relatively little across the range we tested (1.2–1.9 km s^{-1}). The locations we obtained are also generally consistent with the locations we obtained from our body-wave picks. We select a preferred velocity of 1.4 km s^{-1}.

Using this value as the assumed horizontal velocity of the automatically identified amplitude peaks of the signals, we are able to estimate locations for the nearly 28,000 events we identify on the downglacier stations. We perform a grid search over a 250 km $\times$ 250 km region centered on the map area shown in Figure 9, using a dense, 250 m grid for our potential source locations. As the automatically identified amplitude peaks are of varying quality, and the assumed velocity used for the locations is based on a number of simplifying assumptions, we believe the individual locations we determine in this manner are subject to relatively large errors of at least several grid cells. However, given the very large numbers of epicenters we obtain, we believe the overall distribution of the locations we estimate is representative of the true distribution of the events we detect. Our results (Figure 4.9) show that the grid points identified as the locations of the largest numbers of events are those closest to the calving front.

We find that $\sim$80% of the icequakes we detect occur at grid points that are recorded as the location of at least 20 events. These events, shown in Figure 4.9, are fairly tightly clustered with locations most common on or near the calving front. Very few events have estimated locations on bedrock and the shape and character of the distribution leads us to believe that these events are slightly mislocated and actually occurred in glacier ice. Similarly, those events showing locations apparently in the ice mélange are also likely to have occurred in glacer ice, an inference supported

by the strong horizontal-component arrivals we observe.

Although the ice mélange can be quite active and interaction between the icebergs within the mélange is a potential source of seismic emissions [*MacAyeal et al.*, 2008; *Hamilton et al.*, 2010; *Amundson et al.*, 2010]. We expect such signals to be smaller than those from glacier fracturing and we expect them to be depleted in shear-wave energy, as such signals would need to propagate though the fjord water to reach the stations. We observe abundant seismic energy on the horizontal components of all stations for the events we detect, and near-identical records of detections on each component of each station (Figure 4.7. The true velocity structure of the near-terminus region is likely to be complex, and seismograms traveling to the more distant stations (HM01 and HM02) may travel faster paths partially through bedrock. Our simplified velocity model likely biases the event locations downglacier towards the ice mélange.

We emphasize that our goal in location the events is to obtain a general picture of the likely event distribution, rather than highly accurate individual epicenters. We conclude that the majority of the events we observe on the downglacier stations emanate glacier ice at or near the calving front. Events occur across much of the width of the calving front, with the largest number of events located in the central portion of the glacier, which is deforming the most rapidly due to glacier motion. The broad distribution of events indicates that they are not the result of repeated rupture of a single point of failure within the glacier/bed system.

We are not able to estimate event depths from the arrival times. However, the characteristics of the signals we observe do provide some information about the depths of the events. In previous studies of glacier seismicity where denser networks have allowed for accurate determinations of icequake depth, it has been observed that shallow events tend to be distinctly lacking in observable body phases, and are dominated by surface-wave arrivals [*Deichmann et al.*, 2000; *Walter et al.*, 2009, e.g.,]. Our events share these characteristics, suggesting a shallow source for the events.

Additionally, an earlier seismic study of an inland region of the Greenland Ice Sheet found that shallow crevassing icequakes showed energy primarily isolated to the 10–50 Hz range [*Röösli et al.*, 2014]. *Röösli et al.* [2014] made use of instruments sampling at much higher frequency

than this study, and observed larger events, so we are unable to quantitatively compare the spectral content of our signals to that of the surface crevasses in the earlier study. However, our observation that the signals we detect are most apparent at frequencies above 10 Hz with little energy at lower frequencies, is consistent with the overall character of the surface crevassing icequakes observed by *Röösli et al.* [2014]. This is also similar to the frequency content of events observed on a Swiss alpine glacier [*Dalban Canassy et al.*, 2012], and attributed to crack opening. We infer that our events come from shallow regions of the glacier, and are the result of crack opening rather than stick-slip motion, basal crevasse initiation, or other basal processes.

4.5 Discussion

We observe a large number of frequent small earthquakes that occur near the calving front of Helheim Glacier, likely in the glacier ice. The occurrence rate of these icequakes displays a strong $\sim$12 hour periodicity along with a large change in the background seismicity rate near the middle of the study period. The events appear to be shallow, probably associated with near-surface cracking and crevasse opening.

4.5.1 Tidally Modulated Seismicity

The presence of a $\sim$12-hour periodic variation in seismicity in an environment with a clear connection to ocean tides suggests an investigation of the semi-diurnal ocean tides as the driver of the seismicity. We compute a predicted ocean-tide record using the AOTIM-5 tide model [*Padman and Erofeeva*, 2004] at an open-ocean location near the mouth of Sermilik Fjord, which connects Helheim Fjord to the ocean. The prediction point lies $\sim$100 km from the calving front of Helheim Glacier. Synthetic tide data calculated using the AOTIM-5 model for the same point have been used in two previous studies of glacier-tide interactions at Helheim Glacier [*de Juan et al.*, 2010; *Davis et al.*, 2014]. Both of these studies made comparisons of the synthetic tide record to data recorded on a pressure gauge operated $\sim$35 km from the terminus of Helheim Glacier for ap-

proximately one month during the summer of 2007. Both studies found good agreement between the modeled tide data and the observations recorded on the pressure gauge. *de Juan et al.* [2010] note phase alignment between the two signals of less than 3 minutes and amplitude agreement within centimeters. In addition to the small amplitude differences at semi-diurnal and diurnal periods, *Davis et al.* [2014] note longer-period differences that are probably associated with defects in the tide-gauge instrumentation or non-tidal contributions to sea-level changes. We conclude that the tide model produces a tide record of sufficient accuracy for our analysis, which is primarily concerned with the phase of the semi-diurnal component of the ocean tides.

We first compare the synthetic tide record to the record of seismic detections from station HM03 for the duration of the study period, as shown in Figure 4.10. While the long-term variations that we observe in the detections do not have a strong relationship to long-term variations in tide height, the semi-diurnal variations in seismicity and the semi-diurnal variations in tide height are consistently anticorrelated throughout the study period. This relationship is visible when the data are viewed at long timescales, as in the upper panel of Figure 4.10, and becomes especially clear when the data are viewed over shorter time periods, as shown in the lower panels of Figure 4.10. A detailed comparison is shown in Figure 4.11, where we have plotted the tide height at one-minute intervals and the rate of seismicity at 10-minute intervals. In Figure 4.11, we have also inverted the tide signal to emphasize the phase relationship between the two signals. We observe a close relationship between the rate of seismicity on the downglacier stations and the phase of the ocean tide, such that the semi-daily maxima in seismicity occur at low tide, and the semi-daily minima in seismicity occur at high tide.

To quantify this phase relationship, we calculate the best fitting lag of the detection timeseries with respect to the tides. We first split the tide and detection data into one-day segments to account for the large variations in tidal amplitude and for variations in the amplitude of the semi-diurnal oscillations in seismicity. For each day of data we use the seismic detection rate calculated every 10 minutes and the inverted tide height calculated every minute to determine the least-squares fit for a broad range of possible lags. We then identify the best-fitting lag for each day of data, and

calculate the mean lag for the entire study period from these daily values. The detection time series lags the inverted tide height by a mean of 25 minutes ($\sigma = 32$ minutes). This value does not account for tide propagation from the tide gauge to the glacier, which is expected to take $\sim$10 minutes based on observed tsunami propagation times [*Nettles et al.*, 2008a], further shortening the lag between tide height and seismicity. This very short lag between tide height and peak seismicity suggests a direct forcing of the seismicity by the tides.

4.5.2 Relationship of Tidally Modulated Seismicity to Major Calving Events

We observe a large change in the detection rate at the downglacier stations following day 216 (Aug. 4) of 2009 (Figure 4.6). On day 216, we see a rapid increase in the number of detections, which is particularly notable on station HM02, followed by a decrease in background detection rates over about three days. The detection timeseries also shows a brief, sharp drop in the number of detections on day 217. This apparent drop is not real, but an artifact caused by the amplitude of the smoothed envelope remaining above the detection threshold for nearly the entire day, which is recorded by our signal detector as a small number of very long detections. Inspection of the filtered seismograms shows near-continuous excitation, similar to that observed by previous authors near the times of glacial earthquake calving events [*Nettles et al.*, 2008a; *Walter et al.*, 2012a]. We examine the record of global seismic data, along with satellite remote-sensing data, to evaluate whether the glacier state changed significantly at this time.

The published catalog of glacial earthquakes does not include any events at Helheim Glacier on Aug. 4, 2009 [*Veitch and Nettles*, 2012]. We manually review global seismic records from Aug. 4 following the procedure used by *Nettles et al.* [2008a] to identify glacial earthquakes missed using the automated detector [*Ekström*, 2006; *Nettles and Ekström*, 2010] that produces the bulk of the published catalog. We review the global seismic data for the full period of our local seismic deployment, and find one glacial earthquake not previously identified on Aug. 4, 2009, at approximately 17:31 UTC. We believe that this glacial earthquake previously eluded detection due to a combination of low amplitude and signal complexity; the event appears similar to other examples

of missed detections with which we are familiar [*Nettles et al.*, 2008a; *Veitch and Nettles*, 2012; *Murray et al.*, 2015b]. We perform a centroid-single-force source inversion [*Kawakatsu*, 1989] of the type used to produce previously published glacial-earthquake catalogs [*Tsai and Ekström*, 2007; *Veitch and Nettles*, 2012], which allows us to confirm that the event is indeed a glacial earthquake and to obtain more robust timing information for the event. The source parameters we obtain are presented in Table 4.3, and the timing is shown graphically in Figure 4.6. The source is consistent in location and azimuth with other glacial earthquakes reported at Helheim Glacier [*Tsai and Ekström*, 2007; *Veitch and Nettles*, 2012].

The occurrence of a glacial earthquake at Helheim on Aug. 4 (day 216) strongly suggests a large calving event and retreat of the glacier front at that time. We review MODIS and Landsat satellite imagery and previously published calving-front positions [*Bevan et al.*, 2012; *Schild and Hamilton*, 2013]. These data reveal that Helheim Glacier retreated 1–2 km between Aug. 4 (14:40 UTC) and Aug. 5 (13:45 UTC), consistent with the timing of the glacial earthquake. The retreated occurred across the full width of the calving front, probably as several discrete episodes. This was the only major retreat of the glacier during our study period.

The close temporal association between the change in the background seismicity rates at the downglacier stations and a large calving event and retreat of the glacier front suggests a link between physical mechanisms promoting calving and those causing the tidally modulated icequakes we observe.

4.5.3 Mechanism of Tidal Modulation

The abundant icequakes we observe at Helheim Glacier near the downglacier seismic stations appear to occur at shallow depth in the glacier ice, very near the calving front. The rate of icequake occurrence is modulated by the ocean tides such that the maximum occurrence rate coincides with the minimum in tide height, with no significant phase delay. The long-term seismicity rate is affected by iceberg calving such that the number of icequakes increases and peaks at or shortly after the time of a glacial earthquake, during a period of large-scale ice loss. The number of events

then decreases gradually over several days.

Here, we seek to establish a potential mechanism for the tidally modulated seismicity we observe near the calving front of Helheim Glacier. Studies in Antarctica have demonstrated tidal forcing of ice-stream basal seismicity [e.g., *Anandakrishnan and Alley*, 1997; *Bindschadler et al.*, 2003; *Zoet et al.*, 2012], as well seismicity associated with tidally controlled bending of large floating tongues [*von der Osten-Woldenburg*, 1990; *Barruol et al.*, 2013; *Hammer et al.*, 2015], but neither of these mechanisms is likely to be the cause of the shallow seismicity we observe at the nearly grounded Helheim Glacier.

At near-grounded, marine-terminating glaciers like Helheim, large-scale calving is likely promoted by buoyancy induced basal crevassing of the calving front, followed by calving-block rotation during or after block detachment [*James et al.*, 2014; *Murray et al.*, 2015b]. Calving of this type is the cause of glacial earthquakes like the one we observe on Aug. 4, 2009 [*Nettles and Ekström*, 2010; *Veitch and Nettles*, 2012; *Murray et al.*, 2015a]. However, propagation of basal crevasses due to buoyancy-induced forces is not likely to explain the seismicity we observe. Such a mechanism would show the opposite phase relationship to tidal forcing to that we observe, as buoyancy forces on a below-flotation glacier tongue will be maximum at high tide and minimum at low tide, resulting in reduced seismicity at low tide.

Tidal modulation of glacier flow at Helheim has been reported by several authors using GPS data [*de Juan et al.*, 2010; *Davis et al.*, 2014] and terrestrial radar interferometry [*Voytenko et al.*, 2015]. *de Juan et al.* [2010] analyzed data from high-rate GPS sensors placed on the lower regions of the glacier [*Nettles et al.*, 2008a], recording the position of the glacier at multiple points, including stations very close to the calving front. They observed the glacier flow speed to vary semi-diurnally, such that during low tides, the glacier is advanced relative to the position expected from its long-term velocity, and during high tide, the glacier position is retarded relative to that expected from its long-term velocity. The tidal effect is found to decay nearly exponentially in amplitude with distance from the glacier terminus. As a result, the regions of the glacier nearest the calving front experience tidally modulated changes in longitudinal strain, with the strain reaching

a maximum shortly (<1 hour) [*de Juan*, 2011; *de Juan et al.*, in prep.] following low tide, when longitudinal stress is highest, and a minimum shortly following high tide, when longitudinal stress is minimum. The results of *Voytenko et al.* [2015] are generally in agreement with those of *de Juan et al.* [2010].

Combining our results with those of *de Juan et al.* [2010] suggests that icequake seismicity peaks when the longitudinal stress and strain in the glacier are highest, and is at a minimum when the longitudinal stress and strain are minimum. The location of the icequakes near the calving front, at shallow depths, suggests that the events occur as part of crevasse-opening processes, likely through tensile cracking. In this interpretation, the icequakes occur at a background rate controlled by the background glacier strain field, which is extensional in its lower reaches [*Howat et al.*, 2005; *Stearns and Hamilton*, 2007; *Nettles et al.*, 2008a]. Variations in stress due to the tides then modulate the icequake occurrence rate through a triggering mechanism. Surface cracking may also be promoted by the small amount of bending that may occur due to vertical motion of the very short-section of the glacier seaward of the grounding line.

The phase relationship we observe — increased seismicity in phase with the maximum of tidally modulated stress — has been previously reported in both global [*Cochran et al.*, 2004] and regional [e.g., *Wilcock*, 2001; *Stroup et al.*, 2007] studies of tectonic earthquakes. However, while stick-slip seismicity at the glacier base has been previously linked to tidal forcing in Antarctica [e.g., *Anandakrishnan and Alley*, 1997; *Bindschadler et al.*, 2003; *Wiens et al.*, 2008], and *Peng et al.* [2014] linked shallow icequake occurrence to passing Rayleigh waves from larger earthquakes, we know of only a small number of studies linking tidal forcing to large changes in the occurrence of small icequakes. Extensive tidal modulation of small icequakes has been observed at two locations in Antarctica, at Mertz Glacier [*Barruol et al.*, 2013] and the Ekström Ice Shelf [*von der Osten-Woldenburg*, 1990; *Hammer et al.*, 2015]. However, glacier morphology and the relationship between the tides and seismicity observed in these studies is different from what we observe at Helheim Glacier. At Mertz Glacier, seismicity peaks during falling tide when the tidal velocity is maximum [*Barruol et al.*, 2013]. At Ekström Ice Shelf [*Hammer et al.*, 2015] observe

peak seismicity during rising tides, and *von der Osten-Woldenburg* [1990] find seismicity maxima during falling tide. The authors of these studies attribute the seismicity they observe to iceshelf bending resulting in basal crevassing, surface crevassing, or stick-slip behaviour where the iceshelf passes over a small island. None of these studies provides an obvious analog for our results at Helheim Glacier.

Laboratory experiments [*Beeler and Lockner*, 2003; *Savage and Marone*, 2007] on the effects of periodically varying stresses on failure in earth materials have shown that the phase relationship between the peak in seismicity and the peak in applied stress reflects characteristics of the earthquake source. When seismicity is observed to be in phase with the applied stress rate, it is inferred that the nucleation time is shorter than the period of the applied periodic stress. However, when the peak in seismicity is observed to be in phase with the applied periodic stress, the nucleation time for failure is inferred to be longer than the period of the applied stress. We find a number of examples in the literature of failure in glacier ice with nucleation times longer than the period of the semi-diurnal tides. *Weiss* [2004] suggests that a small microcrack within glacier ice will take longer than a month to propagate subcritically into a crack of sufficient size to fail critically. Additionally, modeling and observations of hanging mountain glaciers [*Pralong et al.*, 2003; *Pralong and Funk*, 2005] show many tens of days of slow fracture growth prior to the break-off of large portions of those glaciers in ice avalanches. Thus we believe that a nucleation time of greater than the semi-diurnal tidal period for the events we observe is plausible.

We infer that the tidally modulated seismicity we observe is part of the process of glacier stretching that has been observed in prior GPS deployments [*Nettles et al.*, 2008a] and in satellite remote-sensing data [*Howat et al.*, 2005; *Stearns and Hamilton*, 2007; *Joughin et al.*, 2008a], and that the strain seen in those studies is at least partially accommodated by brittle failure in the ice near the glacier terminus. Based on the laboratory experiments discussed above, these brittle failures must occur via a mechanism whose nucleation time is longer than the $\sim$12 hour period of the semi-diurnal tides.

We interpret the icequakes we observe to be due to glacier extension, and evidence from alpine

glaciers [e.g., *Walter et al.*, 2009; *Dalban Canassy et al.*, 2013] suggests that tensile cracking is the most likely mode of failure for the individual events. However, in the glacier terminus model presented by *Koehn and Sachau* [2014], they argue for the slow development of through-going shear fracture zones within the interiors of glaciers. These zones develop from small shear fractures into zones of shear deformation, which then combine with extensional fractures to allow glacier break-off. The development of these zones is predicted to occur near a glacier's terminus, such that they might play a crucial role in the development of the through-going fractures required for major calving events to occur. The development of such shear zones would occur in the proposed source region for the tidally modulated seismicity we observe, and would require a large number of small shear failures. We cannot rule out a shear-failure mechanism for some or all of the icequakes we observe. An acceptable mechanism for the tidally-modulated seismicity we observe at Helheim Glacier is the failure of small cracks within the glacier that have propagated subcritically from microcracks arising from tide-height-modulated longitudinal stress within the near-terminus region of the glacier. This mechanism is consistent with the source location, inferred depth, very small size, and the long nucleation time implied by the tidal relationship we observe.

4.6 Conclusions

We observe abundant high-frequency seismic arrivals at all stations of a small seismic network deployed around Helheim Glacier, a large, near-grounded, marine-terminating glacier in East Greenland. Seismic events occurring near the downglacier stations are often recorded on multiple stations, while events occurring near the upglacier stations are often recorded on only one station. We focused on the downglacier seismicity for this study, and identified $\sim$28,000 icequakes that occurred over the 37 days for which all three downglacier stations were operational. We were able to determine source locations for many events and found that the vast majority of the events occurred very near the glacier's calving front.

The temporal pattern of arrivals on the downglacier stations shows strong semi-diurnal vari-

ability, which is not observed on the upglacier stations. The semi-diurnal variations are in phase with the inverse of the ocean-tide height near the terminus of Helheim Glacier. The semi-diurnal peak in seismicity is coincident, to within 25 minutes, with the low ocean tide. This phase relationship is consistent with previously published observations of near-terminus tidally modulated flow at Helheim Glacier [*de Juan et al.*, 2010; *Voytenko et al.*, 2015], a flow modulation that leads to increased longitudinal stress within the glacier at low tide. Though the glacier is grounded near the calving front during our observation period, some additional tensional stress may be provided at low tide by glacier bending at the glacier surface.

The phase relationship we observe between downglacier icequake seismicity and a periodic applied stress differs from previously published observations of tidally modulated icequakes. The relationship we observe implies that the source mechanism responsible for the seismicity may have a nucleation time that is long relative to semi-diurnal tide variations, which would suggest that subcritical ice failure plays an important part in the deformation of the lowermost sections of Helheim Glacier. The phase relationship we observe also differs from the phase relationship expected for buoyancy-driven basal crevassing, suggesting multiple modes of brittle failure occur in the glacier's tongue, and should be considered in models of near-terminus brittle glacier deformation.

We also observe a close association between major calving events at Helheim Glacier and the rate of seismicity near its terminus. An increase in seismicity during calving is followed by a large decline in the background rate of seismicity after the calving event, which is associated with a previously undetected glacial earthquake. The increase in seismicity may be linked to failure of the full glacier thickness, and the decrease to removal of the most badly damaged ice and readjustment of the glacier stress state.

Although prior studies of glacier calving have emphasized the stress-rate within the glacier as a control on the calving process [e.g., *Alley et al.*, 2008; *Levermann et al.*, 2012], our findings suggest that stress, applied periodically by semi-diurnal ocean tides, also plays a controlling role in the development of fractures that lead to calving. We believe that tides and other externally applied stresses should be considered in future studies of near-grounded glacier calving.

4.7 Tables

Station	Latitude(°N)	Longitude(°W)
HM01	66.3846	38.0554
HM02	66.3257	38.0811
HM03	66.3361	38.2022
HM04	66.3371	38.4051
HM05	66.4202	38.4802
HM06	66.4830	38.3720

Table 4.1: Locations of the seismic stations used in this study. See Figure 4.1 for map.

Station	Component	A
HM01	HHZ	15.10
HM01	HH1	16.92
HM01	HH2	—
HM02	HHZ	12.92
HM02	HH1	17.93
HM02	HH2	17.27
HM03	HHZ	38.13
HM03	HH1	42.01
HM03	HH2	52.69
HM04	HHZ	32.37
HM04	HH1	45.94
HM04	HH2	49.94
HM05	HHZ	17.97
HM05	HH1	26.66
HM05	HH2	28.85
HM06	HHZ	15.40
HM06	HH1	17.99
HM06	HH2	19.10

Table 4.2: Values of A (detection threshold) in digital counts used for our smoothed-envelope detection method for each station and component. Values are computed as the mean of the smoothed envelope of each seismogram over the duration of the study period, with sections affected by mass recenters and other instrumentation errors removed. A large portion of the record for station HM01, component HH2 contained glitches, and the trace was therefore omitted from our analysis.

Centroid Parameters										Scale		CSF Vector				
Date			Time			Latitude		Longitude		Factor	M					
Y	M	D	h	m	sec	δt_0	λ	$\delta\lambda_0$	ϕ	$\delta\phi_0$	10^{ex}	CSF	V_r	V_θ	V_ϕ	pl.	azim.
2009	8	4	17	31	39.0±0.6	-7.0	66.29±.03	-0.21	-38.37±.08	0.13	18	1.8	-0.58±0.11	1.04±0.14	1.39±0.14	18	127

Table 4.3: Centroid-single-force solution for the glacial earthquake that occurred on Aug. 4, 2009 at Helheim Glacier. See *Veitch and Nettles* [2012] for complete explanation of source parameters.

4.8 Figures

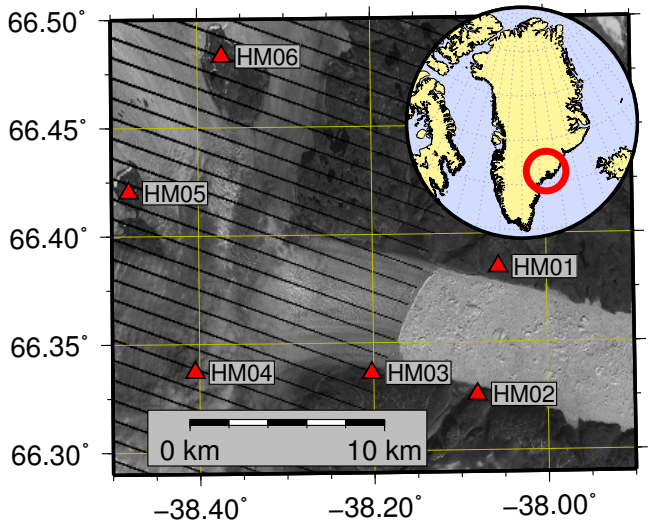

Figure 4.1: The locations of the seismic stations deployed for this study around Helheim Glacier, with the location of Helheim within Greenland indicated in the inset. Seismic stations are indicated by red triangles and identified by their station names. Helheim Glacier flows from northwest to southeast, and terminates in the ocean just east of station HM03, where the change in colour from darker to lighter marks the calving front and the transition from glacier ice to floating ice mélange (densely packed icebergs and ice fragments). The background image is a Landsat 7 pan-chromatic-band scene, captured August 8, 2009.

Figure 4.2: Station HM03; camera view is towards NNW. This installation is representative of the enclosure and setting of the six seismic stations used in this study. The ice visible in the station background is representative of the surface of Helheim Glacier near the calving front, and shows the highly fractured character of the lower reaches of the glacier.

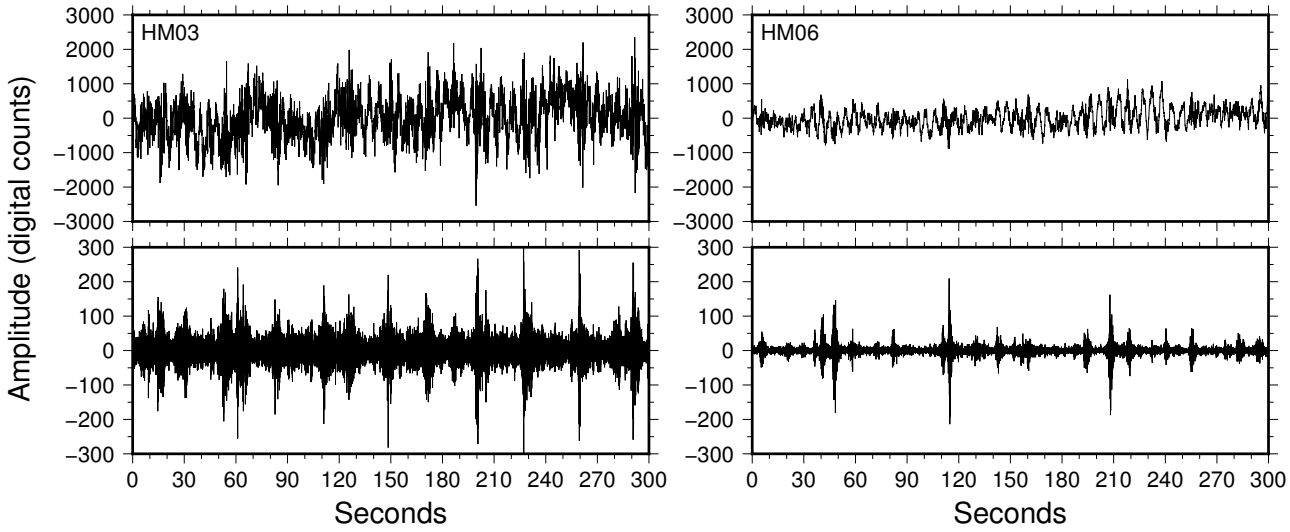

Figure 4.3: Example seismograms from two stations, HM03 and HM06, unfiltered (top) and filtered at 10–25Hz (bottom). These sections are each five minutes in length and are shown in units of digital counts.

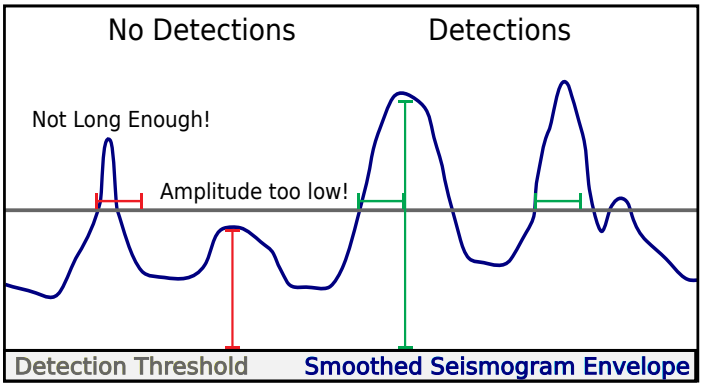

Figure 4.4: A schematic representation of our detection method. In this cartoon, the amplitude of the detection threshold is indicated in grey, with a simplified smoothed envelope represented by the blue line. Examples of sections of the envelope that would be identified as detections are shown on the right side of the figure, while examples of sections of the envelope that would not be identified as detections are shown on the left. The example non-detection peaks would not be detected owing to either a too-short duration (t) or a too-low amplitude (A).

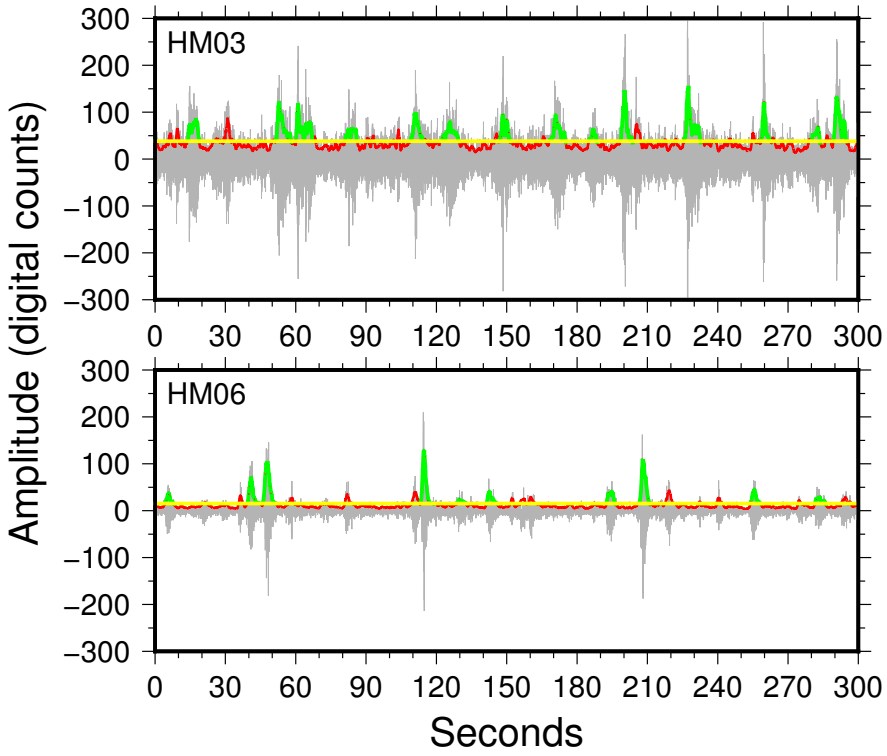

Figure 4.5: An example of our detection method applied to the seismograms shown in Figure 4.3. The detection threshold is indicated by the yellow line, and the smoothed envelope is represented by the green and red line. Sections of the envelope that have been identified as a detection are indicated in green, while sections not identified as a detection are indicated in red.

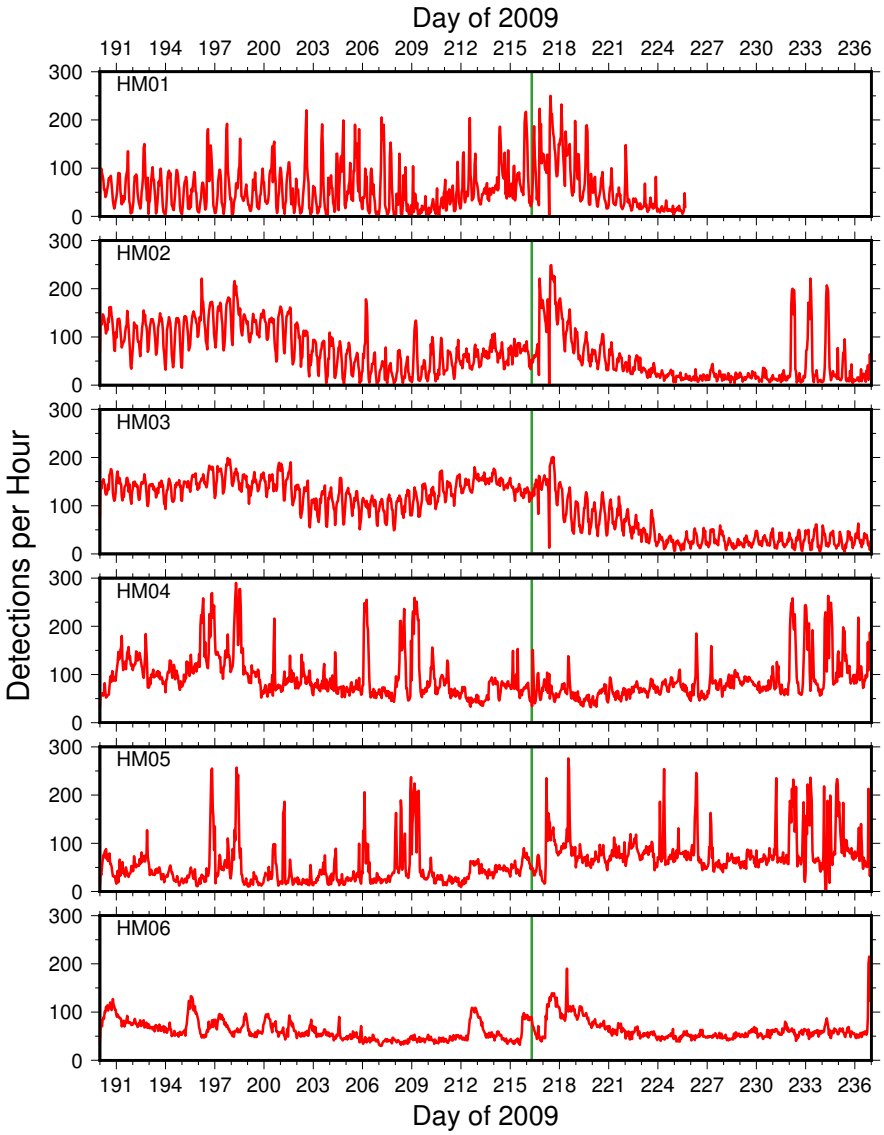

Figure 4.6: Vertical-component detections from all six stations. The number of detections is calculated for one-hour windows with no overlap, centered on the time of plotting. Note the periodic variations in the detection rate at stations HM01–03 (downglacier stations), and the lack of such variation at stations HM04–06 (upglacier stations). The timing of the glacial earthquake that occurred during the study period is indicated in green (Section 4.5.2).

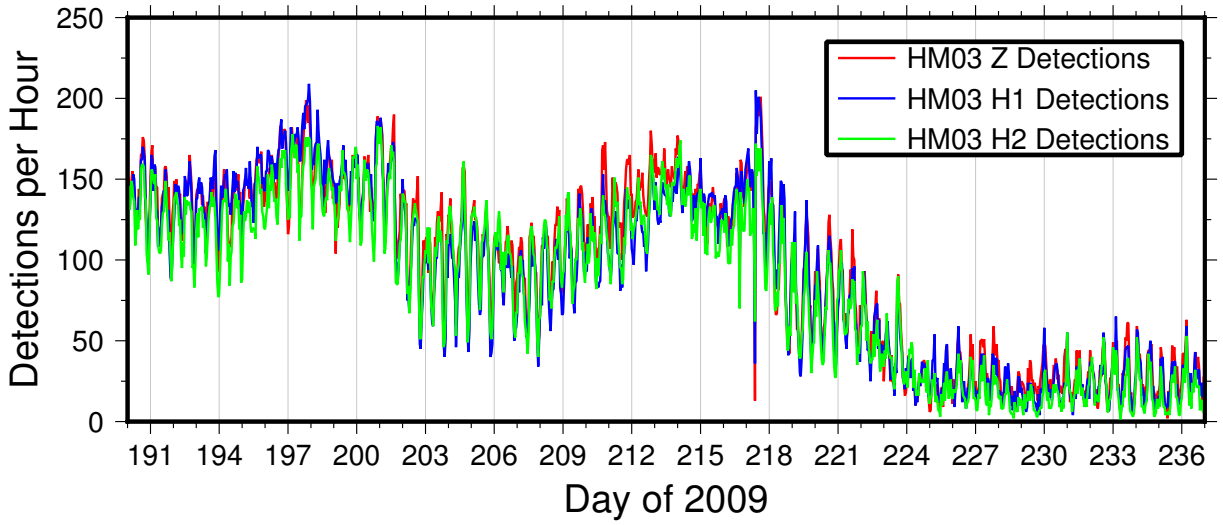

Figure 4.7: Hourly detections from each of the three components of station HM03, computed using a minimum detection time (t) of 3.5 seconds, and the amplitude thresholds (A) as listed in Table 4.2. The vertical component is indicated in red, the first horizontal component in blue and the second horizontal component in green. The number of detections is calculated for one-hour windows with no overlap, centered on the time of plotting.

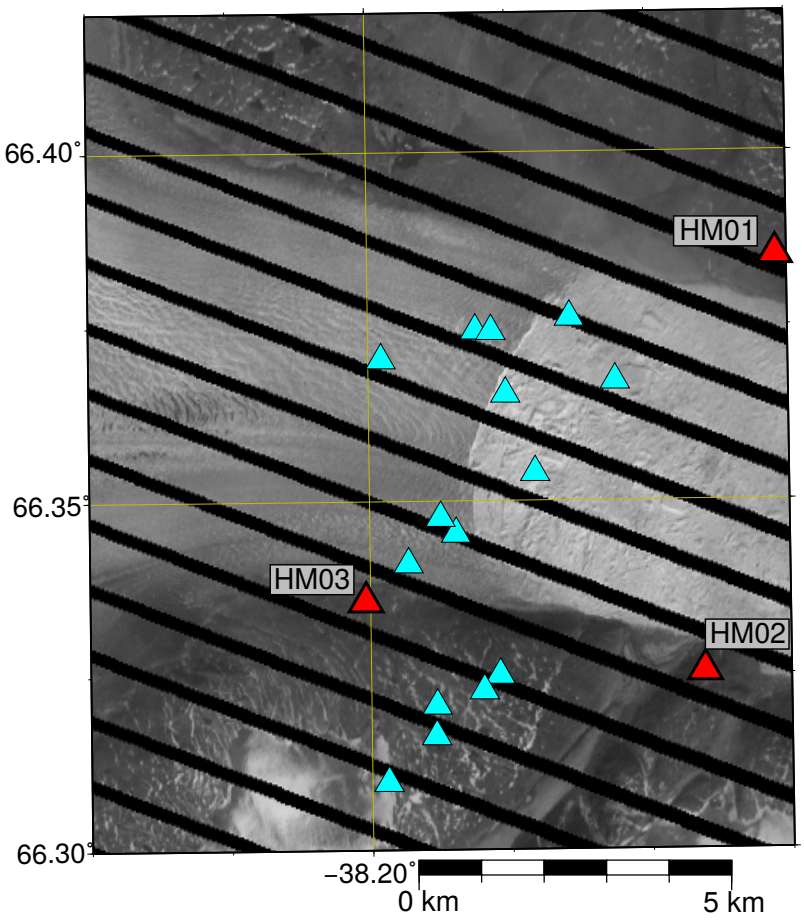

Figure 4.8: Locations (blue triangles) of several events for which we were able to identify body waves, showing event locations scattered in the region around the calving front of Helheim Glacier. Station locations are shown as red triangles. Background image captured on July 14, 2009 by LANDSAT 7 satellite.

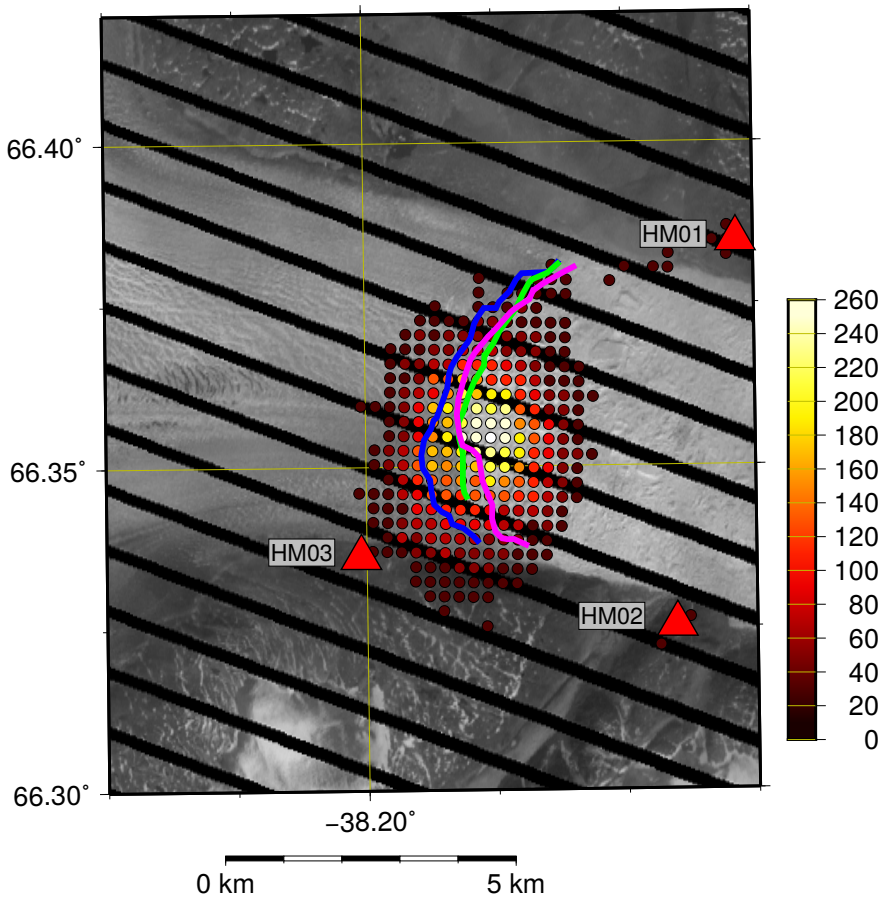

Figure 4.9: Distribution of icequake locations near the terminus of Helheim Glacier showing the large numbers of events located very near the glacier calving front. Only grid points with at least 20 events are plotted (∼80% of all events). Background image is from LANDSAT 7 on July 14, 2009. Solid lines show the location of the calving front on June 30 (magenta), July 14 (green), and August 31 (blue).

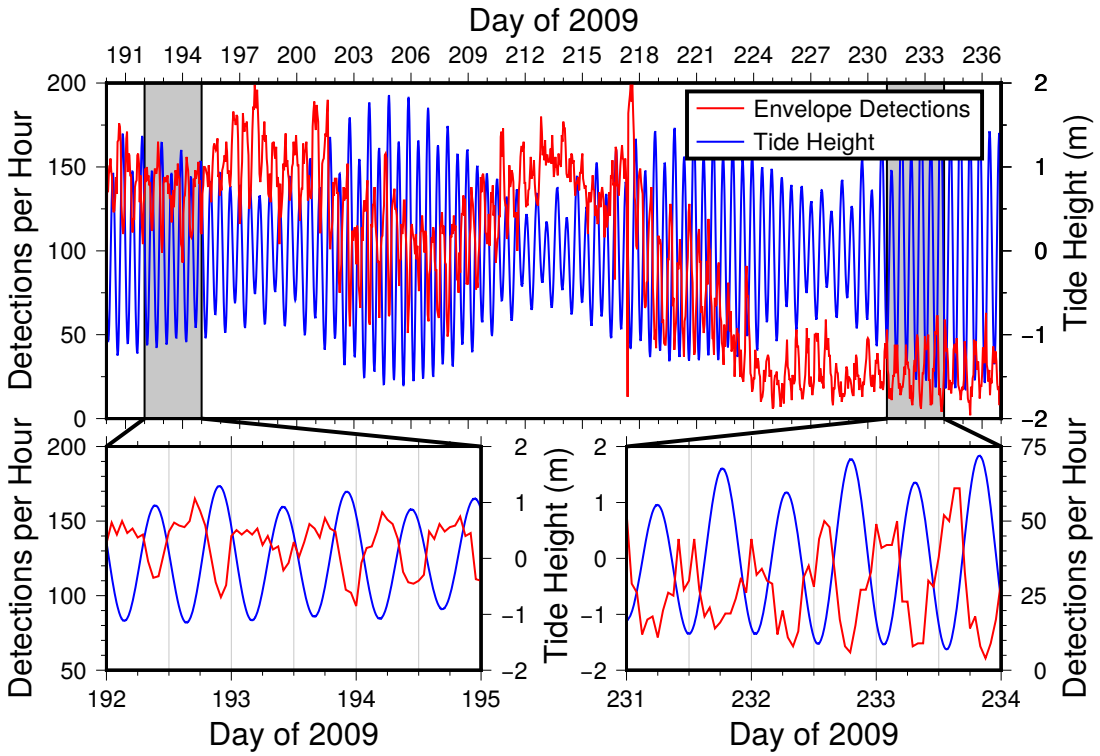

Figure 4.10: Comparison of detections from the vertical component of station HM03, plotted in one-hour increments, with synthetic tides for the ocean near Helheim from the AOTIM-5 tide model [*Padman and Erofeeva*, 2004]. Shown are comparisons over the entire study period (top), and, highlighted with grey backgrounds and in the lower panels, over two short segments in the early and late parts of the study period.

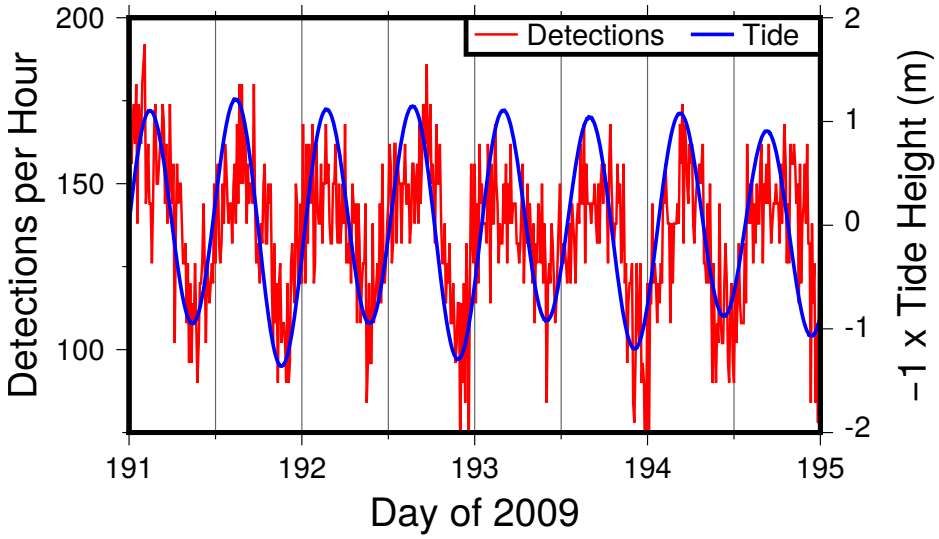

Figure 4.11: A detailed comparison of detections from the vertical component of HM03 and synthetic tide data. Here we have plotted the number of detections in 10-minute bins, but continue to report the values in units of detections per hour, and inverted the tide data (plotted in one-minute intervals) to aid visual comparison.

Chapter 5

Conclusions

In the course of this dissertation, we have expanded our knowledge of the calving process and seismicity related to the calving process at Greenland's marine-terminating outlet glaciers in a number of important ways.

In chapter 2, we presented earthquake source parameters for 121 glacial earthquakes that occurred in Greenland between 2006 and 2010. These source parameters increase the number of glacial earthquakes for which detailed information is available by more than 65%, greatly increasing the amount of data available for rigorous study of glacial earthquakes.

Earlier studies observed a Greenland-wide trend of increasing number of glacial earthquakes. We found that the rapid increase in glacial earthquakes seen prior to 2006 abated, but that overall numbers remained high Greenland wide. We also found a northward spread of glacial-earthquake production in West Greenland that mirrors oceanic warming trends offshore, providing further evidence of a climatic link to glacial-earthquakes.

Using the data from the newly processed as well as previously published glacial earthquake catalogs, we considered the occurrence of glacial earthquakes at several significant producers in light of the capsizing-iceberg model of seismogenesis developed from data obtained from studies conducted at Helheim Glacier. We found that this model was satisfactory to explain glacial earthquakes that occurred in Greenland.

With confirmation of the iceberg capsize source model, we were also able to consider the glacier dynamic conditions needed for such calving events to occur by utilizing both previously published data and original research into the glacier dynamic conditions at glacial-earthquake producing glaciers. We found that glacial earthquakes strongly associated with glaciers with near-grounded termini. We found that the loss of a floating tongue preceded the start of glacial earthquake production and that the presence of a floating tongue was associated with a lack of glacial earthquake production, or cessation of glacial earthquakes at previously active glaciers.

Using our knowledge of the glacial-earthquake source process and the underlying dynamic conditions that are associated with glacial-earthquake seismogenesis, we considered changes in the distribution and occurrence of glacial earthquakes with time. We found that production of glacial earthquakes in West Greenland progressed steadily northward, associated with warming ocean waters off the coast of West Greenland, reinforcing the link between glacial earthquakes and changes in the climate surrounding Greenland.

In chapter 3, we utilized our larger catalog of glacial earthquakes as well as our improved understanding of the dynamics underlying the production of glacial earthquakes in order to assess the accuracy and meaning of the source parameters obtained by waveform-modelling of glacial earthquakes.

We began by considering the active-force azimuth, a parameter that we had previously noted to show a wide range of values. We used satellite remote sensing data estimate the orientation of glacier calving fronts at four glaciers over the time periods that each of those glaciers has produced glacial earthquakes. We then compared the trends and ranges of these values and found the the active-force azimuth to be a good representation of the glacier's orientation at the time of glacial-earthquake seismogenesis.

Using the same data, we also expanded upon an observation we made in chapter 2, that glacial-earthquake locations are elongated in distribution in the direction of glacier advance and retreat. We found that this distribution is due to changes in glacial earthquake location associated with changes in the position of the glacier's calving front.

In chapter 4, we utilized data from a temporary network of seismometers deployed around Helheim Glacier in order to investigate further the dynamics of a seismogenic calving glacier. We found that the data from the Helheim local network recorded abundant high frequency signals, and that those signals showed distinct patterns in different regions of the glacier. In the data recorded on the stations nearest to the calving front, we observed a strong semi-diurnal variation in the number of events. We found that this signal was in phase with the semi-diurnal ocean tides in the fjord of Helheim glacier, in such a way that low tides were associated with increased seismicity. We found that this was consistent with previous geodetic observations of tidally modulated glacier flow.

We also observed that the glacier showed a sharp decrease in high-frequency seismic events during the deployment that was not related to any known tidal cause. We reviewed previously recorded global data and found that a previously undetected glacial earthquake occurred during this time. This finding shows that the tidally modulated seismicity we recorded at Helheim Glacier is strongly linked to the calving process. This implies that semi-diurnal tidal variations, and seismicity driven by these variations are an important part of tide-water glacier calving dynamics. This seismicity may represent the development of failures and weaknesses that will later coalesce into the throughgoing cracks needed for calving to occur.

These findings represent a significant improvement in our understanding of the seismicity and calving process at large Greenland outlet glaciers, and raise a number of potential avenues for future research.

References

Abdalati, W., W. Krabill, E. Frederick, S. Manizade, C. Martin, J. Sonntag, R. Swift, R. Thomas, W. Wright, and J. Yungel (2001), Outlet glacier and margin elevation changes: Near-coastal thinning of the Greenland ice sheet, *Journal of Geophysical Research*, *106*(D24), 33,729–33,741, doi: 10.1029/2001JD900192.

Ahn, Y., and I. Howat (2011), Efficient automated glacier surface velocity measurement from repeat images using multi-image/multichip and null exclusion feature tracking, *Geoscience and Remote Sensing, IEEE Transactions on*, *49*(8), 2838–2846, doi: 10.1109/TGRS.2011.2114891.

Alley, R. B., H. J. Horgan, I. Joughin, K. M. Cuffey, T. K. Dupont, B. R. Parizek, S. Anandakrishnan, and J. Bassis (2008), A simple law for ice-shelf calving, *Science*, *322*(5906), 1344, doi: 10.1126/science.1162543.

Amundson, J. M., M. Truffer, M. P. Lüthi, M. Fahnestock, M. West, and R. J. Motyka (2008), Glacier, fjord, and seismic response to recent large calving events, Jakobshavn Isbræ, Greenland, *Geophysical Research Letters*, *35*(22), L22501, doi: 10.1029/2008GL035281.

Amundson, J. M., M. Fahnestock, M. Truffer, J. Brown, M. P. Lüthi, and R. J. Motyka (2010), Ice mélange dynamics and implications for terminus stability, Jakobshavn Isbræ, Greenland, *Journal of Geophysical Research*, *115*, F01005, doi: 10.1029/2009JF001405.

Amundson, J. M., J. C. Burton, and S. Correa-Legisos (2012), Impact of hydrodynamics on seismic signals generated by iceberg collisions, *Annals of Glaciology*, *53*(60), 106–112, doi: 10.3189/2012/AoG60A012.

Anandakrishnan, S., and R. B. Alley (1997), Tidal forcing of basal seismicity of ice stream C, West Antarctica, observed far inland, *Journal of Geophysical Research: Solid Earth*, *102*(B7), 15,183–15,196, doi: 10.1029/97JB01073.

Anandakrishnan, S., and R. B. Bentley (1993), Micro-earthquakes beneath Ice Streams B and C, West Antarctica: Observations and implications, *Journal of Glaciology*, *39*(133), 455–462.

Andresen, C. S., F. Straneo, M. H. Ribergaard, A. A. Bjørk, T. J. Andersen, A. Kuijpers, N. Nørgaard-Pedersen, K. H. Kjær, F. Schjøth, K. Weckström, and A. P. Ahlstrøm (2012), Rapid response of Helheim Glacier in Greenland to climate variability over the past century, *Nature Geoscience*, *5*(1), 37–41, doi: 10.1038/ngeo1349.

Barruol, G., E. Cordier, J. Bascou, F. R. Fontaine, B. Legrésy, and L. Lescarmontier (2013), Tide-induced microseismicity in the Mertz Glacier grounding area, East Antarctica, *Geophysical Research Letters*, *40*(20), 5412–5416, doi: 10.1002/2013GL057814.

Bartholomaus, T. C., C. F. Larsen, S. O'Neel, and M. E. West (2012), Calving seismicity from iceberg-sea surface interactions, *Journal of Geophysical Research: Earth Surface*, *117*(F4), doi: 10.1029/2012JF002513.

Bassis, J. N., and S. Jacobs (2013), Diverse calving patterns linked to glacier geometry, *Nature Geosci*, *6*(10), 833–836, doi: 10.1038/ngeo1887.

Bassis, J. N., H. A. Fricker, R. Coleman, Y. Bock, J. Behrens, D. Darnell, M. Okal, and J.-B. Minster (2007), Seismicity and deformation associated with ice-shelf rift propagation, *Journal of Glaciology*, *53*(183), 523–536, doi: 10.3189/002214307784409207.

Bassis, J. N., H. A. Fricker, R. Coleman, and J.-B. Minster (2008), An investigation into the forces that drive ice-shelf rift propagation on the Amery Ice Shelf, East Antarctica, *Journal of Glaciology*, *54*(184), 17–27, doi: 10.3189/002214308784409116.

Beeler, N. M., and D. A. Lockner (2003), Why earthquakes correlate weakly with the solid Earth tides: Effects of periodic stress on the rate and probability of earthquake occurrence, *Journal of Geophysical Research: Solid Earth*, *108*(B8), doi: 10.1029/2001JB001518, 2391.

Benn, D. I., C. R. Warren, and R. H. Mottram (2007), Calving processes and the dynamics of calving glaciers, *Earth-Science Reviews*, *82*(3–4), 143–179, doi: 10.1016/j.earscirev.2007.02.002.

Bevan, S. L., A. J. Luckman, and T. Murray (2012), Glacier dynamics over the last quarter of a century at Helheim, Kangerdlugssuaq and 14 other major Greenland outlet glaciers, *The Cryosphere*, *6*(5), 923–937, doi: 10.5194/tc-6-923-2012.

Bindschadler, R. A., M. A. King, R. B. Alley, S. Anandakrishnan, and L. Padman (2003), Tidally controlled stick-slip discharge of a West Antarctic ice, *Science*, *301*(5636), 1087–1089, doi: 10.1126/science.1087231.

Box, J. E., and A. E. Cohen (2006), Upper-air temperatures around Greenland: 1964–2005, *Geophysical Research Letters*, *33*(12), L12706, doi: 10.1029/2006GL025723.

Burton, J. C., J. M. Amundson, D. S. Abbot, A. Boghosian, L. M. Cathles, S. Correa-Legisos, K. N. Darnell, N. Guttenberg, D. M. Holland, and D. R. MacAyeal (2012), Laboratory investigations of iceberg capsize dynamics, energy dissipation and tsunamigenesis, *Journal of Geophysical Research*, *117*(F1), F01007, doi: 10.1029/2011JF002055.

Chen, X., P. M. Shearer, F. Walter, and H. A. Fricker (2011), Seventeen Antarctic seismic events detected by global surface waves and a possible link to calving events from satellite images, *Journal of Geophysical Research*, *116*(B6), B06311, doi: 10.1029/2011JB008262.

Cochran, E. S., J. E. Vidale, and S. Tanaka (2004), Earth tides can trigger shallow thrust fault earthquakes, *Science*, *306*(5699), 1164–1166, doi: 10.1126/science.1103961.

Dalban Canassy, P., J. Faillettaz, F. Walter, and M. Huss (2012), Seismic activity and surface motion of a steep temperate glacier: a study on Triftgletscher, Switzerland, *Journal of Glaciology*, *58*(209), 513–528, doi: 10.3189/2012JoG11J104.

Dalban Canassy, P., F. Walter, S. Husen, H. Maurer, J. Faillettaz, and D. Farinotti (2013), Investigating the dynamics of an Alpine glacier using probabilistic icequake locations: Triftgletscher, Switzerland, *Journal of Geophysical Research: Earth Surface*, *118*(4), 2003–2018, doi: 10.1002/jgrf.20097.

Davis, J. L., J. de Juan, M. Nettles, P. Elósegui, and M. L. Andersen (2014), Evidence for non-tidal diurnal velocity variations of Helheim Glacier, East Greenland, *Journal of Glaciology*, *60*(224), 1169–1180, doi: 10.3189/2014JoG13J230.

Dawes, P. R., and D. van As (2010), An advancing glacier in a recessive ice regime: Berlingske Bræ, North-West Greenland, *Geological Society of Denmark and Greenland Bulletin*, *20*, 79–82.

de Juan, J. (2011), Tidewater glacier flow of Helheim Glacier, Greenland, 2006-2008, using high-rate GPS, Ph.D. thesis, Faculty of Geology, University of Barcelona.

de Juan, J., P. Elósegui, M. Nettles, T. B. Larsen, J. L. Davis, G. S. Hamilton, L. A. Stearns, M. L. Andersen, G. Ekström, A. P. Ahlstrøm, L. Stenseng, S. A. Khan, and R. Forsberg (2010), Sudden increase in tidal response linked to calving and acceleration at a large Greenland outlet glacier, *Geophysical Research Letters*, *37*(12), L12501, doi: 10.1029/2010GL043289.

de Juan, J., M. Nettles, P. Elósegui, J. L. Davis, T. B. Larsen, G. S. Hamilton, and L. A. Stearns (in prep.), Modulation of flow by ocean tides at Helheim Glacier, East Greenland.

Deichmann, N., J. Ansorge, F. Scherbaum, A. Aschwanden, F. Bernardi, and G. Gudmundsson (2000), Evidence for deep icequakes in an alpine glacier, *Annals of Glaciology*, *31*(1), 85–90, doi: 10.3189/172756400781820462.

Dietrich, R., H.-G. Maas, M. Baessler, A. Rülke, A. Richter, E. Schwalbe, and P. Westfeld (2007), Jakobshavn Isbræ, West Greenland: Flow velocities and tidal interaction of the front area from 2004 field observations, *Journal of Geophysical Research*, *112*(F3), F03S21, doi: 10.1029/2006JF000601.

Doyle, S. H., A. L. Hubbard, C. F. Dow, G. A. Jones, A. Fitzpatrick, A. Gusmeroli, B. Kulessa, K. Lindback, R. Pettersson, and J. E. Box (2013), Ice tectonic deformation during the rapid in situ drainage of a supraglacial lake on the Greenland Ice Sheet., *Cryosphere*, *7*(1), 129 – 140, doi: 10.5194/tc-7-129-2013.

Dziewonski, A. M., and D. L. Anderson (1981), Preliminary reference Earth model, *Physics of the Earth and Planetary Interiors*, *25*, 297–356, doi: 10.1016/0031-9201(81)90046-7.

Dziewonski, A. M., T.-A. Chou, and J. H. Woodhouse (1981), Determination of earthquake source parameters from waveform data for studies of global and regional seismicity, *Journal of Geophysical Research*, *86*(B4), 2825–2852, doi: 10.1029/JB086iB04p02825.

Echelmeyer, K., T. S. Clarke, and W. D. Harrison (1991), Surficial glaciology of Jakobshavn Isbræ, West Greenland: Part I. Surface morphology, *Journal of Glaciology*, *37*(127), 368–382.

Ekström, G. (2006), Global detection and location of seismic sources by using surface waves, *Bulletin of the Seismological Society of America*, *96*(4A), 1201–1212, doi: 10.1785/0120050175.

Ekström, G., M. Nettles, and G. A. Abers (2003), Glacial earthquakes, *Science*, *302*(5645), 622–624, doi: 10.1126/science.1088057.

Ekström, G., A. M. Dziewoński, N. N. Maternovskaya, and M. Nettles (2005), Global seismicity of 2003: Centroid-moment-tensor solutions for 1087 earthquakes, *Physics of the Earth and Planetary Interiors*, *148*, 327–351, doi: 10.1016/j.pepi.2004.09.006.

Ekström, G., M. Nettles, and V. C. Tsai (2006), Seasonality and increasing frequency of Greenland glacial earthquakes, *Science*, *311*, 1756–1758, doi: 10.1126/science.1122112.

Ekström, G., M. Nettles, and A. M. Dziewoński (2012), The global CMT project 2004–2010: Centroid-moment tensors for 13,017 earthquakes, *Physics of the Earth and Planetary Interiors*, *200–201*, 1–9, doi: 10.1016/j.pepi.2012.04.002.

Enderlin, E. M., and I. M. Howat (2013), Submarine melt rate estimates for floating termini of Greenland outlet glaciers, *Journal of Glaciology*, *59*(213), doi: 10.3189/2013JoG12J049.

Enderlin, E. M., I. M. Howat, S. Jeong, M.-J. Noh, J. H. van Angelen, and M. R. van den Broeke (2014), An improved mass budget for the Greenland ice sheet, *Geophysical Research Letters*, *41*(3), 2013GL059010, doi: 10.1002/2013GL059010.

Faillettaz, J., A. Pralong, M. Funk, and N. Deichmann (2008), Evidence of log-periodic oscillations and increasing icequake activity during the breaking-off of large ice masses, *Journal of Glaciology*, *54*(187), 725–737, doi: 10.3189/002214308786570845.

Gutenberg, B., and C. F. Richter (1944), Frequency of earthquakes in California, *Bulletin of the Seismological Society of America*, *34*, 185–188.

Hamilton, G. S., S. A. Khan, K. M. Schild, L. A. Stearns, M. Nettles, A. P. Ahlstrøm, M. L. Andersen, J. L. Davis, G. Ekström, P. Elósegui, R. Forsberg, J. de Juan, T. B. Larsen, and L. Stenseng (2008), Iceberg calving and flow dynamics at Helheim Glacier, East Greenland, from time-lapse photography, *EOS Trans. AGU*, *53*(89), abstract C13A–0565.

Hamilton, G. S., K. M. Schild, L. A. Stearns, J. de Juan, P. Elosegui, and M. Nettles (2010), Time-lapse photography yields new insights into Greenland outlet glacier dynamics (Invited), *AGU Fall Meeting Abstracts*, (Abstract IN33B-1313).

Hammer, C., M. Ohrnberger, and V. Schlindwein (2015), Pattern of cryospheric seismic events observed at Ekström Ice Shelf, Antarctica, *Geophysical Research Letters*, *42*(10), 2015GL064029, doi: 10.1002/2015GL064029.

Hanna, E., P. Huybrechts, K. Steffen, J. Cappelen, R. Huff, C. Shuman, T. Irvine-Fynn, S. Wise, and M. Griffiths (2008), Increased runoff from melt from the Greenland Ice Sheet: A response to global warming, *J. Climate*, *21*(2), 331–341, doi: 10.1175/2007JCLI1964.1.

Heeszel, D. S., H. A. Fricker, J. N. Bassis, S. O'Neel, and F. Walter (2014), Seismicity within a propagating ice shelf rift: The relationship between icequake locations and ice shelf structure, *Journal of Geophysical Research: Earth Surface*, *119*(4), 731–744, doi: 10.1002/2013JF002849.

Holland, D. M., R. H. Thomas, B. DeYoung, M. H. Ribergaard, and B. Lyberth (2008), Acceleration of Jakobshavn Isbræ triggered by warm subsurface ocean waters, *Nature Geoscience*, *1*(10), 659–664, doi: 10.1038/ngeo316.

Howat, I. M., and A. Eddy (2011), Multi-decadal retreat of Greenland's marine-terminating glaciers, *Journal of Glaciology*, *57*(203), 389–396, doi: 10.3189/002214311796905631.

Howat, I. M., I. Joughin, S. Tulaczyk, and S. Gogineni (2005), Rapid retreat and acceleration of Helheim Glacier, east Greenland, *Geophysical Research Letters*, *32*, L22502, doi: 10.1029/2005GL024737.

Howat, I. M., I. Joughin, and T. A. Scambos (2007), Rapid changes in ice discharge from Greenland outlet glaciers, *Science*, *315*, 1559–1561, doi: 10.1126/science.1138478.

Howat, I. M., I. Joughin, M. Fahnestock, B. E. Smith, and T. A. Scambos (2008), Synchronous retreat and acceleration of southeast Greenland outlet glaciers 2000–06: ice dynamics and coupling to climate, *Journal of Glaciology*, *54*(187), 646–660, doi: 10.3189/002214308786570908.

Husebye, E. S., B. O. Ruud, and A. M. Dainty (1998), Robust and reliable epicenter determinations: Envelope processing of local network data, *Bulletin of the Seismological Society of America*, *88*(1), 284–290.

James, T. D., T. Murray, N. Selmes, K. Scharrer, and M. O'Leary (2014), Buoyant flexure and basal crevassing in dynamic mass loss at Helheim Glacier, *Nature Geoscience*, *7*(8), 593–596, doi: 10.1038/ngeo2204.

Jiang, Y., T. H. Dixon, and S. Wdowinski (2010), Accelerating uplift in the North Atlantic region as an indicator of ice loss, *Nature Geoscience*, *3*(6), 404–407, doi: 10.1038/ngeo845.

Joughin, I., W. Abdalati, and M. Fahnestock (2004), Large fluctuations in speed on Greenland's Jakobshavn Isbræ glacier, *Nature*, *432*, 608–610, doi: 10.1038/nature03130.

Joughin, I., I. Howat, R. B. Alley, G. Ekström, M. Fahnestock, T. Moon, M. Nettles, M. Truffer, and V. C. Tsai (2008a), Ice-front variation and tidewater behavior on Helheim and

Kangerdlugssuaq Glaciers, Greenland, *Journal of Geophysical Research*, *113*, F01004, doi: 10.1029/2007JF000837.

Joughin, I., I. M. Howat, M. Fahnestock, B. Smith, W. Krabill, R. B. Alley, H. Stern, and M. Truffer (2008b), Continued evolution of Jakobshavn Isbrae following its rapid speedup, *Journal of Geophysical Research*, *113*, F04006, doi: 10.1029/2008JF001023.

Joughin, I., B. E. Smith, I. M. Howat, T. Scambos, and T. Moon (2010), Greenland flow variability from ice-sheet-wide velocity mapping, *Journal of Glaciology*, *56*(197), 415–430, doi: 10.3189/002214310792447734.

Kawakatsu, H. (1989), Centroid single force inversion of seismic waves generated by landslides, *Journal of Geophysical Research*, *94*, 12,363–12,374, doi: 10.1029/JB094iB09p12363.

Khan, S. A., J. Wahr, M. Bevis, I. Velicogna, and E. Kendrick (2010), Spread of ice mass loss into Northwest Greenland observed by GRACE and GPS, *Geophysical Research Letters*, *37*, L06501, doi: 10.1029/2010GL042460.

Koehn, D., and T. Sachau (2014), Two-dimensional numerical modeling of fracturing and shear band development in glacier fronts, *Journal of Structural Geology*, *61*(0), 133 – 142, doi: 10.1016/j.jsg.2012.11.002.

Kollmeyer, R. C. (1980), West Greenland outlet glaciers: an inventory of the major iceberg producers, *Cold Regions Science and Technology*, *1*, 175–181, doi: 10.1016/0165-232X(80)90046-4.

Krabill, W., E. Frederick, S. Manizade, C. Martin, J. Sonntag, R. Swift, R. Thomas, W. Wright, and J. Yungel (1999), Rapid thinning of parts of the southern Greenland ice sheet, *Science*, *283*(5407), 1522–1524, doi: 10.1126/science.283.5407.1522.

Krabill, W., E. Hanna, P. Huybrechts, W. Abdalati, J. Cappelen, B. Csatho, E. Frederick, S. Manizade, C. Martin, J. Sonntag, R. Swift, R. Thomas, and J. Yungel (2004), Greenland ice sheet: Increased coastal thinning, *Geophysical Research Letters*, *31*(24), L24402, doi: 10.1029/2004GL021533.

Levermann, A., T. Albrecht, R. Winkelmann, M. A. Martin, M. Haseloff, and I. Joughin (2012), Kinematic first-order calving law implies potential for abrupt ice-shelf retreat, *The Cryosphere*, *6*(2), 273–286, doi: 10.5194/tc-6-273-2012.

Luckman, A., and T. Murray (2005), Seasonal variation in velocity before retreat of Jakobshavn Isbræ, Greenland, *Geophysical Research Letters*, *32*(8), L08501, doi: 10.1029/2005GL022519.

Luckman, A., T. Murray, R. de Lange, and E. Hanna (2006), Rapid and synchronous ice-dynamic changes in East Greenland, *Geophysical Research Letters*, *33*, L03503, doi: 10.1029/2005GL025428.

Luthcke, S. B., H. J. Zwally, W. Abdalati, D. D. Rowlands, R. D. Ray, R. S. Nerem, F. G. Lemoine, J. J. McCarthy, and D. S. Chinn (2006), Recent Greenland ice mass loss by drainage system from

satellite gravity observations, *Science*, *314*, 1286–1289, doi: 10.1126/science.1130776.

MacAyeal, D. R., T. A. Scambos, C. L. Hulbe, and M. A. Fahnestock (2003), Catastrophic ice-shelf break-up by an ice-shelf-fragment-capsize mechanism, *Journal of Glaciology*, *49*(164), 22–36, doi: 10.3189/172756503781830863.

MacAyeal, D. R., E. A. Okal, R. C. Aster, and J. N. Bassis (2008), Seismic and hydroacoustic tremor generated by colliding icebergs, *Journal of Geophysical Research: Earth Surface*, *113*(F3), F03011, doi: 10.1029/2008JF001005.

McFadden, E. M., I. M. Howat, I. Joughin, B. E. Smith, and Y. Ahn (2011), Changes in the dynamics of marine terminating outlet glaciers in west Greenland (2000-2009), *Journal of Geophysical Research*, *116*(F2), F02022, doi: 10.1029/2010JF001757.

Moon, T., and I. Joughin (2008), Changes in ice front position on Greenland's outlet glaciers from 1992 to 2007, *Journal of Geophysical Research*, *113*, F02022, doi: 10.1029/2007JF000927.

Murray, T., K. Scharrer, T. D. James, S. R. Dye, E. Hanna, A. D. Booth, N. Selmes, A. Luckman, A. L. C. Hughes, S. Cook, and P. Huybrechts (2010), Ocean regulation hypothesis for glacier dynamics in southeast Greenland and implications for ice sheet mass changes, *Journal of Geophysical Research*, *115*, F03026, doi: 10.1029/2009JF001522.

Murray, T., M. Nettles, N. Selmes, L. M. Cathles, J. C. Burton, T. D. James, S. Edwards, I. Martin, T. O'Farrell, R. Aspey, I. Rutt, and T. Baugé (2015a), Reverse glacier motion during iceberg calving and the cause of glacial earthquakes, *Science*, *349*(6245), 305–308, doi: 10.1126/science.aab0460.

Murray, T., N. Selmes, T. D. James, S. Edwards, I. Martin, T. O'Farrell, R. Aspey, I. Rutt, M. Nettles, and T. Baugé (2015b), Dynamics of glacier calving at the ungrounded margin of Helheim Glacier, southeast Greenland, *Journal of Geophysical Research: Earth Surface*, *120*(6), 2015JF003531, doi: 10.1002/2015JF003531.

Neave, K. G., and J. C. Savage (1970), Icequakes on the Athabasca Glacier, *Journal of Geophysical Research*, *75*(8), 1351–1362, doi: 10.1029/JB075i008p01351.

Nettles, M., and G. Ekström (2010), Glacial earthquakes in Greenland and Antarctica, *Annual Review of Earth and Planetary Sciences*, *38*, 467–491, doi: 10.1146/annurev-earth-040809-152414.

Nettles, M., T. B. Larsen, P. Elósegui, G. S. Hamilton, L. A. Stearns, A. P. Ahlstrøm, J. L. Davis, M. L. Andersen, J. de Juan, S. A. Khan, L. Stenseng, G. Ekström, and R. Forsberg (2008a), Stepwise changes in glacier flow speed coincide with calving and glacial earthquakes at Helheim Glacier, Greenland, *Geophysical Research Letters*, *35*, L24503, doi: 10.1029/2008GL036127.

Nettles, M., T. B. Larsen, P. Elósegui, G. S. Hamilton, L. A. Stearns, A. P. Ahlstrøm, J. L. Davis, M. L. Andersen, J. de Juan, S. A. Khan, L. Stenseng, G. Ekström, R. Forsberg, and K. M. Schild

(2008b), Glacier acceleration, glacial earthquakes, and ice loss at Helheim Glacier, Greenland, *EOS Trans. AGU*, *52*(87), abstract G23A–02.

Nick, F. M., A. Vieli, I. M. Howat, and I. Joughin (2009), Large-scale changes in Greenland outlet glacier dynamics triggered at the terminus, *Nature Geoscience*, *2*(2), 110–114, doi: 10.1038/NGEO394.

O'Neel, S., H. P. Marshall, D. E. McNamara, and W. T. Pfeffer (2007), Seismic detection and analysis of icequakes at Columbia Glacier, Alaska, *Journal of Geophysical Research*, *112*, doi: 10.1029/2006JF000595.

Padman, L., and S. Erofeeva (2004), A barotropic inverse tidal model for the Arctic Ocean, *Geophysical Research Letters*, *31*(2), L02303, doi: 10.1029/2003GL019003.

Peng, Z., J. I. Walter, R. C. Aster, A. Nyblade, D. A. Wiens, and S. Anandakrishnan (2014), Antarctic icequakes triggered by the 2010 Maule earthquake in Chile, *Nature Geosci*, *7*(9), 677–681, doi: 10.1038/ngeo2212.

Pralong, A., and M. Funk (2005), Dynamic damage model of crevasse opening and application to glacier calving, *Journal of Geophysical Research: Solid Earth*, *110*(B1), doi: 10.1029/2004JB003104.

Pralong, A., M. Funk, and M. P. Lüthi (2003), A description of crevasse formation using continuum damage mechanics, *Annals of Glaciology*, *37*(1), 77–82, doi: 10.3189/172756403781816077.

Pritchard, H. D., R. J. Arthern, D. G. Vaughan, and L. A. Edwards (2009), Extensive dynamic thinning on the margins of the Greenland and Antarctic ice sheets, *Nature*, *461*(7266), 971–975, doi: 10.1038/nature08471.

Qamar, A. (1988), Calving icebergs: a source of low-frequency seismic signals from Columbia Glacier, Alaska, *Journal of Geophysical Research*, *93*(B6), 6615–6623.

Rial, J. A., C. Tang, and K. Steffen (2009), Glacial rumblings from Jakobshavn ice stream, Greenland, *Journal of Glaciology*, *55*(191), 389–399, doi: 10.3189/002214309788816623.

Rignot, E., and P. Kanagaratnam (2006), Changes in the velocity structure of the Greenland Ice Sheet, *Science*, *311*, 986–990, doi: 10.1126/science.1121381.

Rignot, E., and K. Steffen (2008), Channelized bottom melting and stability of floating ice shelves, *Geophysical Research Letters*, *35*(2), L02503, doi: 10.1029/2007GL031765.

Rignot, E., J. E. Box, E. Burgess, and E. Hanna (2008), Mass balance of the Greenland ice sheet from 1958 to 2007, *Geophysical Research Letters*, *35*(20), L20502, doi: 10.1029/2008GL035417.

Röösli, C., F. Walter, S. Husen, L. C. Andrews, M. P. Lüthi, G. A. Catania, and E. Kissling (2014), Sustained seismic tremors and icequakes detected in the ablation zone of the Greenland ice

sheet, *Journal of Glaciology*, *60*(221), 563–575, doi: 10.3189/2014JoG13J210.

Savage, H. M., and C. Marone (2007), Effects of shear velocity oscillations on stick-slip behavior in laboratory experiments, *Journal of Geophysical Research: Solid Earth*, *112*(B2), B02301, doi: 10.1029/2005JB004238.

Schild, K. M., and G. S. Hamilton (2013), Seasonal variations of outlet glacier terminus position in Greenland, *Journal of Glaciology*, *59*(216), 759–770, doi: 10.3189/2013JoG12J238.

Seale, A., P. Christoffersen, R. I. Mugford, and M. O'Leary (2011), Ocean forcing of the Greenland ice sheet: Calving fronts and patterns of retreat identified by automatic satellite monitoring of eastern outlet glaciers, *Journal of Geophysical Research*, *116*(F3), F03013, doi: 10.1029/2010JF001847.

Shepherd, A., E. R. Ivins, G. A, V. R. Barletta, M. J. Bentley, S. Bettadpur, K. H. Briggs, D. H. Bromwich, R. Forsberg, N. Galin, M. Horwath, S. Jacobs, I. Joughin, M. A. King, J. T. M. Lenaerts, J. Li, S. R. M. Ligtenberg, A. Luckman, S. B. Luthcke, M. McMillan, R. Meister, G. Milne, J. Mouginot, A. Muir, J. P. Nicolas, J. Paden, A. J. Payne, H. Pritchard, E. Rignot, H. Rott, L. S. Sørensen, T. A. Scambos, B. Scheuchl, E. J. O. Schrama, B. Smith, A. V. Sundal, J. H. van Angelen, W. J. van de Berg, M. R. van den Broeke, D. G. Vaughan, I. Velicogna, J. Wahr, P. L. Whitehouse, D. J. Wingham, D. Yi, D. Young, and H. J. Zwally (2012), A reconciled estimate of ice-sheet mass balance, *Science*, *338*(6111), 1183–1189, doi: 10.1126/science.1228102.

Smith, A. M. (2006), Microearthquakes and subglacial conditions, *Geophysical Research Letters*, *33*(24), doi: 10.1029/2006GL028207.

Smith, G. P., and G. Ekström (1997), Interpretation of earthquake epicenter and CMT centroid locations, in terms of rupture length and direction, *Physics of the Earth and Planetary Interiors*, *102*(1-2), 123–132, doi: 10.1016/S0031-9201(96)03246-3.

Sohn, H.-G., K. C. Jezek, and C. J. van der Veen (1998), Jakobshavn Glacier, West Greenland: 30 years of spaceborne observations, *Geophysical Research Letters*, *25*(14), 2699–2702, doi: 10.1029/98GL01973.

Stearns, L. A., and G. S. Hamilton (2007), Rapid volume loss from two East Greenland outlet glaciers quantified using repeat stereo satellite imagery, *Geophysical Research Letters*, *34*, L05503, doi: 10.1029/2006GL028982.

Straneo, F., G. S. Hamilton, D. A. Sutherland, L. A. Stearns, F. Davidson, M. O. Hammill, G. B. Stenson, and A. Rosing-Asvid (2010), Rapid circulation of warm subtropical waters in a major glacial fjord in East Greenland, *Nature Geoscience*, *3*(3), 182–186, doi: 10.1038/ngeo764.

Stroup, D. F., D. R. Bohnenstiehl, M. Tolstoy, F. Waldhauser, and R. T. Weekly (2007), Pulse of the seafloor: Tidal triggering of microearthquakes at 9°50'N East Pacific Rise, *Geophysical Research Letters*, *34*(15), L15301, doi: 10.1029/2007GL030088.

Stuart, G., T. Murray, A. Brisbourne, P. Styles, and S. Toon (2005), Seismic emissions from a surging glacier: Bakaninbreen, Svalbard, *Annals of Glaciology*, *42*(1), 151–157, doi: 10.3189/172756405781812538.

Thelen, W. A., K. Allstadt, S. De Angelis, S. D. Malone, S. C. Moran, and J. Vidale (2013), Shallow repeating seismic events under an alpine glacier at Mount Rainier, Washington, USA, *Journal of Glaciology*, *59*(214), 345–356, doi: 10.3189/2013JoG12J111.

Thomas, R., E. Frederick, W. Krabill, S. Manizade, and C. Martin (2009), Recent changes on Greenland outlet glaciers, *Journal of Glaciology*, *55*(189), 147–162, doi: 10.3189/002214309788608958.

Thomas, R. H., W. Abdalati, T. L. Akins, B. M. Csatho, E. B. Frederick, S. P. Gogineni, W. B. Krabill, S. S. Manizade, and E. J. Rignot (2000), Substantial thinning of a major East Greenland outlet glacier, *Geophysical Research Letters*, *27*(9), 1291–1294, doi: 10.1029/1999GL008473.

Thomas, R. H., W. Abdalati, E. Frederick, W. B. Krabill, S. Manizade, and K. Steffen (2003), Investigation of surface melting and dynamic thinning on Jakobshavn Isbræ, Greenland, *Journal of Glaciology*, *49*(165), 231–239, doi: 10.3189/172756503781830764.

Truffer, M., J. Amundson, M. Fahnestock, I. Joughin, and R. Motyka (2011), Ocean regulation of ice flow, *Proceedings of La Jolla Symposium on Interactions of Ice Sheets and Glaciers with the Ocean, June 6–10*, abstract 60A034.

Tsai, V. C., and G. Ekström (2007), Analysis of glacial earthquakes, *Journal of Geophysical Research*, *112*, F03S22, doi: 10.1029/2006JF000596.

Tsai, V. C., J. R. Rice, and M. Fahnestock (2008), Possible mechanisms for glacial earthquakes, *Journal of Geophysical Research*, *113*, F03014, doi: 10.1029/2007JF000944.

van den Broeke, M., J. Bamber, J. Ettema, E. Rignot, E. Schrama, W. J. van de Berg, E. van Meijgaard, I. Velicogna, and B. Wouters (2009), Partitioning recent Greenland mass loss, *Science*, *326*(5955), 984–986, doi: 10.1126/science.1178176.

Veitch, S. A., and M. Nettles (2012), Spatial and temporal variations in Greenland glacial-earthquake activity, 1993–2010, *Journal of Geophysical Research: Earth Surface*, *117*(F4), doi: 10.1029/2012JF002412.

Velicogna, I. (2009), Increasing rates of ice mass loss from the Greenland and Antarctic ice sheets revealed by GRACE, *Geophysical Research Letters*, *36*(19), L19503, doi: 10.1029/2009GL040222.

Velicogna, I., and J. Wahr (2005), Greenland mass balance from GRACE, *Geophysical Research Letters*, *32*(18), L18505, doi: 10.1029/2005GL023955.

von der Osten-Woldenburg, H. (1990), Icequakes on ekström ice shelf near Atka Bay, Antarctica, *Journal of Glaciology*, *36*(122), 31–36.

Voytenko, D., A. Stern, D. M. Holland, T. H. Dixon, K. Christianson, and R. T. Walker (2015), Tidally driven ice speed variation at Helheim Glacier, Greenland, observed with terrestrial radar interferometry, *Journal of Glaciology*, *61*(226), 301–308, doi: 10.3189/2015JoG14J173.

Walter, F., J. F. Clinton, N. Deichmann, D. S. Dreger, S. E. Minson, and M. Funk (2009), Moment tensor inversions of icequakes on Gornergletscher, Switzerland, *Bulletin of the Seismological Society of America*, *99*(2A), 852–870, doi: 10.1785/0120080110.

Walter, F., D. S. Dreger, J. F. Clinton, N. Deichmann, and M. Funk (2010), Evidence for near-horizontal tensile faulting at the base of Gornergletscher, a Swiss alpine glacier, *Bulletin of the Seismological Society of America*, *100*(2), 458–472, doi: 10.1785/0120090083.

Walter, F., J. M. Amundson, S. O'Neel, M. Truffer, M. Fahnestock, and H. A. Fricker (2012a), Analysis of low-frequency seismic signals generated during a multiple-iceberg calving event at Jakobshavn Isbræ, Greenland, *Journal of Geophysical Research*, *117*, F01036, doi: 10.1029/2011JF002132.

Walter, F., P. Dalban Canassy, S. Husen, and J. F. Clinton (2013), Deep icequakes: What happens at the base of Alpine glaciers?, *Journal of Geophysical Research: Earth Surface*, *118*(3), 1720–1728, doi: 10.1002/jgrf.20124.

Walter, J. I., J. E. Box, S. Tulaczyk, E. E. Brodsky, I. M. Howat, Y. Ahn, and A. Brown (2012b), Oceanic mechanical forcing of a marine-terminating Greenland glacier, *Annals of Glaciology*, *53*(60), 181–192, doi: 10.3189/2012AoG60A083.

Weiss, J. (2004), Subcritical crack propagation as a mechanism of crevasse formation and iceberg calving, *Journal of Glaciology*, *50*(168), 109–115, doi: 10.3189/172756504781830240.

West, M. E., C. F. Larsen, M. Truffer, S. O'Neel, and L. LeBlanc (2010), Glacier microseismicity, *Geology*, *38*(4), 319–322, doi: 10.1130/G30606.1.

Wiens, D. A., S. Anandakrishnan, J. P. Winberry, and M. A. King (2008), Simultaneous teleseismic and geodetic observations of the stick-slip motion of an Antarctic ice stream, *Nature*, *453*(7196), 770–774, doi: 10.1038/nature06990.

Wilcock, W. S. D. (2001), Tidal triggering of microearthquakes on the Juan de Fuca Ridge, *Geophysical Research Letters*, *28*(20), 3999–4002, doi: 10.1029/2001GL013370.

Winberry, J. P., S. Anandakrishnan, D. A. Wiens, R. B. Alley, and K. Christianson (2011), Dynamics of stick-slip motion, whillans ice stream, antarctica, *Earth and Planetary Science Letters*, *305*(3–4), 283–289, doi: 10.1016/j.epsl.2011.02.052.

Wolf, L. W., and J. N. Davies (1986), Glacier-generated earthquakes from Prince William Sound, Alaska, *Bulletin of the Seismological Society of America*, *76*(2), 367–379.

Wouters, B., D. Chambers, and E. J. O. Schrama (2008), GRACE observes small-scale mass loss in Greenland, *Geophysical Research Letters*, *35*(20), L20501, doi: 10.1029/2008GL034816.

Zoet, L. K., S. Anandakrishnan, R. B. Alley, A. A. Nyblade, and D. A. Wiens (2012), Motion of an Antarctic glacier by repeated tidally modulated earthquakes, *Nature Geosci*, *5*(9), 623–626.

Zwally, H. J., J. Li, A. C. Brenner, M. Beckley, H. G. Cornejo, J. DiMarzio, M. B. Giovinetto, T. A. Neumann, J. Robbins, J. L. Saba, D. Yi, and W. Wang (2011), Greenland ice sheet mass balance: distribution of increased mass loss with climate warming; 2003–07 versus 1992–2002, *Journal of Glaciology*, *57*(201), doi: 10.3189/002214311795306682.